МІНІСТЕРСТВО ОСВІТИ І НАУКИ УКРАЇНИ
Національний технічний університет
“Харківський політехнічний інститут”

ВІСНИК
НАЦІОНАЛЬНОГО ТЕХНІЧНОГО УНІВЕРСИТЕТУ “ХАРКІВСЬКИЙ ПОЛІТЕХНІЧНИЙ ІНСТИТУТ”

Серія: Радіофізика та іоносфера

№ 47 (1089) 2014

Збірник наукових праць

Видання засноване у 1961 р.

Харків
НТУ “ХПІ”, 2014

ISSN 2078-9998

Вісник Національного технічного університету "Харківський політехнічний інститут". Збірник наукових праць. Серія: Радіофізика та іоносфера. – Х.: НТУ "ХПІ". – 2014. – № 47 (1089). – 108 с.

Державне видання
Свідоцтво Держкомітету з інформаційної політики України
КВ № 5256 від 2 липня 2001 року

Збірник виходить українською та російською мовами.

Вісник Національного технічного університету "ХПІ" внесено до "Переліку наукових фахових видань України, в яких можуть публікуватися результати дисертаційних робіт на здобуття наукових ступенів доктора і кандидата наук", затвердженого Постановою президії ВАК України від 26 травня 2010 р., № 1 – 05 (Бюлетень ВАК України, № 6, 2010 р., с. 3, № 20).

У квітні 2013 р. Вісник Національного технічного університету "ХПІ", серія "Радіофізика та іоносфера", включений у довідник періодичних видань бази даних ***Ulrich's Periodicals Directory (New Jersey, USA)****.*

Рекомендовано до друку Вченою радою НТУ "ХПІ",
протокол № 8 від 26 вересня 2014 р.

MINISTRY OF EDUCATION AND SCIENCE OF UKRAINE
National Technical University
“Kharkiv Polytechnic Institute”

BULLETIN of the
NATIONAL TECHNICAL UNIVERSITY "KHARKIV POLYTECHNIC INSTITUTE"

Series: Radiophysics and ionosphere

№ 47 (1089) 2014

Scientific Papers

Published since 1961

Kharkiv
NTU “KhPI”, 2014

ISSN 2078-9998

Bulletin of the National Technical University "Kharkiv Polytechnic Institute". Scientific Papers. Series: Radiophysics and ionosphere. – Kharkiv: NTU "KhPI". – 2014. – № 47 (1089). – 108 p.

State edition
Certificate of the State Committee of Ukraine for Information Policy
KB № 5256 from July 2, 2001

Proceedings are published in Ukrainian and Russian.

Bulletin of the National Technical University "KPI" included in the "List of scientific professional publications of Ukraine, where the results can be published dissertations for academic degrees of doctor and candidate of sciences", approved by the Presidium of Higher Certification Commission of Ukraine of 26 May 2010 p., № 1 - 05 (Bulletin of Higher Certification Commission of Ukraine, № 6, 2010, p. 3, № 20).

In April 2013 Bulletin of the National Technical University "KhPI" series "Radiophysics and ionosphere", included in the ***Ulrich's Periodicals Directory*** *database* ***(New Jersey, USA)****.*

Recommended for publication by Scientific Council of NTU "KhPI"
protocol No. 8 on September 26, 2014

UDC 628.396

D.V. SHAPOVALOVA, student, NTU "KhPI"
V.A. PULYAYEV, D.Sc., Prof., deputy director, Institute of Ionosphere, Kharkiv

REFINEMENT OF THE INCOHERENT SCATTER RADAR CONSTANT

Examined a variant of the software for procedure realization for comparing the level of noise at the input of the incoherent scatter radar, order to improve its constants without using information from the ionospheric station.

Keywords: scattering signal, the constant radar, software algorithms, ionospheric station, the parameters of the ionosphere.

Introduction. Dynamic processes, which occur in the ionospheric plasma and largely determine the structure of the field F, we have enormous influence on the radio waves propagation channel. The study of these processes is associated with the need to predict the state of the ionosphere and determine the optimum conditions for the short-wave communication. The electron density N_e is one of the main defined parameters of the ionospheric plasma.

The method of incoherent scatter (IS) to obtain information about the basic parameters of the ionosphere suggests as one of the options, attraction the IS radar constant C_{et}, which show the state of its technical systems [1]. However, some difficulties encountered, when we using a constant. These include situation in which the current state of technical systems varies and differs from the primary, when was determined the constant C_{et} for radar.

The periodic heating and cooling of the large surfaces waveguide lines, which occur due to changes network supply voltage and fluctuations the ambient temperature is the main causes of instability of the characteristics of hardware. Also the situation is complicated with change of solar activity during magnetic and ionospheric storms. It is causing the necessity in adjusting the amplitude for the input signal dynamic range of the ADC by changing the amplification factor in the receiver. The result is a divergence with the radar constant C_{et}. To resolve this, is applied periodic refinement a constant using the automatic ionospheric station – the ionosonde.

In [2] proposed a variant of carrying out correction for the values of the constant C_{et} in another way – using the information about changing the noise power $P_c(t)$, which present at the input of the IS radar on the current day of the experiment.

The purpose of this article is to develop software algorithms for the implementation the procedure refinement for the IS radar constant by information about changing the noise power at the radar input.

Implementation of program for the processing mode. In [2] analyzed the components of the background noise that enters the area of the antenna pattern.

For information about the changing technical characteristics of the IS radar will compare next graphic lines: the diurnal cycle power $P_{et}(t)$, recorded during the calculation of the constants C_b in the test day, with noise power $P_c(t)$, obtained within the time $t = \overline{0,T}$ on the current day (see block diagram in Fig. 1).

For convenience, such a comparison will put the condition that the array $P_{et}(t)$ consisted of $N = 365$ samples, allowing to realize a cyclic shift of the graph along the time axis with a step of $1/N$, corresponding to $\Delta t \approx 4$ min. This shift corresponds to a change of position of the Earth in relation to the sky for a period of one day. Similarly, in an array $P_c(t)$ readings must attend with the same discreteness. And since in the IS method for the formation of the daily line taken receive counts of the noise power for each interval of 15 minutes, using the programmatic transformation primarily necessary spend interpolation between points for values $P_c(t)$, aligning dimension of arrays.

After interpolation, necessary implement the cyclic shift of one of the graphs (Fig. 2) along a horizontal line, and simultaneously run the iterative procedure for finding the minimum value of $\Delta(n)$ in the form [2].

$$\Delta(n)\Big|_{n=\overline{0,N}} = \sum_{t=0}^{T} \left\{P_{et}(t) - [P_c(t - n\Delta t)\right\}^2 \Rightarrow \min .$$

The following procedure will give the opportunity to fix the coincidence of minima and maxima of the two lines along the horizontal. Incidentally, at this point ($t_0\big|_{\Delta(n)=\min} = t - n_0\Delta t$), spending the count for number of shifts ($n_0 = 304$ in Fig. 3), can refine the date of the measurements.

In the next step alternately will changing the values of variables k and d (step depends by precision) and must be implemented the procedures of finding a minimum meaning of $\Delta(k, d)$ as [2]

$$\Delta(k,d)\Big|_{\substack{k=\overline{-2,+2}\\ d=\overline{-2000,+2000}}} = \sum_{t=0}^{T} \left\{P_{et}(t) - k \cdot [P_c(t_0) + d]\right\}^2 \Rightarrow \min ,$$

which gives an opportunity to compare the lines ($k_0 = 0{,}5$ and $d_0 = 1132$ in Fig. 4), but along the vertical.

Execution completes these procedures the constant C_c in current day is calculated as [2]

$$C_c = \frac{C_{et}}{k_0}\left[1 - \frac{k_0 \cdot d_0}{P_=}\right] = C_{et} \cdot 0{,}5 ,$$

where $P_= = 750$ – a component of the noise level, which is fixed during the definition of the constant C_{et} at the IS radar, using the transmitter, which is currently is disabled.

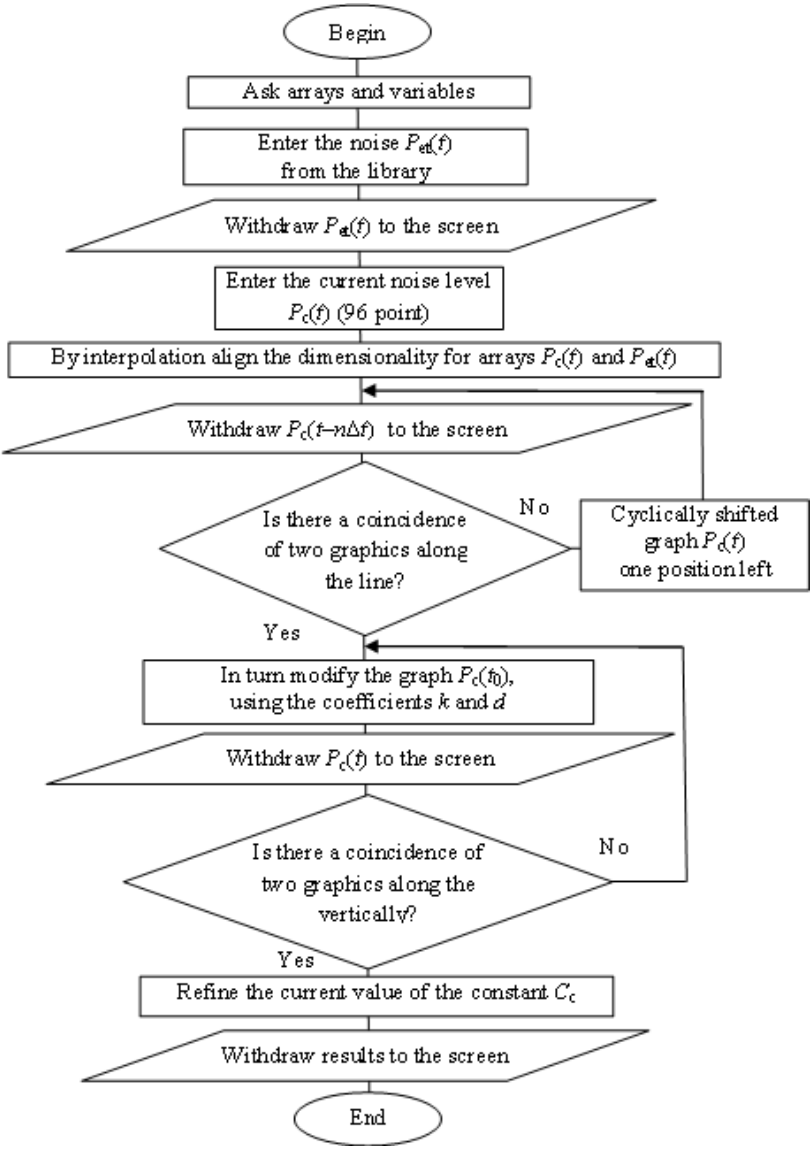

Fig. 1 – The flowchart of algorithm for correction of constant C_c

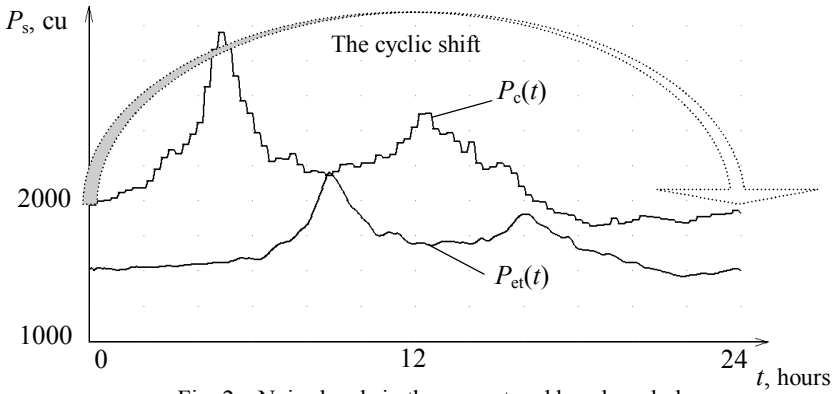

Fig. 2 – Noise levels in the current and benchmark days

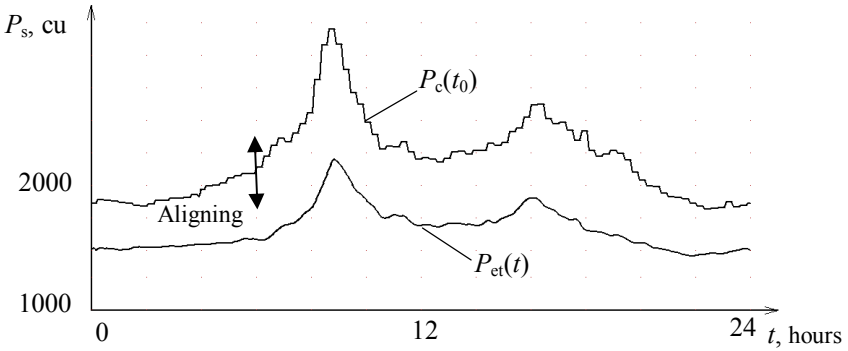

Fig. 3 – Moment of aligning lines along the horizontal

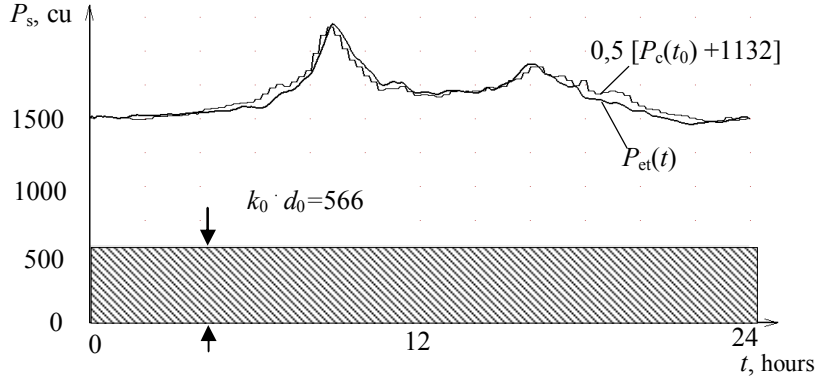

Fig. 4 – Moment of aligning lines along the vertical

Conclusions. In this article describes the procedure that implements the checking and refinement the constant of IS radar and making possible to use it in the future for more accurately assess of the electron density N_e in the ionosphere by the measured the scattering signal.

It is shown that the constant does can not track changes in the characteristics of the technical systems of radar in time, for its refinement is necessary the station for vertical sounding. In the above work, alternatively, for independent verifying the constants considered the way, based on the using of information that provided by the noise and obtained by the receiving antenna. Flowchart and software, using the language operators of *FreeBASIC*, was developed for implementation of this method. Using the mathematical transformations for arrays which containing information about the distribution of the noise power in the etalon and in one of the working days of the measurements, have been demonstrated the one is example for comparing the noise elements.

The comparison results showed that, with ratio to the benchmark day (C_{et} constant was determined June 1), the information of the current day was obtained by the cyclically shift left on n_0 = 304 positions that correspond to the calendar date on April 2.

After that there were obtained coefficients k_0 = 0,5 and d_0 = 1132, which provided information on changes in the receiving and transmitting IS radar systems, which led to the nonconformity of reality for the constant C_{et} on 50%.

References: 1. *Evans J.W.* Theoretical and practical issues to investigate the ionosphere by means of incoherent scattering of radio waves / *J.W. Evans* // PIEEE. – 1969. – Vol. 57, № 4. – P. 139-175. **2.** *Pulyayev V.A.* Defining the parameters of the ionosphere method of incoherent scattering of radio waves: Monograph / *V.A. Pulyayev, D.A. Dzyubanov, I.F. Domnin*. – Kharkiv: NTU "KhPI", 2011. – 240 p.

Received 20.05.2014

UDC 628.396

Refinement of the incoherent scatter radar constant / D.V. Shapovalova, V.A. Pulyayev // Bulletin of NTU "KhPI". Series: Radiophysics and ionosphere. - Kharkiv: NTU "KhPI", 2014. – No. 47 (1089). – P. 5-9. Ref.: 2 titles.

Рассмотрен вариант реализации процедуры программного сравнения уровня шума на входе радара некогерентного рассеяния для уточнения его константы без использования информации с ионосферной станции.

Ключевые слова: сигнал рассеяния, константа радара, программные алгоритмы, ионосферная станция, параметры ионосферы.

Розглянуто варіант реалізації процедури програмного порівняння рівня шуму на вході радару некогерентного розсіяння для уточнення значення його константи, не використовуючи при цьому інформацію з іоносферної станції.

Ключові слова: сигнал розсіяння, константа радару, програмні алгоритми, іоносферна станція, параметри іоносфери.

UDC 621.396, 004.457

O.V. BOGOMAZ, research scientist, Institute of ionosphere, Kharkiv;
D.V. KOTOV, PhD, research scientist, Institute of ionosphere, Kharkiv

A LIBRARY OF ROUTINES FOR INCOHERENT SCATTER RADAR DATA PROCESSING

The structure of the developed dynamic link library of routines for incoherent scatter radar data processing and incoherently scattered signals simulation and the examples of its application are described.

Keywords: incoherent scatter, data processing, simulation, numerical computing routines.

Introduction. Incoherent scatter radar data processing is produced by the complicated program packages GUISDAP and UPRISE for example [1, 2].

GUISDAP (Grand Unified Incoherent Scatter Design and Analysis Package) is used on EISCAT radars and needs a MATLAB environment in the Linux or Windows operating system (OS). The MATLAB application is built around the own high-level language and provides a lot of numerical computing routines for data processing. These features make GUISDAP sources more clear to understand and simpler to improve.

UPRISE (Unified Processing of the Results of Incoherent Scatter Experiments) package is used for processing of the data obtained by means of Kharkiv incoherent scatter radar (ISR). The package includes programs for viewing the initial data, interference filtering, time integration, altitudinal correction and estimating of ionospheric plasma parameters. It is written using FreeBASIC, runs in Windows OS and doesn't need any third-party software. The most used routines for UPRISE were exported to the dynamic link library (DLL) *albom.dll* written in C programming language.

Purpose of the article is to present the developed dynamic link library of routines for incoherent scatter radar data processing.

Library structure. *Albom.dll* consists of more than 100 functions that can be divided into several groups.

The first group is represented by functions for manipulating the initial data. The library can handle files produced by all Kharkiv ISR data processing systems operating since 1996. There are functions for loading and saving files of data processing system based on TMS320 signal processors [3], multichannel programmed correlator [4] and the data acquisition system based on E20-10 analog-to-digital conversion module [5]. There are functions for file testing and metadata reading and writing.

Functions for calculating altitude of the scattered volume are also present in this group. An altitude h can be calculated using $h = H_0 + \Delta h \cdot i$ formula, where Δh –

an altitude step (4.583 or 9.81 km), i – a current altitude position, H_0 – an altitude for the first position. Constants H_0 for every ISR data processing system were verified using the reflections from the International Space Station (fig. 1).

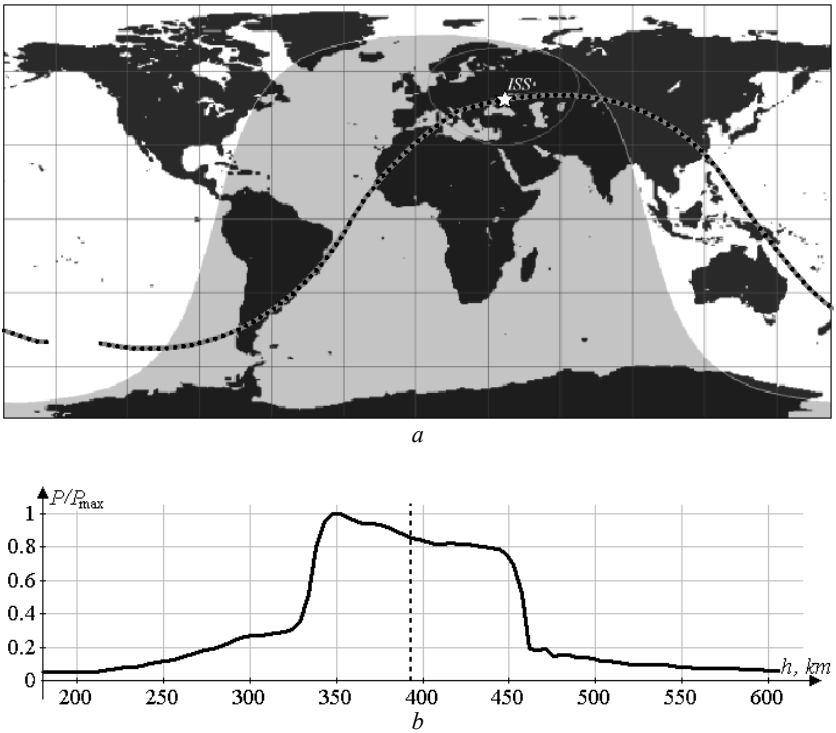

Fig. 1 – International Space Station (ISS) location on August 11, 1999 at 2:41 EEST (*a*) and recieved by the Kharkiv radar reflected power profile showing distance to the ISS is equal 393 km (*b*)

The group also includes functions for working with files in the specified directory in the disk file system. For example it is possible to make a list of files in a directory and get its length using only one function. There is a need to perform this task often because the number of initial files always varies.

The second group of functions contained in the *albom.dll* gathers ones for output data manipulating. This data can be binary or text files with IS signal autocorrelation functions (ACFs) or estimated ionospheric plasma parameters (such as ion and electron temperatures, ion composition, velocity etc.). It is possible to work with buffer in memory as with a file and after writing to it file is flushed to disk.

The third group provides time and date functions. The one of the main of them converts date to UNIX timestamp. It is used for sorting the initial data. Inverse conversion is also available. Another function returns the next day value. It checks if the date is valid, takes into account number of days in the month and determines whether the year is leap. For example if the input date is February 29, 2012, the function will return March 1, 2012.

The fourth group contains functions for calculating IS signals' spectra and ACFs. Wavelength is taken to be 1.9 m. Such other parameters as sampling interval, ion composition, ion and electron temperatures and electron density are definable. As ACF calculating is time-consuming operation, it is not desirable to carry out it in the real time while the inverse problem is solving for example. So routines for building of ACF libraries and working with them are also present in the DLL.

Lastly a lot of routines for data processing are implemented in the fifth group of functions.

Statistical routines are presented by functions for distribution law, arithmetic mean, standard deviation and variance of a list of numbers calculating.

A set of functions is intended for arrays manipulation (maximum and minimum values searching, trends building, normalization of series, convolution between two series, element-wise addition, subtraction, multiplication and division).

ISR data can be interpolated and approximated using a number of functions (linear and spline interpolation, polynomial approximation).

The discrete Fourier transform, fast Fourier transform and their inverses are implemented in the library and are widely used in the UPRISE package.

Two functions in the library generate random real numbers with uniform and normal distributions. The initial value can be set by lower 32 bits of the Time Stamp Counter (TSC) when x86 architecture processor is used. RDTSC (Read TSC) instruction returns the number of cycles since processor's reset and is available starting from Pentium.

Other applications of the albom.dll. The library using is quite wide in programs developed in the Institute of ionosphere.

First of all it is programs for the initial data export to analyze them using third-party software. These programs have a simple user interface (fig. 2). One click is needed to choose directory with files and one more to choose directory to export data to text files.

Secondly, programs using *albom.dll* are designed for incoherently scattered signals simulation. The developed software for signal simulation allows to obtain statistical errors of ionospheric plasma parameters estimation [6] and to test ISR data acquisition systems [7].

Data stored in the DLL. Besides the code of routines, the *albom.dll* contains data related to the Kharkiv ISR characteristics such as frequency response, impulse response and ACF of impulse response for analog low-pass filters that are used in the radar receiver (fig. 3). Appropriate functions easily fill arrays and there is no

need to store data in many files and to load them from disk.

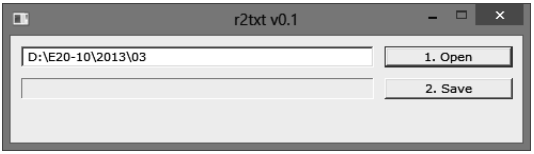

Fig. 2 – Graphical user interface of the program for the initial data exporting that uses *albom.dll*

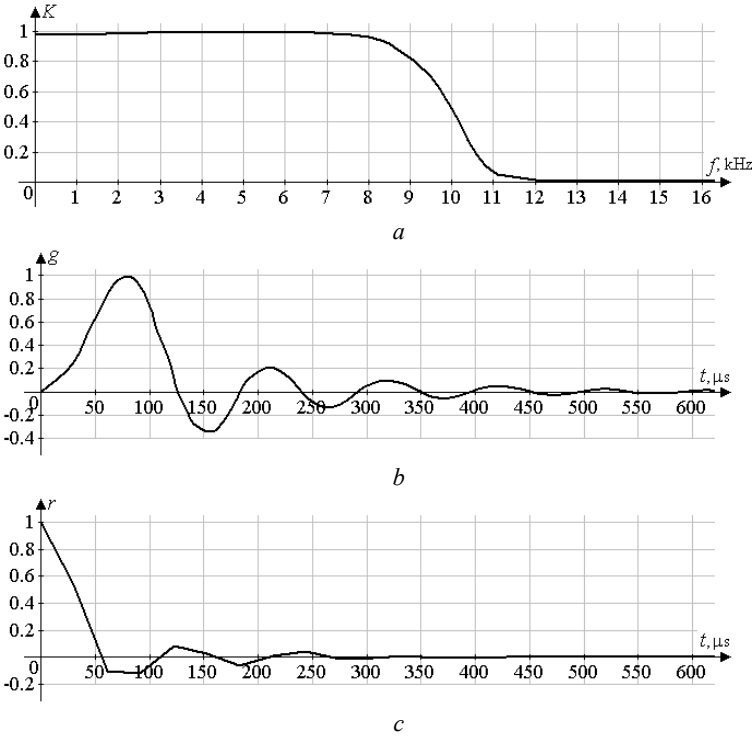

Fig. 3 – Frequency response (*a*), impulse response (*b*) and ACF of impulse response (*c*) for 9.5 kHz low-pass filter used in Kharkiv incoherent scatter radar receiver

Conclusions. The *albom.dll* library contains a lot of routines that significantly simplify the process of development of programs for ISR data

processing and incoherently scattered signals simulation. It can be used with almost all modern programming language (C/C++, Delphi, Python, FreeBASIC etc.).

References: 1. *Lehtinen M.S.* General incoherent scatter analysis and GUISDAP / *M.S. Lehtinen*, *A. Huuskonen* // J. Atmos. Terr. Phys. – 1996. – Vol. 58. – № 1–4. – P. 435-452. **2.** *Bogomaz O.V.* Unified Processing of the Results of Incoherent Scatter Experiments (UPRISE), a new generation program package for incoherent scatter radar data processing / *O.V. Bogomaz*, *D.V. Kotov* // Bulletin of National Technical University "Kharkiv Polytechnic Institute": Special Issue "Radiophysics and ionosphere". – 2013. – № 28 (1001). – P. 29-37. (in Russian) **3.** *Lysenko V.N.* Programmable correlator to measure the ionospheric parameters using the incoherent scatter method / *V.N. Lysenko* // Bulletin of the Kharkiv State Polytechnic University. – 1999. – № 31.– C. 96-99. (in Russian) **4.** *Lysenko V.N.* Correlation processing of incoherent scatter signal / *V.N. Lysenko*, *A.F. Kononenko*, *Yu.V. Chernyak* // Bulletin of National Technical University "Kharkiv Polytechnic Institute", Special Issue "Radiophysics and ionosphere". – 2004. – № 23. – P. 49-62. (in Russian) **5.** *Iskra D.A.* Improving the accuracy of determining the autocorrelation functions of incoherently scattered signal / *D.A. Iskra* // International School-Conference "Remote radio sounding of the ionosphere (ION-2013)", September, 30 – October, 4, 2013, Maly Mayak (Big Alushta), Crimea, Ukraine. – Book of abstracts. – 2013. – P. 45. (in Russian) **6.** *Bogomaz O.V.* Simulation of random errors in ionospheric parameters estimation obtained by means of incoherent scattering / *O.V. Bogomaz* // Bulletin of North-Caucasus Federal University. – 2013. – № 6 (39). – P. 9-15. (in Russian) **7.** *Bogomaz O.V.* Hardware and software complex for incoherently scattered signal simulation / *O.V. Bogomaz*, *D.A. Iskra* // Bulletin of National Technical University "Kharkiv Polytechnic Institute": Special Issue "Radiophysics and ionosphere". – 2013. – № 33 (1066). – P. 3-7. (in Russian)

Received 12.05.2013

UDC 621.396, 004.457

A library of routines for incoherent scatter radar data processing / O.V. Bogomaz, D.V. Kotov // Bulletin of NTU "KhPI". Series: Radiophysics and ionosphere. - Kharkiv: NTU "KhPI", 2014. – No. 47 (1089). – P. 10-14. Ref.: 7 titles.

В статье описана структура разработанной динамической библиотеки процедур для обработки данных радара некогерентного рассеяния и имитации некогерентно рассеянных сигналов, а также приведены примеры её применения.

Ключевые слова: некогерентное рассеяние, обработка данных, моделирование, численные вычислительные процедуры.

У статті описано структуру розробленої динамічної бібліотеки процедур для обробки даних радара некогерентного розсіяння та імітації некогерентно розсіяних сигналів, а також приведено приклади її використання.

Ключові слова: некогерентне розсіяння, обробка даних, моделювання, чисельні обчислювальні процедури.

UDC 550.388

I.F. DOMNIN, D.Sc., Prof., director, Institute ionosphere, Kharkov;
C. LA HOZ, Prof., UiT the Arctic University of Norway, Tromsø;
M.V. LYASHENKO, PhD, scientific secretary, Institute ionosphere, Kharkov

VARIATIONS OF THE ELECTRIC FIELD ZONAL COMPONENT, THE VERTICAL COMPONENT OF THE PLASMA DRIFT AND NEUTRAL WIND VELOCITIES IN IONOSPHERE OVER KHARKOV (UKRAINE) DURING AUGUST 5 – 6, 2011 AND NOVEMBER 13 – 15, 2012 MAGNETIC STORMS

The modeling results of the zonal electric field and the vertical component of the plasma transfer velocity due to electromagnetic drift during August 5–6, 2011 and November 13 – 15, 2012 magnetic storms were presented. Confirmed that has a penetration of electric fields from magnetospheric origin in the mid-latitude ionosphere during strong geomagnetic disturbances. For the considered disturbed periods the neutral wind parameters were calculated using Kharkov incoherent scatter radar data.

Keywords: ionosphere, geospace storm, zonal electric field, plasma drift.

Introduction. It is well known that in quiet conditions the contribution of magnetospheric sources in electric fields and currents in the middle and low latitudes is fairly small. As the presented in [1 – 4], the results of experimental studies and theoretical calculations, the magnitude of the electric field in the mid-latitude ionosphere without geomagnetic disturbances does not exceed several mV/m. At altitudes of the ionospheric F2-peak the plasma drift caused by these fields is small compared to the transport processes of charged particles due to ambipolar diffusion and neutral winds. During strong geomagnetic disturbances has penetration of electric fields at the altitudes of the mid-latitude ionosphere and, consequently, increasing the plasma velocity in crossed electric and magnetic fields. It should be noted that the transfer of the plasma due to the electromagnetic drift during geomagnetic storms have a significant impact on the altitudinal distribution of the parameters of the mid-latitude ionosphere.

The aim of this work is to calculate the parameters of the zonal electric field in the ionosphere over Kharkov (Ukraine), as well as modeling the transport velocity variations due to the electromagnetic plasma drift and neutral wind during August 5 – 6, 2011 and November 13 – 15, 2012 magnetic storms.

The observation means. For modeling of the neutral wind parameter variations were used the Kharkov incoherent scatter radar (ISR) (geographic coordinates: 49,6º N, 36,3º E; geomagnetic coordinates: 45,7º, 117,8º) data. At present time the Kharkov ISR is the only reliable and most informative data source of the geospace plasma state at the mid-latitudes of Central Europe.

Radar allows measuring with high accuracy (usually error is 1 – 10%) and acceptable altitude resolution (10 – 100 km) the following ionospheric parameters:

electron density N, electron T_e and ion T_i temperatures, a vertical component of the plasma drift velocity v_z, and ion composition. The investigated altitude range is 100 – 1500 km.

The general information about magnetic storms parameters. *The magnetic storm on August 5 – 6, 2011*. Super-strong magnetic storm (MS) began on August 5, 2011 at 19:03 UT. The K_p index of geomagnetic activity during the MS main phase reached magnitude 8 – and D_{st} = –113 nT. The solar wind (SW) velocity during the main phase ranged 570 – 620 km/s, the SW particle temperature reached a value $6{,}4 \cdot 10^5$ K, the density of SW particles $N_{sw} \approx 1{,}9 \cdot 10^7$ m^{-3}. The value of the interplanetary magnetic field (IMF) B_z-component was –(15–18) nT, and the IMF magnetic induction by modulus was 25 – 27 nT. The auroral activity index $AE_{max} \approx 1740$ nT. The value of the Akasofu function $\varepsilon \approx 37$ GJ/s.

The magnetic storm on November 13 – 15, 2012. Geomagnetic storm began on November 13 at 15:00 UT. The main phase of the magnetic storm took place from 18:00 UT on November 13 to 06:00 UT on November 14. The extreme values of the geomagnetic activity indices during the MS were: AE_{max} = 1009 nT, $K_{p\,max}$ = 6+, D_{st} = –108 nT. The value of the IMF B_z-component was –(17 – 18) nT. The value of the Akasofu function was ~26–30 GJ/s.

Initial theoretical relations. As is known, without perturbation the electric fields effects in the mid-latitudes can be neglected. However, during strong geomagnetic storms have amplification of electric fields due to the magnetospheric convection, which significantly affects on dynamics of the mid-latitude ionosphere. During disturbed conditions in the mid-latitudes, and neglecting the effects of the geomagnetic field declination the main contribution to the vertical transport of plasma makes zonal electric field. Electric field directed to the east, causing the plasma drift upwards and field directed to the west – the transfer of ionospheric plasma down. We estimate the value of the zonal component of the electric field, as well as the contribution of the vertical component of plasma motion due to the electromagnetic drift in the dynamic mode of the ionosphere during magnetic storms on August 5 – 6, 2011 and on November 13 – 15, 2012.

As shown by the calculations presented in [5], there is a correlation between AE index and the values of the zonal component of the electric field E_y. In this case, the electric fields of magnetospheric origin and geomagnetic plasma heating are the main sources of dynamic processes in the ionosphere in mid-latitudes during strong geomagnetic disturbances.

To calculate E_y use the empirical relation between the magnitude of the electric field and auroral activity index, given in [5]:

$$E_y = (0{,}55 - 0{,}01AE) \cdot 10^{-3},$$

where AE – auroral activity index (in nT).

Expression to calculate the velocity of plasma transport due to electromagnetic drift neglecting effects declination has the form [6]

$$v_{EB} \approx (E_y/B)\cos I,$$

where B – the geomagnetic field modulus, I – the geomagnetic field inclination (for Kharkov city $I = 66{,}85^{\circ}$).

In mid-latitudes the drag wind velocity vertical component of ions due meridional component of the velocity of the neutral gas horizontal motion. Neutral wind directed toward the equator causes the plasma upward along magnetic field lines, and the wind, having the direction of the pole down motion of the plasma along the geomagnetic field lines [6].

Expression for calculating the meridional component of the neutral wind velocity v_{nx} neglecting the effects of the geomagnetic field decline has the form [6]:

$$v_{nx} = (v_z - v_{dz} - v_{EB})/(\sin I \cos I),$$

$$v_{dz} = -D_a \sin^2 I \left(\frac{1}{H_p} + \frac{1}{N}\frac{\partial N}{\partial z} + \frac{1}{T_p}\frac{\partial T_p}{\partial z} \right).$$

Here v_z – the vertical component of the plasma velocity (Kharkov ISR data), v_{dz} – the vertical component of the plasma transport velocity due to ambipolar diffusion, D_a – ambipolar diffusion coefficient, $H_p = kT_p/mg$ – the plasma scale height, k – Boltzmann constant, $T_p = T_e + T_i$ – the plasma temperature, T_e and T_i – the electron and ion temperatures (Kharkov ISR data), m – the oxygen ion mass, ν_{in} – the total ion collision frequencies with the major components of the neutral gas, g – the free fall acceleration, N – the oxygen ions density (Kharkov ISR data), z – the altitude, v_{EB} – the velocity of plasma transport due to electromagnetic drift.

Calculation results. Figures 1 and 2 shows the temporal variations of the zonal component of the electric field in the mid-latitude ionosphere at the altitude of 300 km during August 5 – 6, 2011 and November 13 – 15, 2012 magnetic storms.

The calculations show that the value of E_y reached –17 mV/m during the main phase of the MS on August 5 – 6, 2011. Whereas in quiet conditions, the magnitude of the zonal component of the electric field does not exceed –5 mV/m. During the November 13 – 15, 2012 MS the value of the electric field zonal component was –9,5 mV/m. In quiet conditions, the value of E_y does not exceed units of mV/m.

In general, the results agree well with the results obtained by other authors [1, 3, 6].

Figures 3 and 4 shows the calculation results of the temporal variations of the plasma velocity vertical component due to the electromagnetic drift during the considered magnetic storms and quite conditions at altitude of 300 km.

In the main phase of August 5 – 6, 2011 magnetic storm the v_{EB} velocity reached values of –150 m/s, while the magnetically quiet conditions, plasma transport due to electromagnetic drift practically absent. For November 13 – 15, 2012 magnetic storm obtained that the v_{EB} velocity reached its peak shortly after the beginning of the magnetic storm and equaled –85 m/s.

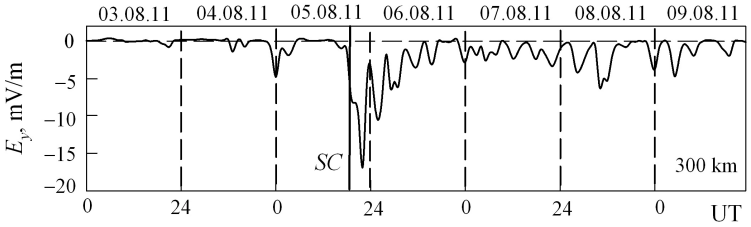

Fig. 1 – The temporal variations of the zonal component of the electric field during August 5 – 6, 2011 magnetic storm

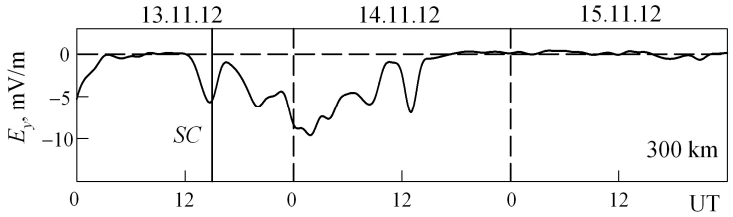

Fig. 2 – The temporal variations of the zonal component of the electric field during November 13 – 15, 2012 magnetic storm

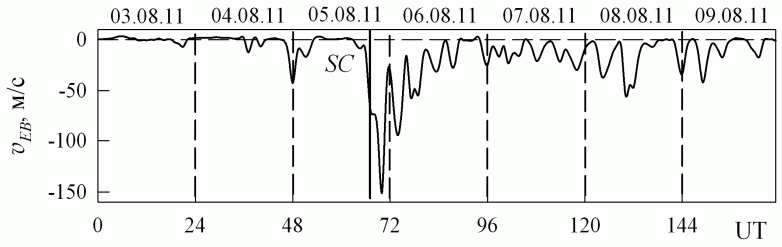

Fig. 3 – The temporal variations of the plasma velocity vertical component due to the electromagnetic drift during the magnetic storm on August 5 – 6, 2011

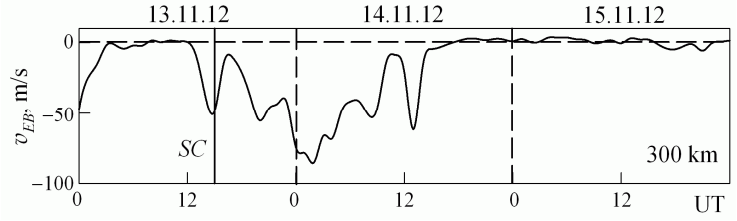

Fig. 4 – The temporal variations of the plasma velocity vertical component due to the electromagnetic drift during the magnetic storm on November 13 – 15, 2012

Figures 5 and 6 shows the temporal variation of the meridional component of the neutral wind during August 5 – 6, 2011 and November 13 – 15, 2012 magnetic storms. Calculations showed that in quiet conditions v_{nx} velocity ranges from 0 to –150 m/s. The highest rate of v_{nx}, as shown by calculations, reaching a value of 350 m/s on August 6, 2011 and 150 m/s on November 14, 2012. This behavior of v_{nx} indicates that the effects of the magnetic storm well manifested in the variations of the global thermospheric circulation parameters. Such behavior of the neutral wind velocity was also observed during September 25, 1998 magnetic storm [7]. The calculation results agree with the results of other authors presented in [8, 9].

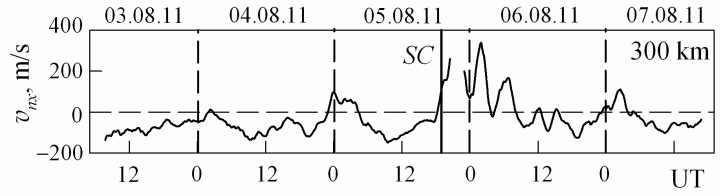

Fig. 5 – The variations of the neutral wind velocity meridional component during August 5 – 6, 2011 magnetic storm

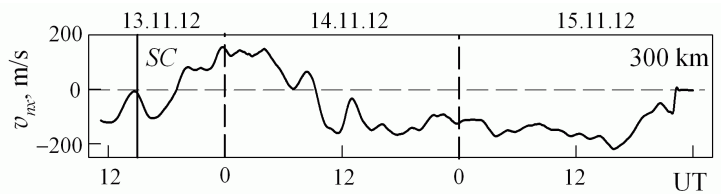

Fig. 6 – The variations of the neutral wind velocity meridional component during November 13 – 15, 2012 magnetic storm

Conclusion. 1) The calculations show that the magnitude of the electric field zonal component reaches the value of –17 and –9,5 mV/m in the main phase of

magnetic storms on August 5 – 6, 2011 and November 13 – 15, 2012, respectively. In quiet conditions, the E_y value does not exceed units of mV/m.

2) The effects of considered magnetic storms were well manifested in variations of dynamic processes in the ionosphere. The magnitude of the vertical component of the plasma velocity due to the electromagnetic drift reached values of –150 and –85 m/s during magnetic storms on August 5 – 6, 2011 and November 13 – 15, 2012, respectively. In undisturbed conditions plasma transport due to electromagnetic drift was negligible.

3) The effects of magnetic storms were well manifested in the variations of the global thermospheric circulation. During magnetic storms occurred strengthening the neutral wind, toward the poles. The calculations show that the neutral wind velocity reached values 350 and 150 m/s during magnetic storms on August 5 – 6, 2011 and November 13 – 15, 2012, respectively.

References: 1. *Blanc M., Amayenc P., Bauer P., Taieb C.* Electric field induced from the French incoherent scatter facilities // J. Geophys. Res. – 1977. – Vol. 82, 1. – P. 87-97. **2.** *Blanc M., Amayenc P.* Seasonal variations of the ionospheric *E×B* drift above Saint-Santin on quite days // J. Geophys. Res. – 1979. – Vol. 84, A6. – P. 2691-2704. **3.** *Ogawa T., Tanaka Y., Huzita A., Yasuhara M.* Horizontal electric fields in the middle latitude // Planet. Space Sci. – 1975. – Vol. 23. – P. 825-830. **4.** *Richmond A.D., Blanc M., Emery B.A., Wand R.H., Fejer B.G., Woodman R.F., Ganguly S., Amayenc P., Behnke R.A., Calderon C., Evans J.V.* An empirical model of quite-day ionospheric electric fields at middle and low latitudes // J. Geophys. Res. – 1980. – Vol. 85, A9. – P. 4658-4664. **5.** *Sergeenko N.P.* Estimates of electric fields during ionospheric disturbances // Ionospheric forecasting. – Moscow: Nauka, 1982, p. 91-96, (in Russian). **6.** *Bryunelli B.E., Namgaladze A.A.* Physics of the Ionosphere – Moscow: Nauka, 1988, 528 p. (in Russian). **7.** *Grigorenko E.I., Lazorenko S.V., Taran V.I., Chernogor L.F.* Wave disturbances in the ionosphere accompanied the solar flare and the strongest magnetic storm of September 25, 1998 // Geomagnetism and Aeronomy. – 2003. – Vol. 43, 6. – P. 718-735. **8.** *Richards P.G., Torr D.G., Buonsanto M.J., Sipler D.P.* Ionospheric Effects of the March 1990 Magnetic Storm: Comparison of Theory and Measurement // J. Geophys. Res. – 1994. – Vol. 99, A12. – P. 23,359–23,365. **9.** *Buonsanto M.J.* Millstone Hill Incoherent Scatter F Region Observations During the Disturbances of June 1991 // J. Geophys. Res. –1995. – Vol. 100, A4. – P. 5743-5755.

Received 14.05.2014

UDC 550.388

Variations of the electric field zonal component, the vertical component of the plasma drift and neutral wind velocities in ionosphere over Kharkov (Ukraine) during August 5 – 6, 2011 and November 13 – 15, 2012 magnetic storms / I.F. Domnin, C. La Hoz, M.V. Lyashenko // Bulletin of NTU "KhPI". Series: Radiophysics and ionosphere. - Kharkiv: NTU "KhPI", 2014. – No. 47 (1089). – P. 15-21. Ref.: 9 titles.

Представлено результати моделювання варіацій зонального електричного поля та вертикальної компоненти швидкості переносу плазми за рахунок електромагнітного дрейфу під час магнітних бур 5 – 6 серпня 2011 р. та 13 – 15 листопада 2012 р. Підтверджено, що під час сильних геомагнітних збурень має місце проникнення електричних полів магнітосферного походження у середньоширотну іоносферу. Для розглянутих збурених періодів розраховано параметри нейтрального вітру з використанням даних Харківського радара некогерентного розсіяння.

Ключові слова: іоносфера, геокосмічна буря, зональне електричне поле, дрейф плазми.

Представлены результаты моделирования вариаций зонального электрического поля и вертикальной компоненты скорости переноса плазмы за счет электромагнитного дрейфа во время магнитных бурь 5 – 6 августа 2011 г. и 13 – 15 ноября 2012 г. Подтверждено, что во время сильных геомагнитных возмущений имеет место проникновение электрических полей магнитосферного происхождения в среднеширотную ионосферу. Для рассмотренных возмущенных периодов рассчитаны параметры нейтрального ветра с использование данных Харьковского радара некогерентного рассеяния.

Ключевые слова: ионосфера, геокосмическая буря, зональное электрическое поле, дрейф плазмы.

UDC 621.311:621.314

I.F. DOMNIN, D.Sc., Prof., director, Institute of Ionosphere, Kharkiv;
O.O. LEVON, PhD student, NTU "KhPI";
V.V. VARVYANSKAYA, senior lecturer, NTU "KhPI"

FUZZY LOGIC BASED CONTROL SYSTEM OF CONVERTER FOR POWERFUL SOUNDING PULSES GENERATOR

This thesis deals with the design of control system for powerful sounding pulses generator using Fuzzy Logic based decision structure and implementation using the 68HC12 microcontroller. Some practical cases with Fuzzy Tech are presented to check the proposed control performance. Conclusions of obtained results are presented.

Key words: fuzzy-controller, microprocessor realization, fuzzification, membership functions.

The purpose of article is to implement microprocessor realization of level higher harmonics fuzzy-controller, which determines the deviation from the nominal value of the selected parameter and leads it to the established norms.

Introduction. Fuzzy logic implementation is becoming increasingly important, and finding applications in diverse areas of current interest, such as control, pattern recognition, robotics, and other decision making applications. Fuzzy decision process offer a significant advantage over crisp decision process which is the ability to process different levels of truth instead of only 1 or O levels. Fuzzy Logic does not require precise inputs, it is inherently robust, and can process any reasonable number of inputs but system complexity increases rapidly with more inputs and outputs. Distributed processors would probably be easier to implement. Simple, plain-language IF X AND Y THEN Z rules are used to describe the desired system response in terms of linguistic variables rather than mathematical formulas. The number of these is dependent on the number of inputs, outputs, and the designer's control response goals. The new Motorola 68HC12 MCU has an embedded fuzzy logic instruction set. Using this instruction set, it can be implemented complex fuzzy logic systems using only a few hundred bytes of ROM that cycle compute in less than a millisecond.

In [1, 2] describes a method for designing a fuzzy controller in the control system of compensation inactive components of the total power device. Fuzzy controller implements a fuzzy inference procedure and makes it possible to obtain the required values of regulated and controlled process parameters, namely controls the amplitude level of selected harmonic current mains *k*i and brings it to the required value. This can be achieved by varying the voltage on the capacitor of the inverter Uc by control signals *delta*_Uc of additional output control circuit [1]. In the proposed control system based on fuzzy logic fuzzy controller input signals and output control actions are considered as linguistic variables, qualitatively characterized by the term-sets.

Each term is considered as a fuzzy set, and formalized using the membership function. Formation of the control action performed on the basis of linguistic control rules that establish means of natural language communication between the states of a dynamic system and manage the impact of the control system of the converter [2].

Hardware realization of fuzzy microcontroller fuzzy-controller can be done using special-purpose microcontrollers. As a special-purpose microcontroller with hardware support for fuzzy logic was selected microcontroller 68HC12 from Motorola.

The 68HC12 is a high-speed, 16-bit processing unit that has a programming model identical to that of the industry standard M68HC11 CPU. The 68HC12 instruction set is a proper superset of the M68HC11 instruction set, and M68HC11 source code is accepted by 68HC12 assemblers with no changes. The 68HC12 has full 16-bit data paths and can perform arithmetic operations up to 20 bits wide for high-speed math. An instruction queue buffers program information so the CPU has immediate access to at least three bytes of machine code at the start of every instruction.

A fuzzy inference kernel for the 68HC12 requires one-fifth as much code space, and executes fifteen times faster than a comparable kernel implemented on a typical midrange microcontroller. The 68HC12 includes four instructions that perform specific fuzzy logic tasks. In addition, several other instructions are especially useful in fuzzy logic programs. The overall C-friendliness of the instruction set also aids development of efficient fuzzy logic programs.

The four fuzzy logic instructions are MEM, which evaluates trapezoidal membership functions; REV and REVW, which perform unweighted or weighted MIN-MAX rule evaluation; and WAV, which performs weighted average defuzzification on singleton output membership functions.

Other instructions that are useful for custom fuzzy logic programs include MiNA, EMIND, MAXM, EMAXM, TBL, ETBL, and EMACS. For higher resolution fuzzy programs, the fast extended precision math instructions in the 68HC12 are also beneficial. Flexible indexed addressing modes help simplify access to fuzzy logic data structures stored as lists or tabular data structures in memory. A microcontroller based fuzzy logic control system has two parts. The first part is a fuzzy inference kernel which is executed periodically to determine system out-puts based on current system inputs. The second part of the system is a knowledge base which contains membership functions and rules.

The knowledge base can be developed by an application expert without any microcontroller programming experience. Membership functions are simply expressions of the expert's understanding of the linguistic terms that describe the system to be controlled. Rules are ordinary language statements that describe the actions a human expert would take to solve the application problem.

Rules and membership functions cm be reduced to relatively simple data structures (the knowledge base) stored in nonvolatile memory. A fuzzy inference kernel cm be written by a programmer who does not know how the application system works. The only thing the programmer needs to do with knowledge base information is store it in the memory locations used by the kernel.

The design process begins by associating fuzzy sets with the input and output variables. These fuzzy sets are described by membership function of the type shown in figure below. These fuzzy set values are labeled. The shape of the membership functions are, in general, trapezoids that may have no top (triangles) or may have no vertical sides. A functional diagram of a fuzzy-controller is shown in the following figure.

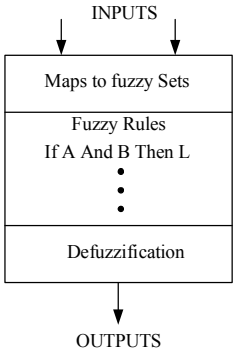

Fig. 1 – Functional Diagram of a Fuzzy Controller

The fuzzy controller shown above consists of three parts. The fuzzification of inputs. The processing of rules, and the defuzzification of the output. The inputs to a fuzzy controller are assigned to the fuzzy variables with a degree of membership given by the membership functions. After applying al1 of the fuzzy rules to a given set of input variables, the output will belong to more than one fuzzy set with different weights. The weighted output fuzzy sets are combined in a manner to be described below and then a centroid defuzzification process is used to obtain a single crisp output value.

The system structure identifies the fuzzy logic inference flow from the input variables to the output variables. The fuzzification in the input interfaces translates analog inputs into fuzzy values. The fuzzy inference takes place in rule blocks which contain the linguistic control rules. The output of these rule blocks are linguistic variables. The defuzzification in the output interfaces translates them into analog variables. The following figure shows the whole structure of this fuzzy system including input interfaces, rule blocks and output interfaces. The connecting 1ines symbolize the data flow. A Structure of the Fuzzy Logic System in Fuzzy Tech is shown in Fig.2

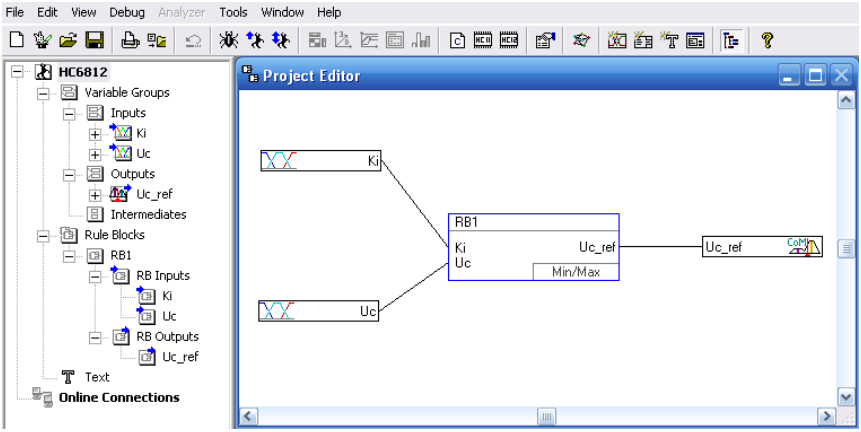

Fig. 2 – Structure of the Fuzzy Logic System

The appearance of interface Fuzzy Tech project in debug mode is shown in Fig. 3. View graphic table editor of fuzzy inference system is shown in Fig. 4.

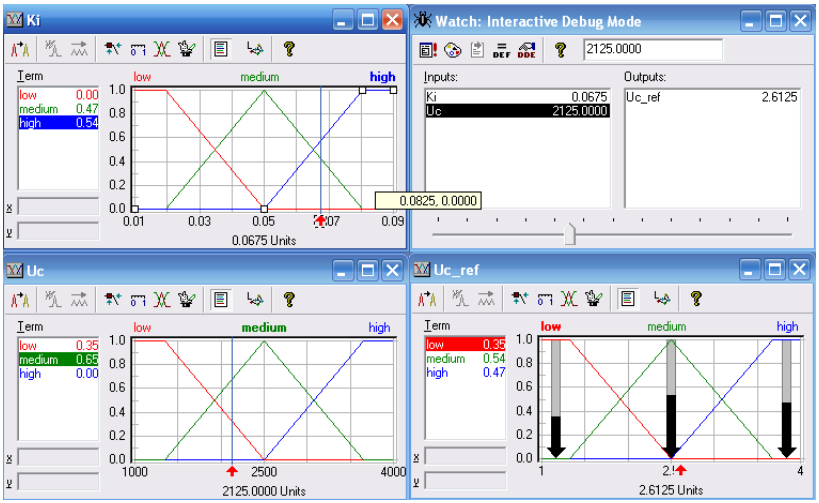

Fig. 3 – The appearance of interface Fuzzy Tech project

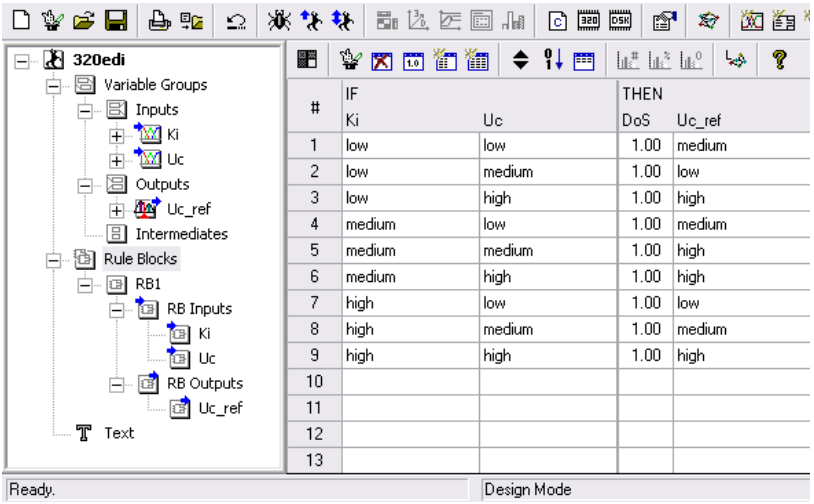

#	IF Ki	Uc	THEN DoS	Uc_ref
1	low	low	1.00	medium
2	low	medium	1.00	low
3	low	high	1.00	high
4	medium	low	1.00	medium
5	medium	medium	1.00	high
6	medium	high	1.00	high
7	high	low	1.00	low
8	high	medium	1.00	medium
9	high	high	1.00	high
10				
11				
12				
13				

Fig. 4 – Table editor window block rules Fuzzy Tech fuzzy inference system

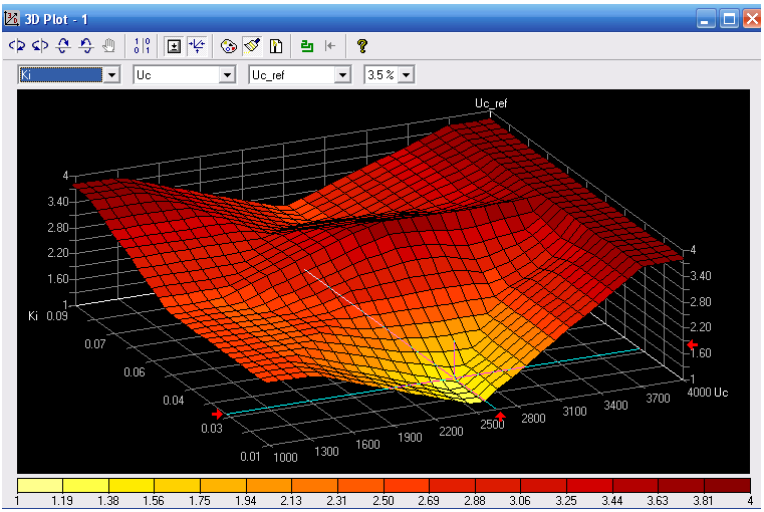

Fig. 5 – Three-dimensional surface of the fuzzy inference system

Software implementation of fuzzy-control loop mains current harmonics in Assembler and C language is realized in Fuzzy Tech code editor and based on fuzzy logic microcontroller Motorola 68HC12.

Summary and conclusion. This article is concerned with the design techniques for fuzzy logic and its implementation in the control system of converter for powerful sounding pulses generator. Due to the new series of microcontrollers 68HC12, which has dedicated instructions for programming and implementation of fuzzy logic it has become easy to write a smaller code which can overcome the memory constraints of earlier versions of microcontrollers. The Fuzzy Tech design software has made it very easy to design a control system using fuzzy logic. This design approach using fuzzy logic is practically feasible and many other applications are open venues for further research and future work.

References: 1. *Domnin I.F., Levon O.O.* Multiloop control system of filter-device // Technical electrodynamics. Thematic issue "Power electronics and energy efficiency". – 2010. – Part 2. – P. 44-47 (in Russian). **2.** *Levon O.O.* Fuzzy control device compensation of total power inactive components // Technical electrodynamics. Thematic issue "Power electronics and energy efficiency". – 2011 .– Part 1. – P. 184-188 (in Russian).

Received 19.05.2014

UDC 621.311:621.314

Fuzzy logic based control system of converter for powerful sounding pulses generator / I. F. Domnin, O. O. Levon, V. V. Varvyanskaya // Bulletin of NTU "KhPI". Series: Radiophysics and ionosphere. – Kharkiv: NTU "KhPI", 2014. – No. 47 (1089). – P. 22-27. Ref.: 2 titles.

В статье описан вариант микропроцессорной реализации fuzzy-регулятора системы управления двухканальным компенсатором неактивных составляющих полной мощности для формирователя мощных зондирующих импульсов. Представлены результаты проектирования системы нечеткого логического вывода в программе Fuzzy Tech.

Ключевые слова: нечеткий регулятор, микропроцессорная реализация, фаззификация, функции принадлежнности.

У статті описаний варіант мікропроцесорної реалізації fuzzy-регулятора системи керування двоканальним компенсатором неактивних складових повної потужності для формувача потужних зондуючих імпульсів. Представлені результати проектування системи нечіткого логічного виводу в програмі Fuzzy Tech.

Ключові слова: нечіткий регулятор, мікропроцесорна реалізація, фазифікація, функції приналежності.

UDC 550.388.1:551.510.535:621.396

I.F. DOMNIN, D.Sc., Prof., director, Institute of Ionosphere, Kharkiv;
Ya.M. CHEPURNYY, chief engineer, Institute of Ionosphere;
L.Ya. EMELYANOV, PhD, head of department, Institute of Ionosphere;
S.V. CHERNYAEV, head of sector, Institute of Ionosphere;
A.F. KONONENKO, head of sector, Institute of Ionosphere;
D.V. KOTOV, PhD, research scientist, Institute of Ionosphere;
O.V. BOGOMAZ, research scientist, Institute of Ionosphere;
D.A. ISKRA, junior research scientist, Institute of Ionosphere

KHARKIV INCOHERENT SCATTER FACILITY

The structure, parameters and operating modes of the incoherent scatter radar of the Institute of Ionosphere, Kharkiv are presented. Some results of the ionosphere research obtained by this facility are shown.

Keywords: incoherent scatter radar, ionosonde, ionospheric observatory, ionospheric parameters, incoherent scatter method.

Introduction. Incoherent scattering (IS) is the most informative technique of radio-physical exploration of near-Earth space. It allows measuring a wide set of ionospheric parameters at the same time and in a large range of heights. IS radars are used for this technique realization. These radars are complex technical systems, which include powerful transmitters, large size antennas, high sensitivity receivers and high-performance computer data processing systems. Currently there are 11 active IS radars in the world. One of them is the IS radar of Institute of Ionosphere of National Academy of Sciences of Ukraine and Ministry of Education and Science of Ukraine.

Purpose of the article is to present the current state of the IS equipment in the Ionosphere observatory of Institute of Ionosphere, to show radar potential and to introduce techniques for the parameters of the ionosphere measurement and ionospheric data processing.

Facility. Ionospheric Observatory of the Institute of Ionosphere is located in 50 km to the south-east from Kharkiv city (49.676º N, 36.292º E; InvDip=45.74º). This location is best one to carry out studies of the longitude and latitude effects in the ionosphere together with radars in Millstone Hill (43° N, 71° W), Irkutsk (52° N, 104° E) and Tromsø (78° N, 19° E).

The Ionospheric Observatory facilities include the VHF IS radar equipped with the zenith parabolic Cassegrain antenna of 100 m diameter; the VHF IS radar equipped with the fully steerable parabolic antenna of 25 m diameter; ionosonde “Bazis” [1].

Radar with 100-m antenna was put into operation in the 1970s [1–3] and being modernized right along.

Radar allows to measure with high accuracy (usually error is 1–10 %) and acceptable altitude resolution (10–100 km) the following ionospheric parameters: electron density N_e, electron T_e and ion T_i temperatures, a vertical component of the plasma drift velocity V_z, and ion composition [1, 4]. The investigated altitude range is 100–1500 km.

At the present time, the main parameters of IS radar are as follows: the frequency is about 158 MHz, the effective aperture of the 100-m antenna is about 3700 m^2, the two way half-power antenna beam width is close to 1.3°, the peak pulse power of the transmitter is up to 3.6 MW and the average power is 100 kW, pulse repetition frequency is 24.4 Hz, and the polarization is circular or linear. The noise temperature of the receiver is 120 K and the receiver bandwidth is 11–19 kHz. The effective noise temperature of system is 470–980 K.

Block diagram of IS radar is shown on Fig. 1.

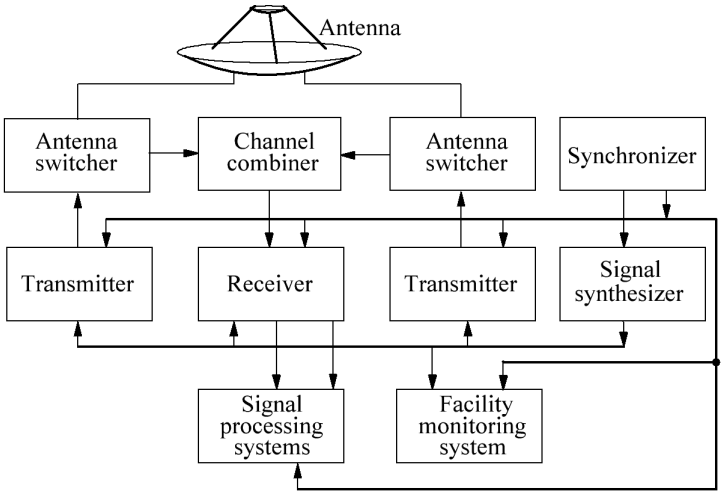

Fig. 1 – Block diagram of IS radar of Institute of Ionosphere

Antenna (Fig. 2) allows to transmit and receive circular and linear polarized signals due to the presence of two orthogonal dipoles [5]. The antenna pattern was measured using the reflections of the sounding signal from spacecrafts. The antenna pattern is shown in Fig. 3 [6].

Feeder circuit is based on dual-channel scheme. It is built on 1330×660 mm rectangular waveguide section and partially on 160/70 mm rigid coaxial lines.

Feeder length in each of the channels is more than 200 m. It consists of coaxial and waveguide sections, high power waveguide-coaxial transitions, waveguide expansion compensators (thermal expansion compensators), ball switches, coaxial and waveguide directional couplers. Isolation between radio receiving and transmitting devices is provided in each of the two channels of the waveguide feeder line by using balanced antenna waveguide switches performed on gas-filled surge arrester.

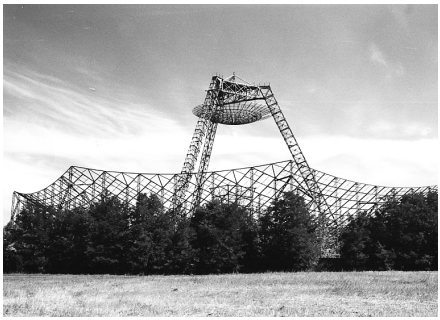

Fig. 2 – The 100-m-diameter parabolic antenna

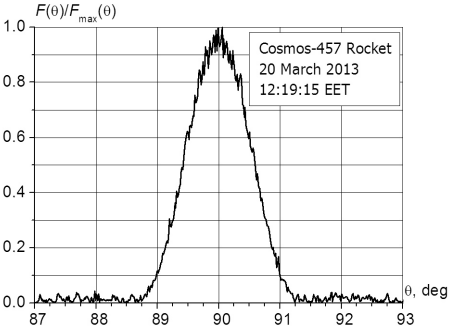

Fig. 3 – Cross-section of the 100-m antenna pattern in the plane of φ = 203°, measured by reflections from Cosmos-457 Rocket

Transmitter consists of two channels of high-power amplifiers operating with an external excitation by common signal synthesizer [7]. Peak pulse power of each channel is up to 1.5 MW. Usually it is about 1 MW. Transmitted pulse duration is defined by measurement mode. The total pulse length does not exceed 800 μs. Pulse repetition frequency is 24.4 Hz.

To transmit signals with linear or circular polarization, the desired phase difference between the signals of two channels (either 0 or 90 degrees, respectively) is set. Block diagram of the transmitter is shown in Fig. 4. Each channel consists of a preamplifier, power amplifier, system of the formation of the pulse anode voltages (modulator and high voltage rectifier), and the power supply and cooling equipment.

Driving signal with power of about 130 mW comes from the synthesizer to inputs of the preamplifiers. These preamplifiers are made as multistage scheme with metal-ceramic electron tubes. Output three-stage power amplifiers are made with powerful triodes cooled distilled water. Modulator is a pulse voltage source for these stages. It consists of a multisection LC charge integrator with full discharge of energy via the pulse transformer. All elements of the modulator are matched so as to minimize the transmitter noise level in the interpulse periods. It is

possible to operate using four transmitter channels with the pairwise summation of their signals via coaxial combiner bridges. In this case, a total peak power reaches up to 3.5 MW.

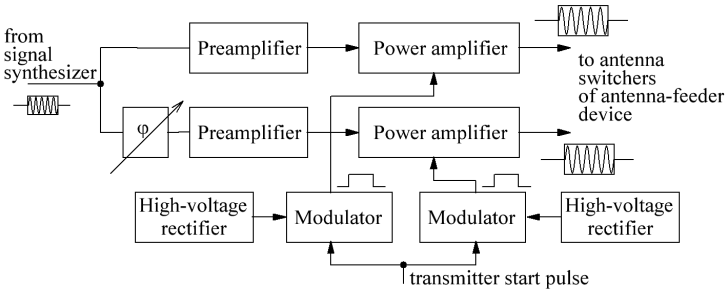

Fig. 4 – Block diagram of the IS radar transmitter

Radio receiver of IS radar is a multi-channel receiver with a triple frequency transformation [8]. The spectrum of the received signal is sequentially translated from the carrier frequency (158 MHz) to a low frequency region where correlation processing is carried out. The receiving equipment is located near the outputs of antenna-feeder system in order to minimize signal power losses at the receiver input and reduce interference.

Block diagram of receiver for the reception of two signals spaced apart in frequency is shown in Fig. 5.

A system of the received signal polarization choice (consisting of a phase shifter and coaxial combiner of the signals from two feeder line channels), a circulator for a better match of input resistance to the feeder line impedance (75 ohm), blank switch device (to close the receiver during pulsing), and a low noise transistor amplifier VHF1 are at the receiver input. Receiver blanking is provided using two high-speed electronic switches of radio-frequency path (with p-i-n diodes) to avoid overload of the receiver and analog-to-digital converters (ADC) of processing devices. The amplifier VHF1 provides sufficient for VHF radio receiver sensitivity: the receiver noise factor is equal to 1.4. A number of pairs of quadrature signals in outputs of receiver are formed (for correlation processing) by synchronous detection and low-pass filtering. The receiver bandwidth depends on the low-pass filters. Usually the 7th-order Cauer filters with the bandwidth of ΔF=9.5 kHz and ΔF=5.5 kHz, as well as the third-order Gauss filters with ΔF=6.0 kHz are used. Unevenness of the flat part of amplitude-frequency characteristic of these filters does not exceed 0.18 dB.

The receiver heterodyne signals are formed from signals of synthesizer to ensure coherence of IS radar systems. Due to this we are able to detect small (relative to width of the IS signal spectrum) Doppler frequency shifts, which are used for determining the radial velocity of the ionospheric plasma.

A first heterodyne signal with the frequency f_{g1} is formed from the synthesizer signal with frequency ($f_{g1}/8$) using frequency multiplier. Since the carrier frequency of the sounding signal is formed by the synthesizer according to the expression $f_0=((f_{g1}/8)–2f_\beta)\cdot 8$, the first intermediate frequency (IF) is $f_{if1}=f_{g1}–f_0=16f_\beta$. Thus, it is known accurate to a Doppler shift of the IS signal spectrum due to the plasma motion. Second heterodyne signal is formed according to the expression: $f_{g2}=16f_\beta+f_{sg}$. Third (synchronous) heterodyne signal is formed by quartz crystal filtering of the synthesizer signal with the frequency f_{sg}. Therefore the second intermediate frequency f_{if2} coincides with the frequency f_{sg} of the synchronous heterodyne (up to Doppler shift). As a result of the synchronous detection, the signal is translated to the zero frequency with Doppler shift. Thus, the coherent radar system operation is achieved and the possibility of the ionospheric plasma drift velocity measurement is provided.

Signal synthesizer system is designed to form the signals required for operation of the transmitter, receiver and facility monitoring system. In particular, the driving signal for transmitter and heterodyne signals for receiver are formed. All signals are synthesized from the highly stable reference oscillator signal with frequency of 5 MHz.

Synchronization system is intended to ensure synchronous operating of the equipment. It produces a signal of start of transmitting, a strobe pulse for synchronizer to form driving signal for transmitter, a blank pulse to close the receiver input during transmitting, and other control signals for radar systems.

Several independently working signal processing systems are used in the Kharkiv IS radar. All systems work in one local area network.

Two dual-channel correlators based on the TMS320 family signal processors operate since 1996 [9]. Each correlator runs the own program and allows to obtain unique data. For example, one of them is intended to calculate autocorrelation functions (ACFs) for the electron density, ion composition, ion and electron temperatures estimation. At the same time another correlator calculates quadrature ACFs for the plasma velocity estimation.

Four-channel programmable correlator consists of four 10-bit precise high-speed successive approximation ADC and the general-purpose personal computer (PC) [10]. It was put into operation in 2003. In contrast to correlators based on the TMS320 family signal processors, the four-channel programmable correlator

allows to obtain a full set of the IS signal ACFs for all ionospheric plasma parameters estimation.

Since 2012, a new data processing system based on E20-10 ADC module operates in structure of the IS facility. It provides continuous acquisition of 16-bit data with processing rate up to 10 MHz and their transfer to PC using USB 2.0 interface. The software developed for system maintenance is an application for Microsoft Windows operating system. It sets up E20-10 appropriate mode, records signal data for every radar scan (1464 scans are response to 1 min session of measurement), calculates IS signal ACFs, and visualizes obtained data. High-speed interface and a high-performance PC allowed significantly increase sampling rate (currently up to 6 times) [11].

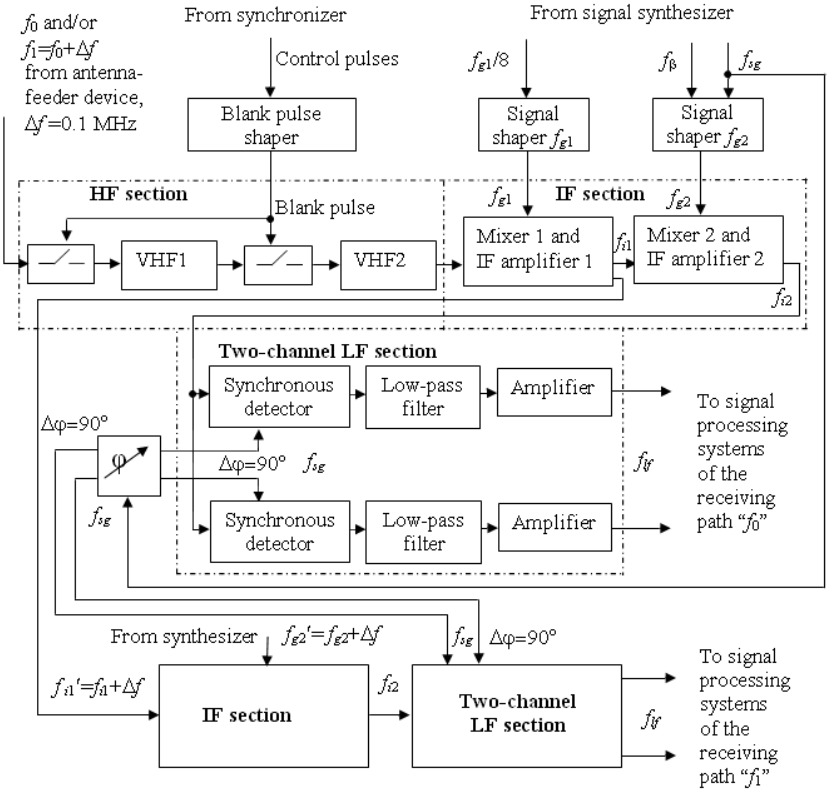

Fig. 5 – Block diagram of the IS radar receiver

Fig. 6 – The fully steerable 25-m-diameter antenna

Facility monitoring system is designed to test the radar operation. It produces a harmonic or random signal with characteristics similar to the IS signal. These signals are transmitted by the control antenna with orthogonal vibrators and received via 100-m antenna and feeder circuit to the receiver input.

Radar with a steerable 25-m antenna (Fig. 6) was put into operation in 1980s and has a similar structure of transmitter, receiver and feeder system [1, 3]. The effective aperture of the 25-m antenna is about 290 m^2, the two ways half-power antenna beam width is close to 5.1°. Radar is used to study the dynamics and wave disturbances of the ionosphere.

From time to time we work simultaneously using two radars (with zenith and steerable antennas). Because of this, it is possible to study the spatial structure of the ionosphere over Ukraine, to measure the full vector of the ionospheric plasma motion velocity, and to research in detail wave effects in the ionosphere.

Ionosonde "Bazis" allows to provide vertical, oblique and transionospheric pulse sounding of the ionosphere [12, 13]. Ionosonde is used independently to determine the basic parameters of the ionosphere (electron density, critical frequency, etc.) and in conjunction with the IS radar for binding measured value of the electron density at the maximum of ionization and normalized altitudinal profile of N_e. The ionosonde of Institute of Ionosphere can work in the international network of ionospheric stations, in particular, to observe the latitude and longitude effects in co-operation with the

ionosonde in Pruhonice (Czech Republic, 50.0° N, 14.6° E), Dourbes (Belgium, 50.1° N., 4.6° E), Moscow (Russia, 55.5° N, 37.3° E) [14–16].

Main technical characteristics of the ionosonde "Bazis" are: peak pulse power of transmitter is not less than 15 kW, operating frequency range in vertical sounding mode is 1–20 MHz, frequency sweeping law is linearly increasing one with a discrete step in the range of 1 to 100 kHz, a number of operating frequencies are 400, pulse repetition frequency is 100 Hz, pulse duration is 100 ms. Antennas are rhombic ones with vertical radiation. Receiving and transmitting antennas are identical and located orthogonally.

The main elements of the "Bazis" are transmitter, receiver, control unit and recording device with PC.

Operating modes. Kharkiv IS radar can operate in the following modes (Fig. 7) [2, 17]:

– Sounding with a pulse of about 800 μs length to measure the parameters of the upper ionosphere and the ionosphere at the altitudes near the peak of the ionospheric F layer with altitude resolution of about 120 km (polarization is circular to avoid Faraday fading of the IS signals).

– Sounding with a cyclic sequence of double pulses (65 or 135 μs length) with a variable delay between pulses from one period of sounding to another. Every delay is equal to the respective lag of measured correlation function. Polarization is circular. This mode is used for measurement of the ionospheric parameters at altitudes of 100–550 km with altitude resolution of about 10 or 20 km respectively. Space between the double pulses is filled by the signal with an offset carrier frequency (f_1=f_0+0.1 MHz) to ensure stable operation of the transmitter and to reduce error of the ionospheric plasma drift velocity measurement, as well as because of the transmitter specifics [18]. This mode was actively used during the peak of solar cycle 23 [19].

– Sounding with a signal of 135 μs length with linear polarization to determine the electron density using the Faraday effect [20].

Since 2006, the main mode of the IS radar operation is radio sounding of the ionosphere using composite two-frequency radio pulse, where the first element has a pulse length of about 650 μs (the carrier frequency f_0 = 158 MHz) and the second element has the pulse length of about 135 μs (the frequency f_1 = (158 + 0.1) MHz) [3, 21]. As a result of receiving and processing of the first signal element scattered by the ionosphere, the electron density, the electron and ion temperatures, the vertical component of the plasma velocity, and the ion composition are measured for the altitudes near the peak of the ionospheric F layer and in the upper ionosphere. The height resolution for the first pulse element is about 120 km. Return signal from the second pulse element allows to determine the altitude profile of the IS signal power at the altitudes of 100 to 550 km with the height resolution of 20 km to correct the altitude electron density profile. Polarization of both pulse elements is circular.

The 135 μs pulse element is transmitted and received with linear polarization by two orthogonal antenna vibrators in case of need to determine the electron density using the Faraday effect.

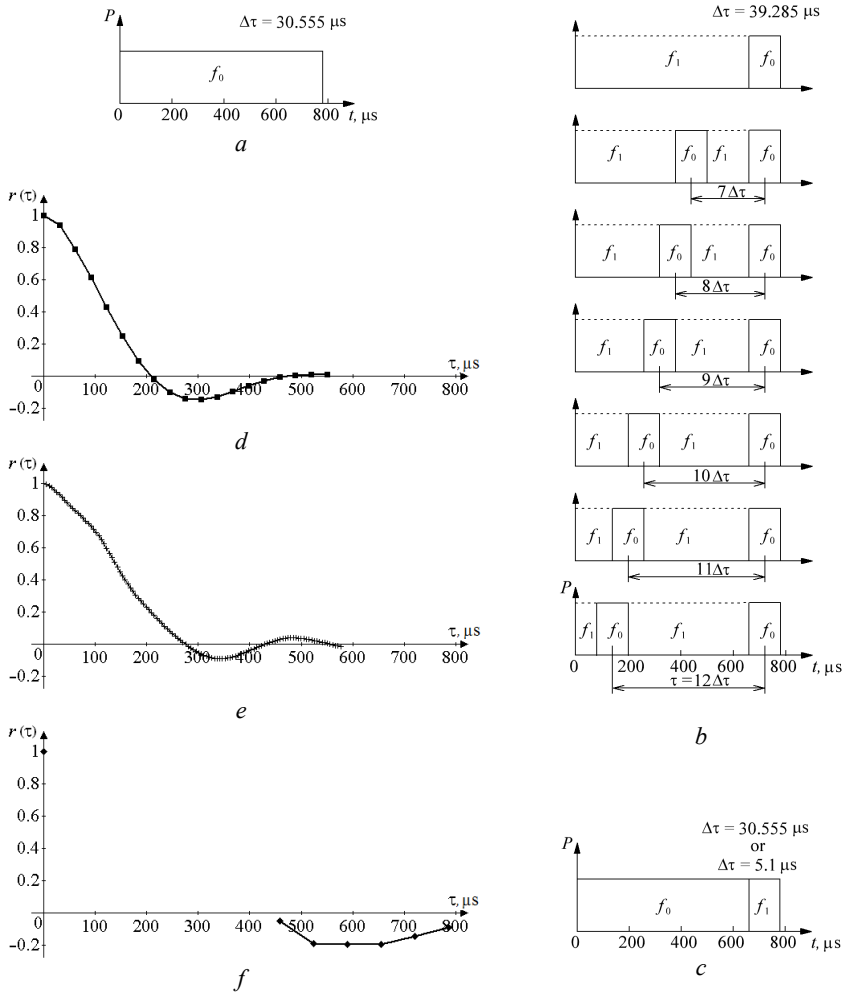

Fig. 7 – Diagrams of sounding signal for three main modes of Kharkiv IS radar: *a* – one-pulse mode, *b* – double-pulses mode, *c* – dual frequency sounding with long and short radio pulses. IS signal ACFs: *d* – lag step Δτ equals 30.555 μs, *e* – 5.1 μs, and *f* – 39.285 μs.

Processing techniques. Parameters of the ionospheric plasma for a number of discrete heights are determined as follows [4, 22]. For each signal delay, which is corresponding to height of the center of the scattering volume, ACFs of mixture of signal and noise are estimated using a variety of realizations. IS signal ACFs are calculated for several discrete delays as the difference between the measured mixture of signal and noise ACFs and noise ACFs averaged using a number of measurements at the end of scan where IS signal is negligible. Temperatures T_i and T_e are obtained using IS signal ACFs. Altitude N_e profile normalized to the peak of electron density is calculated using the obtained temperatures and the signal-to-noise ratio. Absolute values of N_e are determined by binding its normalized profile to the maximum value measured by the ionosonde. The ionospheric plasma velocity is determined using the measured IS signal ACFs quadrature components.

IS radar data processing software was developed in the Institute of Ionosphere. UPRISE (Unified Processing of the Results of Incoherent Scatter Experiments) package based on optimal techniques of IS radar data analysis includes programs for viewing the initial data, interference filtering, time integration, altitudinal data correction and ionospheric plasma parameters estimation [23].

Software development at the Institute is aimed to use of advanced networking technologies and databases [24, 25]. Thus, for example, a developed data processing system works on a remote server and uses the database of the radiophysical experiments. Its main task is to give information in text and graphics form about the data presented in the database. Information about size and quality of data is provided using a web interface to the system.

Some results of the ionosphere research. The research activity of the Institute of Ionosphere includes a broad spectrum of research topics devoted to the mid-latitude ionosphere. The observation of seasonal and diurnal variations in the electron density, ion and electron temperatures, plasma drift velocity, and hydrogen ions fraction during the winter and summer solstices, the vernal and autumnal equinoxes in the altitude range 200–1000 km is carried out [26]. The model of the mid-latitude ionosphere CERIM IION (Central Europe Regional Ionospheric Model) was developed using the Kharkiv IS radar data obtained over a period of more than two cycles of solar activity (from 1986 to 2011) [27]. Large variety of studies addressed different types of ionospheric perturbations, the ionospheric plasma dynamics in general [28, 29], and the wave disturbances in the ionosphere caused by the solar terminator [30], by the launches of rockets [31], and by the effect of high power HF radio transmission on the ionospheric plasma [32, 33]. The Institute also continues

to study the response of the ionosphere to geomagnetic storms [34–36] and solar eclipses [29, 37, 38]. A model of ion composition of the topside ionosphere over Kharkiv is currently under development [39, 40].

As an example, the altitude-time variations of ionospheric parameters in the quiet conditions (Fig. 8) and during magnetic storm (Fig. 9) are presented.

The scientific results are regularly presented at topical conferences, symposia and seminars also at many international forums. The Institute of Ionosphere coordinates its activity with foreign scientific institutions that are actively involved in ionospheric studies.

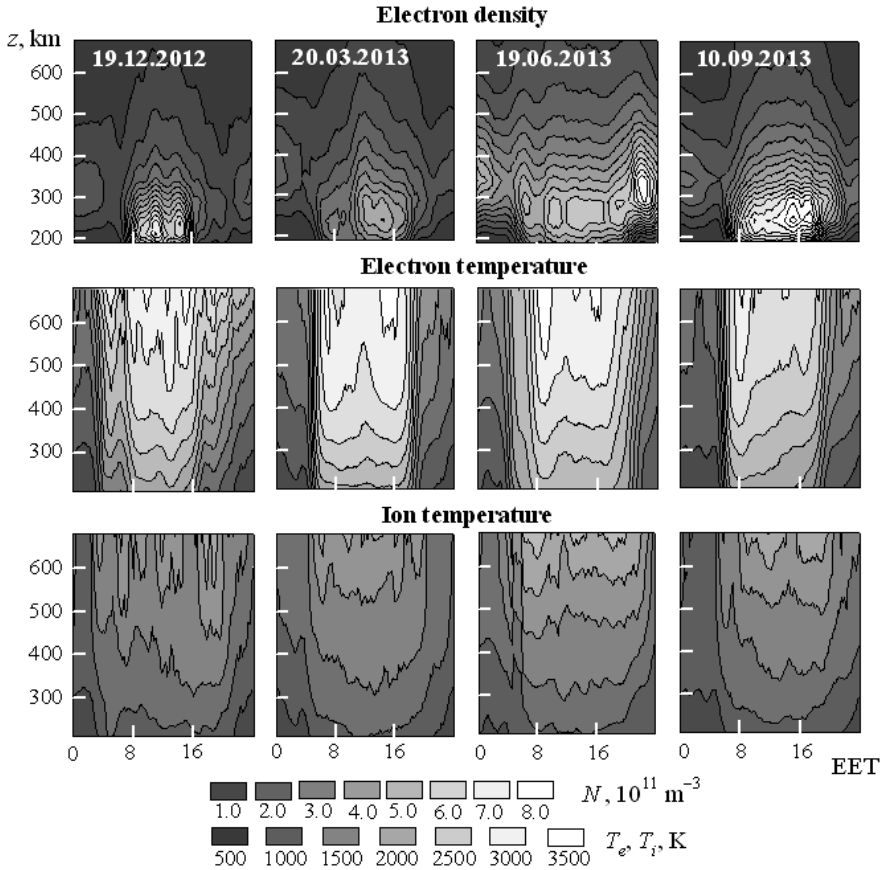

Fig. 8 – Altitude and temporal variations of electron density (top panel), electron (middle panel) and ion (bottom panel) temperatures for typical geophysical periods according to the Kharkiv incoherent scatter radar data

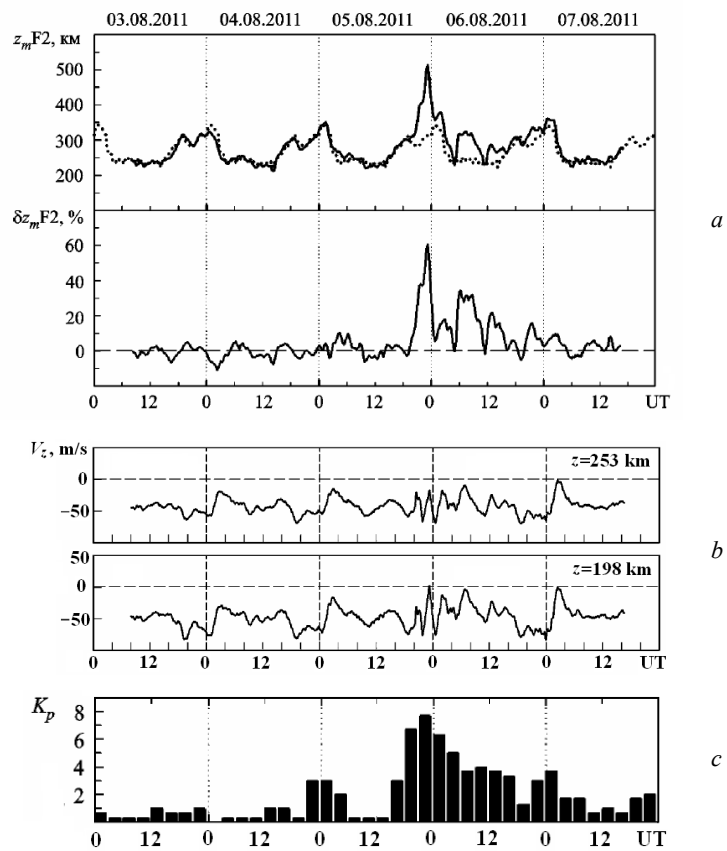

Fig. 9 – Temporal variations in z_mF2 height (upper panel) on 3–7 August 2011 (solid line) and its relative deviation δz_mF2 (lower panel) (*a*), the variations in the vertical component of the ionospheric plasma drift velocity V_z at altitudes 198 and 253 km (*b*), obtained by the IS Kharkiv radar, and distribution of geomagnetic index K_p (from http://www.swpc.noaa.gov/). The dashed line shows the temporal variations in z_mF2 obtained by averaging data of 3, 4 and 7 August 2011 when conditions were magnetically quiet

Conclusions.

– Kharkiv incoherent scatter facility is a powerful tool for study of the ionosphere. It is the only one in the middle latitudes of the Central European region and it is used to study the longitude and latitude effects in the ionosphere together with the similar foreign facilities.

– Due to significant modernization of the IS facility, the development of measurement techniques of ionospheric parameters, algorithms, and software for processing of ionospheric data, we obtain reliable information about the state of the ionosphere over Ukraine at a high level.

– The Institute of Ionosphere database of ionosphere parameters (http://database.iion.org.ua/) is developed.

– Experimental researches of the ionospheric parameters variations in a wide range of altitudes (100–1000 km) over Ukraine (Central Europe) during over 3 solar activity periods were carried out with Kharkiv IS radar.

– Experimental and theoretical studies of the effects in geospace during a number of geomagnetic storms of various intensity (from weak to very strong) and solar eclipses were carried out.

– Study of the aperiodic and quasi-periodic disturbances in the ionosphere during rocket launches and the ionosphere modification by high power HF radio transmission far from the antenna beam pattern of the heater (at the distance of about 1000 km) are carried out using the IS facility of the Institute of Ionosphere.

References: **1.** *Taran V.I.* Ionosphere research by incoherent scatter radars in Kharkiv / *V.I. Taran* // Bulletin of the Kharkiv State Polytechnic University. – 1999. – № 31.– P. 3-9 (in Russian). **2.** *Golovin V.I.* Observations of the ionosphere using the incoherent scatter method / *V.I. Golovin*, *E.V. Rogozhkin*, *V.I. Taran*, *S.V. Chernyaev* // Bulletin of the Kharkiv Polytechnic Institute "The study of ionosphere by the incoherent scatter method". – 1979. – № 155, Issue 1. – P. 12-22 (in Russian). **3.** *Emelyanov L.Ya.* History of the development of IS radars and founding of the Institute of Ionosphere in Ukraine / *L.Ya. Emelyanov*, *T.G. Zhivolup* // History of Geo- and Space Sciences. – 2013. – № 4. – P. 7-17, doi:10.5194/hgss-4-7-2013. **4.** *Pulyaev V.A.* Determination of the ionospheric parameters using the incoherent scattering technique: Monograph / *V.A. Pulyaev*, *D.A. Dzyubanov*, *I.F. Domnin*. – Kharkiv: NTU "KhPI", 2011. – 240 p. (in Russian). **5.** *Gukasov Yu.G.* Measurement of NDA-100 antenna patterns by currents on the mirror surface / *Yu.G. Gukasov*, *V.N. Ivchenko* // Bulletin of the Kharkiv Polytechnic Institute "The study of ionosphere by the incoherent scatter method". – 1979. – № 155, Issue 1.– P. 29-33 (in Russian). **6.** *Chepurnyy Ya.M.* Measurement of NDA-100 antenna pattern using the reflections from the man-made space objects / *Ya.M. Chepurnyy*, *L.Ya. Emelyanov*, *D.A. Iskra* // Bulletin of National Technical University "Kharkiv Polytechnic Institute": Special Issue "Radiophysics and ionosphere". – 2013. – № 28 (1001). – P. 14-18 (in Russian). **7.** *Smaglo N.A.* Radio transmitting device the meter band radar / *N.A. Smaglo, A.D. Koval, V.K. Bogovskiy* // Bulletin of the Kharkiv State Polytechnic University. – 1999. – № 31. – P. 113-116 (in Russian). **8.** *Emelyanov L.Ya.* Radio receiver system of the incoherent scatter radar / *L.Ya. Emelyanov* // Bulletin of the Kharkiv State Polytechnic University. – 1999. – № 31. – P. 108-112. (in Russian). **9.** *Lysenko V.N.* Features of correlation processing incoherent scatter signal by sounding the ionosphere in the VHF band with the radio pulses of 800 μs duration / *V.N. Lysenko* // Bulletin of the Kharkiv State Polytechnic University. – 1999. – № 31. – P. 90-95 (in Russian). **10.** *Lysenko V.N.* Programmable correlator to measure the ionospheric parameters using the incoherent scatter method / *V.N. Lysenko*, *A.F. Kononenko*, *Yu.V. Chernyak* // Bulletin of National Technical University "Kharkiv Polytechnic Institute", Special Issue "Radiophysics and ionosphere". – 2004. – № 23.– P. 49-62 (in Russian). **11.** *Iskra D.A.* Improving the accuracy of determining the autocorrelation functions of incoherently scattered signal / *D.A. Iskra* // Bulletin of National Technical University "Kharkiv Polytechnic Institute": Special Issue "Radiophysics and ionosphere". – 2013. – № 33 (1066). – P. 34-37 (in Russian). **12.** *Emelyanov L.Ya.* Ionosonde "Bazis" of the Institute of Ionosphere as a tool for monitoring the state of the ionosphere / *L.Ya. Emelyanov, A.A. Kononenko* // Radiotekhnika: All-Ukr. Sci. Interdep. Mag. – 2011. – № 167. – P.

30-33 (in Russian). **13.** *Emelyanov L.* Analysis of variations of the critical frequency f_0F2 of the ionosphere over Kharkiv during two solar cycles / *L. Emelyanov*, *A. Kononenko* // International School-Conference "Remote radio sounding of the ionosphere" (ION-2013) September, 30 – October, 4, 2013. – Maly Mayak (Big Alushta), Crimea, Ukraine. – Book of Abstracts. – 2013. – P 48. **14.** Pruhonice / Digisonde-4D / Czech Republic. – http://147.231.47.3 **15.** Dourbes / Digisonde DPS-4/ Belgium – http://digisonde.oma.be **16.** Moscow / Digisonde DPS-4 / Russia – http://dps.izmiran.ru/ **17.** *Rogozhkin E.V.* Sounding signals to study the ionosphere by the incoherent scattering: Monograph / *E.V. Rogozhkin*, *V.A. Pulyaev*, *V.N. Lysenko*. – Kharkiv: NTU "KhPI", 2008. – 256 p. (in Russian) **18.** *Emelyanov L.Ya.* Issues of reducing the effect of the sounding signal to the accuracy of the determination of the ionospheric plasma drift velocity / *L.Ya. Emelyanov, I.B. Sklyarov*, *S.V. Chernyaev* // Bulletin of National Technical University "Kharkiv Polytechnic Institute", Special Issue "Radiophysics and ionosphere". – 2002. – Vol. 5, № 9. – P. 25-28 (in Russian). **19.** *Siusiuk M.M.* Features of investigation of the middle ionosphere by incoherent scatter technique / *M.M. Siusiuk* // Bulletin of National Technical University "Kharkiv Polytechnic Institute": Special Issue "Radiophysics and ionosphere". – 2013. – № 33 (1066). – P. 62-65 (in Russian). **20.** Patent 71162. Ukraine, G01S 13/95. A method of measuring the parameters of the ionosphere and magnetosphere / *L.Ya. Emelyanov*, *T.A. Skvortsov*, *I.B. Sklyarov*, *A.V. Fesun*.; patented 14.11.2011; published 10.07.2012, Bulletin N 13 (in Ukrainian). **21.** *Lysenko V.N.* Dual-frequency measuring channel for determining the parameters of the ionosphere by the incoherent scattering / *V.N. Lysenko*, *Yu.V. Chernyak* // Radiophysics and electronics. – 2004. – Vol. 10, № 2.– P. 217-223 (in Russian). **22.** *Emel'yanov L.Ya.* Incoherent Scatter Measurement of the Electron Density Altitude Profiles / *L.Ya. Emel'yanov* // Geomagnetism and Aeronomy. – 2002. – Vol. 42, № 1. – P. 109-113. **23.** *Bogomaz O.V.* Unified Processing of the Results of Incoherent Scatter Experiments (UPRISE), a new generation program package for incoherent scatter radar data processing / *O.V. Bogomaz*, *D.V. Kotov* // Bulletin of National Technical University "Kharkiv Polytechnic Institute": Special Issue "Radiophysics and ionosphere". – 2013. – № 28 (1001). – P. 29-37 (in Russian). **24.** *Miroshnikov A.E.* Kharkiv Institute ionosphere incoherent scatter radar (Ukraine) express data processing on a remote server and visualization of results / *A.E. Miroshnikov*, *O.V. Bogomaz* // 16th International EISCAT symposium, 12–16 August 2013, Lancaster, United Kingdom. – Lancaster, 2013. – http://eiscat2013.lancs.ac.uk/wp-content/uploads/2013/08/3_Miroshnikov_Miroshnikov_Abstract.pdf **25.** *Bogomaz O.V.* Express incoherent scatter radar data processing on a remote server / *O.V. Bogomaz, A.E. Miroshnikov* // Bulletin of National Technical University "Kharkiv Polytechnic Institute": Special Issue "Radiophysics and ionosphere". – 2013. – № 28 (1001). – P. 63-68 (in Russian). **26.** *Chernogor L.* Study of ionospheric processes over Ukraine / *L. Chernogor*, *I. Domnin*, *L. Emelyanov*, *D. Kotov*, *M. Lyashenko* // Space Research in Ukraine / By Ed. O. Fedorov. – 2012. – P. 47-67 (in Russian). **27.** *Lyashenko M.* Development of Central Europe Regional Ionospheric Model (CERIM IION) based on Kharkiv incoherent scatter data / *M. Lyashenko*, *I. Domnin*, *L. Chernogor* // Workshop on Assessment and Validation of Space Weather Models (Alcala de Henares, Spain, 16–17 March, 2011). – 2011. – P. 23–24. **28.** *Yemelyanov L.Ya.* The Peculiarities of Mid–Latitude Ionosphere Plasma Drift Velocity Determination / *L.Ya. Yemelyanov*, *D.A. Dzyubanov* // Telecommunications and Radio Engineering. – 2007. – Vol. 66, № 14. – P. 1313-1327. **29.** *Domnin I.F.* Dynamics of the ionospheric plasma above Kharkiv during the January 4, 2011 solar eclipse / *I.F. Domnin*, *L.Ya. Emelyanov*, *L.F. Chernogor* // Radio Physics and Radio Astronomy. – 2012. – Vol. 3, № 4. – P. 311-324. **30.** *Burmaka V.P.* Wave Disturbances in the Ionosphere during a Lasting Solar Activity Minimum / *V.P. Burmaka*, *L.F. Chernogor* // Geomagnetism and Aeronomy. – 2012. – Vol. 52, № 2. – P. 183-196. **31.** *Burmaka V.P.* Complex Diagnostics of Disturbances in the Ionospheric Plasma Parameters Far from the Trajectories of Launched Rockets / *V.P. Burmaka*, *L.F. Chernogor* // Geomagnetism and Aeronomy. – 2009. – Vol. 49, № 5.– P. 637-652. **32.** *Burmaka V.P.* Variations in the parameters of scattered signals and the ionosphere connected with plasma modification by high-power radio waves / *V.P. Burmaka*, *I.F. Domnin*, *V.P. Uryadov*, *L.F. Chernogor* // Radiophysics and Quantum Electronics. – 2009. – Vol. 52, № 11. – P. 774-795. **33.** *Domnin I.F.* Results of Radiophysical Study of Wave Disturbances in the Ionospheric Plasma During Its Heating by High-Power HF Radio Transmission of "Sura" Facility /

I.F. Domnin, *S.V. Panasenko*, *V.P. Uryadov*, *L.F. Chernogor* // Radiophysics and Quantum Electronics. – 2012. – Vol. 55, N 4. – P. 253-265. **34.** *Grigorenko Ye.I.* Analysis and classification of ionospheric storms at the midlatitudes of Europe / *Ye.I. Grigorenko*, *V.N. Lysenko*, *V.I. Taran*, *L.F. Chernogor* // Kosmichna nauka i technologiya. – 2007. – Vol. 13, № 5. – P. 58-96 (in Russian). **35.** *Chernogor L.* Ionospheric storm effects above Kharkiv during the August 5–6, 2011 / *L. Chernogor*, *I. Domnin*, *L. Emelyanov*, *S. Kharytonova*, *M. Lyashenko* // EGU General Assembly 2012, Vienna, Austria, 22–27 April 2012. – Geophysical Research Abstract. – EGU2012-630-1. – 2012. – P. 14. **36.** *Domnin I.F.* Dynamic processes in the ionosphere during a very moderate magnetic storm on 20–21 January 2010 / *I.F. Domnin*, *L.Ya. Emelyanov*, *S.A. Pasura*, *S.V. Kharitonova*, *L.F. Chernogor* // Kosmichna nauka i technologiya. – 2011. – Vol. 17, № 4. – P. 26-40 (in Russian). **37.** *Emelyanov L.Ya.* Effects in geospace plasma during the partial solar eclipse on August 1, 2008 over Kharkiv. 1. The results of observations / *L.Ya. Emelyanov*, *M.V. Lyashenko*, *L.F. Chernogor* // Kosmichna nauka i technologiya. – 2009. – Vol. 15, № 3. – 70-81 (in Russian). **38.** *Chernogor L.F.* Effects in the geospace during partial solar eclipses over Kharkiv / *L.F. Chernogor*, *Ye.I. Grigorenko*, *M.V. Lyashenko* // International Journal of Remote Sensing. – 2011. – №. 32. – P. 3219-3229. **39.** *Kotov D.V.* Spatial and temporal variation in the hydrogen ions fraction under various space weather conditions / *D.V. Kotov*, *L.F. Chernogor* // Proceedings of XII Conference of Young Scientists "Interaction of fields and radiation with substance" (Irkutsk, Russia, September, 19–24, 2011). – Irkutsk. – 2011. – P. 202-204 (in Russian). **40.** *Kotov D.* The upper transition height over the Kharkiv incoherent scatter radar before, during and after the extreme minimum of the solar activity: Observational results and comparison with the IRI-2012 model / *D. Kotov*, *V. Truhlik*, *P. Richards*, *J. Huba*, *L. Chernogor*, *O. Bogomaz*, *I. Domnin* // EGU General Assembly 2014, Vienna, Austria, 27 April–2 May 2014. – Geophysical Research Abstract. – EGU2014-5652. – 2014.

Received 16.05.2014

UDC 550.388.1:551.510.535:621.396

Kharkiv incoherent scatter facility / I. F. Domnin, Ya. M. Chepurnyy, L. Ya. Emelyanov, S. V. Chernyaev, A. F. Kononenko, D. V. Kotov, O. V. Bogomaz, D. A. Iskra // Bulletin of NTU "KhPI". Series: Radiophysics and ionosphere. – Kharkiv: NTU "KhPI", 2014. – No. 47 (1089). – P. 28-42. Ref.: 40 titles.

Наведено структуру, параметри і режими роботи радара некогерентного розсіяння Інституту іоносфери (м. Харків). Показано деякі результати спостережень іоносфери за допомогою цього обладнання.

Ключові слова: радар некогерентного розсіяння, іонозонд, іоносферна обсерваторія, параметри іоносфери, метод некогерентного розсіяння радіохвиль.

Представлены структура, параметры и режимы работы радара некогерентного рассеяния Института ионосферы (г. Харьков). Показаны некоторые результаты наблюдений ионосферы с помощью этого оборудования.

Ключевые слова: радар некогерентного рассеяния, ионозонд, ионосферная обсерватория, параметры ионосферы, метод некогерентного рассеяния радиоволн

UDC 621.371.25

A.A. KOLCHEV, PhD, associate professor, MarSU, Yoshkar-Ola, Russia;
A.E. NEDOPEKIN, PhD, MarSU, Yoshkar-Ola, Russia;
V.V. SHUMAEV, PhD, senior researcher, "ADASIS" Ltd., Yoshkar-Ola, Russia

SIMULTANEOUS DETERMINE OF DOPPLER SHIFT AND GROUP DELAY TIME USING AMPLITUDE MODULATED CHIRP-SIGNAL

New method of the simultaneous measurement of the frequency dependencies of Doppler shift and group delay time of separate ionosphere modes by means of amplitude modulated chirp signal is presented in this paper. The algorithms of data processing are presented.

Keywords: ionosphere, chirp-sounder, phase, Doppler shift.

Formulation of the problem. LFM ionosonde powerful tool for monitoring the state of the ionosphere. Recently chirp sensing capabilities expand [1]. One of the main parameter of radio channel is differential Doppler shift between rays, which effect to reliability and noise-immunity of radio systems work. References 0 shows method of simultaneous determine of dependences group delay time and Doppler shift from radiation frequency of separately HF-signal propagation separate modes by means periodical frequency-modulated wave. Large time measuring on some frequency and large step of frequency are deficiencies of this method.

Analysis of the literature. Method of simultaneous definition group delay and Doppler shift of separate ionosphere modes, based on three-element frequency-modulated wave described in reference 0. Usage of phase measuring allow to reduce measuring time at same frequency channel, but measuring are realized discrete at channels defined previously, using three time-displaced signals with push-type parameters.

Reference 0 suggest way of simultaneous determine group delay and Doppler shift for each mode, using two continuous frequency-modulated wave (FMCW), but it's straightforward realization require two identical transmitters and two identical receivers.

Purpose of the article. This work describe methodic for realization of last way, using single transmitter and single receivers. It is more useful than straightforward realization.

Main equations. Let transmitter radiate continuous amplitude-modulated FMCW, which is expressed in the following way:

$$a_I(t) = a_0 \exp[j(2\pi \cdot f_M(t - t_0))] \times \exp[j(2\pi \cdot f_H(t - t_0) + \pi \cdot df(t - t_0)^2)], \quad t \in [t_0, t_0 + t_K], \tag{1}$$

where f_M is the modulate frequency; $df = df/dt$ is the chirp frequency change rate; f_{H} is initial radiation frequency; a_0 is the signal amplitude; t_0 is the time of radiation start; t_{K} is the radiation duration.

Amplitude-modulated signal may be represented as sum of two signals:

$$a_I(t) = a_0 \exp[j(2\pi(f_{\text{H}} + f_M)(t - t_0) + \pi \cdot df(t - t_0)^2)] + \\ + a_0 \exp[j(2\pi(f - f_M)(t - t_0) + \pi \cdot df(t - t_0)^2)],\ t \in [t_0, t_0 + t_{\text{K}}] \quad (2)$$

Processing of accepted chirp signal in the receiver using compression method in the frequency range is multiplication of chirp signal by the heterodyne signal, complex-conjugated to the signal being radiated, and in analysis of the accepted difference signal spectrum. For second term of (2):

$a_2(t) = a_0 \exp[j(2\pi(f - f_M)(t - t_0) + \pi \cdot df(t - t_0)^2)],\ t \in [t_0, t_0 + t_{\text{K}}]$ following mathematical ratios correspond to those operations:

$$A_2(t) = a_{2\text{out}}(t)a^*(t)$$
$$S_2(\Omega) = \int_{-\infty}^{\infty} A_2(t)e^{-j\Omega t}dt, \quad (3)$$

where * is the sign of complex conjugation; $A_2(t)$ is the differential signal corresponding to $a_2(t)$; $S_2(\Omega)$ is its spectrum; $a_{2\text{out}}(t)$ is the signal at the output from ionosphere (at the input of the receiver).

To determine group delay time of separate ionosphere modes of propagation, SW signal of differential frequency is divided into N elements being T_{E} long at a distance between elements T and for each element Fourier transformation is calculated. Since $\Delta f_{\text{E}} = df \cdot T_{\text{E}} << f$ (f is a current frequency), each element of differential signal is referred to the central frequency of element Δf_E. Accordingly, spectrum of the signal element also can be referred to this frequency.

In case of multi-beam non-stationary channel of propagation a transfer function can be expressed in the following way:

$$H(\omega,t) = \left|H\ (\omega,t)\right| \cdot \exp j\,\varphi(\omega,t) = \sum_{i=1}^{m} \left|H_i(\omega,t)\right| \cdot \exp j\,\varphi_i(\omega,t), \quad (4)$$

where $\left|H_i(\omega,t)\right|$ is modulus of the path transfer function for individual beam; $\varphi_i(\omega,t)$ is the path phase in ionosphere; m is the number of propagation modes.

The chirp element occupies a certain band of $\Delta f_{\text{E}} = df \cdot T_{\text{E}}$ near the frequency f_0. Considering the signal to be quasi-stationary for small scales of time $\Delta t = t - t_0$, in the absence of frequency dispersion, we can expand the

transfer function phase of the individual beam in the Taylor power series $\Delta\omega = 2\pi \cdot (f - f_0)$ and Δt, having been restricted by linear summands, and considering $\left|H_i(\omega,t)\right| \cdot$ as constant:

$$\begin{aligned} &\varphi_i(\omega,t) \approx \varphi_i(\omega_0,t_0) + \varphi'_{it}(\omega_0,t_0)\Delta t + \varphi'_{i\omega}(\omega_0,t_0)\Delta\omega; \\ &\left|H_i(\omega,t)\right| = \left|H_{0i}\right| = const \end{aligned} \tag{5}$$

The first phase derivative considering frequency equals to the group signal-delay time τ :

$$\varphi'_{i\omega}(\omega_0;t_0) = \tau_i(\omega_0;t_0) \tag{6}$$

The first phase derivate considering time equals the Doppler frequency shift:

$$\varphi'_{it}(\omega_0;t_0) = -\omega_{\partial i}(\omega_0;t_0) = -2\pi F_{\partial i}(\omega_0;t_0) \tag{7}$$

The absence of the frequency dispersion and quasi-stationary imply that within frequency band of signal element during its length time values $\tau_i(\omega;t)$ and $F_{\partial i}(\omega;t)$ do not change, i.e.:

$$\tau_i(\omega;t) = \tau_i(\omega_0;t_0) = \tau_{0i} = const$$

and

$$F_{\partial i}(\omega;t) = F_{\partial i}(\omega_0;t_0) = F_{\partial i0} = const\ .$$

When propagating in the ionosphere, $T_{\mathrm{E}} >> \tau_{0i}$. In this case, from Eq. (3), we obtain:

$$A_2(t) = {a_0}^2 \sum_{i=1}^{m} \left|H_{0i}\right| \exp[j(\psi_i(\omega_0,t_0) + 2\pi(t - t_0)f_{0i}], \tag{8}$$

where

$$\begin{aligned} &\psi_i(\omega_0,t_0) = \varphi_i(\omega_0,t_0) - \tau_{0i} \cdot \omega_0 + 2\pi\, \mathrm{f_H}\tau_{0i} - 2\pi f_M \tau_{0i} - \pi \cdot df \cdot {\tau_{0i}}^2, \\ &\omega_0 = 2\pi(f_{\mathrm{H}} - f_M);\ f_{0i} = df\tau_{0i} + f_M - F_{\partial i0} \end{aligned} \tag{9}$$

It can be seen from Eq. (8), a separate element of the differential signal in the course of T_{E} is a section of harmonic fluctuation. In this case we can obtain $S_2(\Omega)$ in the following way:

$$\begin{aligned} S_2(\Omega) = {a_0}^2 T_{\mathrm{E}} \sum_{i=1}^{m} \left|H_{0i}\right| \exp[j\psi_i(\omega_0,t_0)] \times \\ \times \sin c\left(\frac{\Omega - 2\pi(df\tau_{0i} - F_{\partial i0} + \mathrm{f}_M)}{2} T_{\mathrm{E}}\right) \end{aligned} \tag{10}$$

where $\sin c(x) = \dfrac{\sin x}{x}$.

Methodic of data treatment. Individual modes are distinguished according to the procedures described in [6]. In element wise treatment of FMCW every *k*-th element of differential signal corresponding to time t_0 we denoted as $A_I(t)$, and every *(k+1)*-th element correspond to time $t_0 + T$ we denoted as $A_{II}(t)$. Time displacement of *(k+1)*-th element from *k*-th element defined in the following way:

$$T = \frac{2f_M}{df} \tag{11}$$

In spectrum of differential signal for each propagation mode we can see two spectrum components with difference of frequency $2f_M$ because signal has amplitude modulation. The second spectrum component for *i*-th mode of *k*-th element of differential signal is defined as $S_{Ii,2}(\Omega)$ and illustrated in Fig. 1a). It corresponds to Eq. (10). The first spectrum component for *i*-th mode of *(k+1)*-th element of differential signal is defined as $S_{IIi,2}(\Omega)$ and illustrated in Fig. 1b).

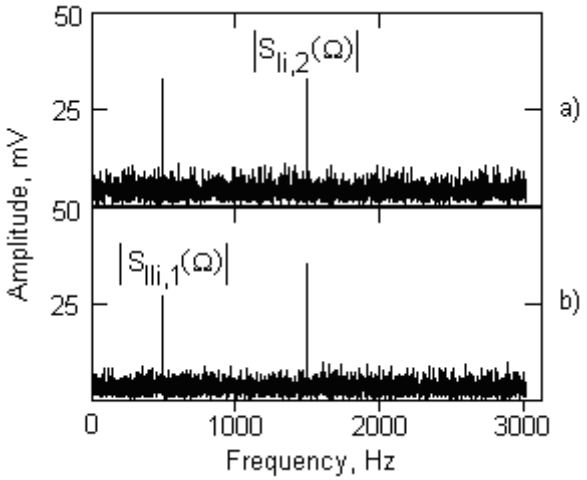

Fig.1 Spectrums of differential signal elements: a) *k*-th element of I signal; b) *(k+1)*-th element of signal

In equation of radiating signal first summand of Eq. (2) correspond to this spectrum component. Subject to time displacement T this summand is:

$$\begin{aligned} a_{II,1}(t) = a_0 \exp[j(2\pi(f - f_M)(t - t_0) - f_{\text{H}}T - f_M T + \\ + \pi \cdot df(t - t_0)^2 + \pi \cdot dfT^2)], \ t \in [t_0 + T, t_0 + t_K + T]. \end{aligned} \tag{12}$$

For differential signal of *(k+1)*-th element we obtained:

$$S_{II,1}(\Omega) = a_0{}^2 T_{\mathrm{E}} \sum_{i=1}^{m} \left| H_{0i} \right| \exp[j\psi_i(\omega_0, t_0 + T)] \times \sin c\left(\frac{\Omega - 2\pi(df\tau_{0i} - F_{\partial i0} - \mathrm{f_M})}{2} T_{\mathrm{E}}\right). \quad (13)$$

where

$$\psi_i(\omega_0, t_0 + T) = \varphi_i(\omega_0, t_0 + T) - \tau_{0i} \cdot \omega_0 + 2\pi f_{\mathrm{H}} \tau_{0i} - 2\pi f_M \tau_{0i} - \pi \cdot df \cdot \tau_{0i}{}^2 + 2\pi \cdot f_M T + 2\pi \cdot TF_{\partial i0}. \quad (14)$$

We see that both expressions for spectrums Eq. (10) and Eq. (13) have same amplitudes and different phases. Obviously phases differ on two summands. Equation (14) contains terms $2\pi F_{\partial i0} \cdot T$ and $2\pi \cdot f_M T$, therefore for define of Doppler shift we must change f_M and T so that product $f_M \cdot T$ become an integer number. For instance, if time displacement between signal elements T equals 0.01 s and f_M =500 Hz, then value of $2\pi \cdot f_M T$ is 20π — whole number of phase rotations.

If $\Delta\psi_i$ is difference between phases of spectral components $S_{Ii,2}(\Omega)$ and $S_{IIi,1}(\Omega)$, then with condition of Eq. (7) we have:

$$\Delta\psi_i = \varphi_i(\omega_0, t_0 + T) - \varphi_i(\omega_0, t_0) = 2\pi F_{\partial i0} \cdot T \quad (15)$$

There is necessity to change displacement T so that $\left|\Delta\psi_i\right| = \left|2\pi F_{\partial i0} T\right| \in (0; \pi)$. At the same time we have condition $T \in \left(0; \frac{1}{2\left|F_{\partial i0}\right|}\right)$. Usually in case of ionospheric propagation for short waves Doppler shift satisfy the condition $F_{\partial i0} < 10\,\mathrm{Hz}$, hence we can change value of data treatment displacement T < 0.05 s and amplitude modulation frequency 1000 Hz for good visibility of spectral components.

Making such treatment, we obtain two sequences of complex spectral samples for each element of differential signal.

If φ_{Iik} and φ_{IIik} are phases of spectral components for the *k*-th and the *(k+1)*-th elements of differential signal, then Doppler shift for element of the signal each *i*-th mode with central frequency $f_{0k} = f_{\mathrm{H}} + \dot{f} \cdot T\,(k - 1/2)$ can be defined in the following way:

$$F_{\partial ik} = \frac{\varphi_{IIik} - \varphi_{Iik}}{2\pi T}. \quad (16)$$

Registering variations of position for maximums of modulus of differential signal spectrum from element to element when operating frequency varies within the range of from f_{H} to f_{K}, we get frequency dependency for group delay $\tau_{ki}(f_{0k})$. Computing on Eq. (16) values of $F_{\partial ik}$ for each signal element, we obtain frequency dependency for Doppler shift $F_{\partial ik} = F_{\partial i}(f_{0k})$.

To define group delay, amplitude spectrum $S_{Ii,2}(\Omega)$ of differential signal $A_I(t)$ is used. For instance, modules $\left|S_{Ii,2}(\Omega)\right|$ have maximums on frequencies $\Omega_{I,2_{ki}} = 2\pi(df\tau_{ki} + f_M - F_{\partial ik})$.

In conditions of ionospheric propagation Doppler shift $F_{\partial ik}$ far less than product $df \cdot \tau_{ki}$, therefore group delay for central frequency $f_{0k} = f_{\text{H}} + df \cdot T(k - 1/2)$ is:

$$\tau_{ki} \approx \frac{\Omega_{I,2_{ki}} - 2\pi \cdot f_M}{2\pi \cdot df} \qquad (17)$$

Thus we obtain frequency dependency group delay for separate modes.

Conclusion. This methodic permit make straight forward element wise measurements of group delay time and Doppler shift by means phase values, without great averaging in great time interval. This advantage gives facility for Doppler-gram tracing with high temporal resolution. Methodic not requires many technical consumptions and wants only one transmitter and one receiver. Methodic usage in work of systems for FMCW radio sounding of ionosphere can give resource for define frequency dependences Doppler shift and propagation time of radio signal in ionospheric channel for whole decameter range. It will refine possibility of chirp-sounder as estimations tool for non-stationary short-wave channel.

References: **1.** *Vertogradov G.G.* Oblique sounding and modeling of the ionospheric HF channel / *G.G. Vertogradov, V.G. Vertogradov, V.P. Uryadov* // Radiophysics and Quantum Electronics. – 2005. – Vol. 48, № 6. – P. 405-419. **2.** *Ivanov V.A.* Effect non-stationary single-beam short wave channel to characteristics of extended spectrum signal / *V.A. Ivanov, A.A. Kolchev, V.V. Shumaev* // Problems of diffraction and propagation electromagnetic waves. – Moscow: Moscow Institute for Physics and Technology, 1994, p. 73-79. **3.** *Batukhtin V.I.* Measurement of the Doppler Frequency Shift on Individual Rays Using a Chirp Ionosonde / *V.I. Batukhtin, V.A. Ivanov, A.A. Kolchev, S.V. Rozanov* // Radiophysics and Quantum Electronics. – 2000. – Vol. 43, № 12. – P. 938-947. **4.** *A.M.V. Pool* Advanced sounding. The FMCW alternative / *A.M.V. Pool* // Radio Science. – 1985. – Vol. 20, № 6. – P. 1609-1616. **5.** *Kolchev A.A.* Measurement of Doppler shift using double chirp signal / *A.A. Kolchev, V.V. Shumaev* / Proceedings of 12th International ionospheric effects symposium (IES'2008, Alexandria, VA). – 2008. – P. 698-703. **6.** *Kolchev A.A.* Application of techniques for separating anomalous samples during the processing of SW LFM Signal / *A.A. Kolchev, A.E. Nedopekin, D.V. Khober* // Radioelectronics and Communications Systems. – 2012. – Vol. 55, № 9. – P. 418-425.

Received 31.05.2014

UDC 621.371.25
Simultaneous determine of Doppler shift and group delay time using amplitude modulated chirp-signal / A. A. Kolchev, A. E. Nedopekin, V. V. Shumaev // Bulletin of NTU "KhPI". Series: Radiophysics and ionosphere. – Kharkiv: NTU "KhPI", 2014. – No. 47 (1089). – P. 43-49. Ref.: 6 titles.

Представлено новий метод одночасного вимірювання частотних залежностей допплерівського зсуву і часу групової затримки окремих іоносферних мод з використанням безперервного ЛЧМ сигналу з амплітудною модуляцією. Наведено порядок обробки даних під час вимірювання.

Ключові слова: іоносфера, ЛЧМ іонозонд, фаза, допплерівський зсув.

Представлен новый метод одновременного измерения частотных зависимостей доплеровского сдвига и времени групповой задержки отдельных ионосферных мод с использованием непрерывного ЛЧМ сигнала с амплитудной модуляцией. Приведен порядок обработки данных при измерении.

Ключевые слова: ионосфера, ЛЧМ ионозонд, фаза, доплеровский сдвиг.

UDC 550.388

***T.G. ZHIVOLUP*,** PhD, research scientist, Institute of Ionosphere, Kharkiv

THE F2-LAYER PARAMETER VARIATIONS DURING SPRING EQUINOX 2013, ACCORDING TO THE KHARKIV AND EISCAT INCOHERENT SCATTER RADARS DATA

The investigations of temporal variations of the electron density in the F2-layer maximum, ion and electron temperatures in the mid-and high latitudes during the 2013 year spring equinox are conducted. The features of the temporal variations of the parameters of the F2-layer in Kharkiv and Tromsø during the spring equinox are revealed. It was established that during the spring equinox changes amplitude electron and ion temperatures in the ionosphere over Tromsø less than the amplitude of temperature changes of electrons and ions in the ionosphere over Kharkiv on the entire time interval of joint observations from 07:00 to 24:00 UT.

Keywords: the spring equinox, the temporal variations of the parameters of the F2-layer in middle and high latitudes.

Statement of the problem. The incoherent scatter (IS) radar in Kharkiv and radar EISCAT Observatory's radars form the European chain of IS radars , which allows you to gain knowledge about the ionosphere structure at mid- and high latitudes, as well as to create modern ionosphere and thermosphere models. The comparative analysis of temporal variations of the electron concentration in the F2-layer maximum, ion and electron temperatures in the mid- and high latitudes for quiet period during different seasons allows improving the theory region F2 and thermosphere. The creation of reliable theoretical ionosphere region F2 model for middle and high latitudes, taking into account different heliogeophysical conditions, is of interest both for the development of the theory of ionosphere, and for solving applied tasks of radio waves.

The analysis of the literature. The F2 region research at different latitudes are conducted by IS radars and other methods. The [1] presents the results of studies of seasonal variations of maximum electron concentration of the F2-layer ($n_{em}F2$) and electron and ion temperatures in high and middle latitudes. It was noted that in equinox season in Tromsø not observed before-sunset high $n_{em}F2$, which is observed in Kharkiv, and that after sunset in Tromsø there is more rapid decrease $n_{em}F2$ compared with decrease $n_{em}F2$ after sunset in Kharkiv. In [2], the results of study temperatures of electrons and ions, as well as $n_{em}F2$ in Kharkiv and Tromsø during a strong magnetic storm on August 5 – 6, 2011 are presented. The sharp monotonous decrease $n_{em}F2$ in Kharkiv and Tromsø after beginning of the magnetic storm and unusual intermittent night ionospheric plasma in Kharkiv to daytime temperatures of electrons and ions there was observed. In [3] the variations $n_{em}F2$ with 13 stations vertical sounding located at different latitudes were investigated. It was noted that during high solar activity (index $F_{10,7}$ was

equal to 140) standard changes n_{em}F2 make up 20% at day and 33% at night. Seasonal changes n_{em}F2, especially, the increase n_{em}F2 during the equinox were marked. In [4], the results of the study temperatures of electrons and ions for summer, winter and equinox seasons at different latitudes and at different levels of solar activity are presented. It was noted that the daily values of electron temperature exceeds its average night values in 2.8 – 4.6 times in the transition from solar activity minimum to its maximum, and day values of ion temperature – in 1.2 – 2.2 times.

The aim of the article – to reveal the specific features of temporal variations of electron concentration in the F2-layer maximum, ion and electron temperatures in the mid-and high latitudes during spring equinox at a moderate solar activity.

Heliogeophysical environment 14 and 20 March 2013. Measurements with IS radars in Kharkiv and Tromsø held March 19 – 22, 2013 (Kharkiv) and March 14, 2013 (Tromsø) in accordance with the International Geophysical Calendar.

On March 20, 2013 the index of solar activity $F_{10,7}$ mattered 108 (solar activity was moderate). Planetary the daily index of geomagnetic activity A_p for March 20 had a value of 9 and three-hour planetary K_p-index matter not exceeding 3 (basically had value equal to 2, in the period of measurements from 07:00 to 24:00 UT), i.e. this period of time was absolutely quiet.

On March 14, planetary the daily index of geomagnetic activity A_p had a value of 5, and three-hour planetary K_p-index matter not exceeding 2 (generally equal to 1), i.e. this period of time was absolutely quiet. Index of solar activity $F_{10,7}$ had a value of 123, i.e. solar activity was moderate.

Variations of electron concentration in the F2-layer maximum of March 14, 2013, according to Tromsø radar data, and March 20, 2013, according to Kharkiv radar data. The main interest in the study F2-region are temporal variations of electron concentration n_{em} in the F2-layer maximum in the mid-and high latitudes in different seasons. Fig.1 shows a comparison of the temporal variations lgn_{em}F2 on the time interval 07:00 to 24:00 UT according to Tromsø and Kharkov radar data in a quiet day 14 and 20 March 2013. As can be seen from Fig. 1 the time course of lgn_{em}F2 for Kharkiv has two distinct local maximum at 08:00 and 13:00 UT, as the time course of lgn_{em}F2 for Tromsø with a local maximum at 13:00 UT. In Tromsø electron concentration in the maximum of the F2-layer (n_{em}F2) monotonically decreases slowly after 13:00 to 17:00 UT, and after 17:00 UT is more rapid decrease of the electron concentration in the F2-layer maximum is observed. In Kharkiv n_{em}F2 also monotonically decreases after 13:00 till 18:00 UT, and after 18:00 UT more quickly decreases, and the decrease n_{em}F2 in Kharkiv slower compared to Tromsø.

The Fig. 1 shows the values of lgn_{em}F2 for Kharkiv exceed the values of lgn_{em}F2 for Tromsø almost in the whole time interval joint observations from 08:00 to 24:00 UT. The value n_{em}F2 for Kharkiv at 08:00 UT exceeds the value n_{em}F2 for Tromsø by 23%, and the value n_{em}F2 at 13:00 UT – by 3% (value n_{em}F2 in Kharkiv

and Tromsø almost the same). The value n_{em}F2 for Kharkiv at 17:00 UT exceeds the value n_{em}F2 for Tromsø by 29%, at 18:00 UT – by 91%, at 21:00 UT – by 79%, and at 24:00 UT n_{em}F2 in Kharkiv exceeds n_{em}F2 in Tromsø by 74%.

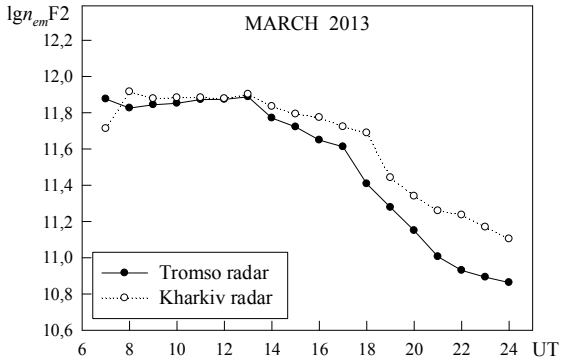

Fig. 1 – Comparison of the temporal variations of lgn_{em}F2, according to Tromsø radar data for 14.03.2013 and Kharkiv radar data for 20.03.2013

In Kharkiv until sunset at an altitude of 300 km at 17:41 UT there is slow monotonous decrease n_{em}F2, and after 18:00 UT there is faster descending n_{em}F2. In Tromsø there is slow monotonous decrease n_{em}F2 from 13:00 to 17:00 UT, and after sunset at 16:40 UT in Tromsø there is more rapid decrease n_{em}F2, moreover, this reduction faster in comparison with the reduction n_{em}F2 after sunset in Kharkiv. It should be noted that before-sunset highs n_{em}F2 in Tromsø and Kharkiv are not observed.

Thus, in the period of spring equinox n_{em}F2 in Kharkiv exceeds n_{em}F2 in Tromsø in the whole time interval joint observations from 08:00 to 24:00 UT. Before-sunset highs n_{em}F2 in Tromsø and Kharkiv are not observed. After sunset in Tromsø there is more rapid decrease n_{em}F2 compared with decrease n_{em}F2 after sunset in Kharkiv.

Electron temperature variations on March 14, 2013, according to Tromsø radar data, and March 20, 2013, according to Kharkiv radar data. Variations of electron temperature T_e on March 14, 2013 at the height of 344 km in Tromsø and at a height of 342 km on March 20, 2013 in Kharkov are shown in Fig. 2.

From Fig. 2 you can see that the electron temperature T_e in Tromsø more electron temperature in Kharkiv in the whole time interval joint observations from 07:00 to 24:00 UT. The temperature of electrons in Kharkiv, starting from 08:00 UT, gradually increases to its maximum value – 2120 K at 14:00 UT. After 14:00 UT with the sunset in magneto-conjugated with Kharkiv point (Madagascar island) at 14:59 UT electron temperature is slowly reduced, and with the sunset in

Kharkov 15:49 UT there is more rapid decrease T_e to its minimum value 827 K that it takes at 22:00 UT. The amplitude changes T_e, i.e. the difference between the maximum and minimum temperatures of electrons in Kharkiv is 1293 K.

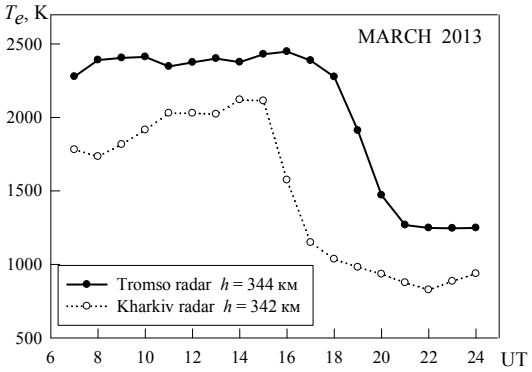

Fig. 2 – Comparison of temporal variations of T_e, according to Tromsø radar data for 14.03.2013 and Kharkiv radar data for 20.03.2013

In Tromsø electron temperature gradually increases to its first local maximum 2412 K at 10:00 UT, the second local maximum T_e – 2401 K is observed at 13:00 UT. After this, the electron temperature gradually increases to its maximum value 2448 K that it takes at 16:00 UT, and with the sunset at 16:40 UT T_e quickly reduced to its minimum 1246 K that it takes at 23:00 UT. The amplitude changes T_e in Tromsø is 1202 K, i.e. in Tromsø amplitude changes of electron temperature on the time interval 07:00 – 24:00 UT 91 K less, than in Kharkiv.

The temperature of electrons in Tromsø exceeds the temperature of electrons in Kharkov: in the interval from 07:00 to 15:00 UT – 497 – 311 K, and in the interval 16:00 – 24:00 UT – 874 – 311 K.

Thus, in the period of spring equinox electron temperature in Tromsø exceeds the temperature of electrons in Kharkiv in the whole time interval joint observations from 07:00 to 24:00 UT. The temperature of electrons in Kharkiv has a pronounced maximum at 14:00 UT, with the sunset in magneto-conjugated with Kharkiv point (Madagascar island) at 14:59 UT electron temperature is slowly reduced, and with the sunset in Kharkov at 15:49 UT there is more rapid decrease T_e to its minimum value. In Tromsø rapid decrease of the electron temperature is observed only after sunset in Tromsø at 16:40 UT. In Tromsø amplitude changes of electron temperature on the time interval 07:00 – 24:00 UT 91 K less, than in Kharkiv. This is because in Tromsø on the heights of 300 km and more 14.03.2013 the Sun never sets, and at these heights dominates the polar day.

Ion temperature variations on March 14, 2013, according to Tromsø radar data, and March 20, 2013, according to Kharkiv radar data. Variations

of ion temperature T_i on March 14, 2013 at the height of 344 km in Tromsø and at a height of 342 km on March 20, 2013 in Kharkov are shown in Fig. 3.

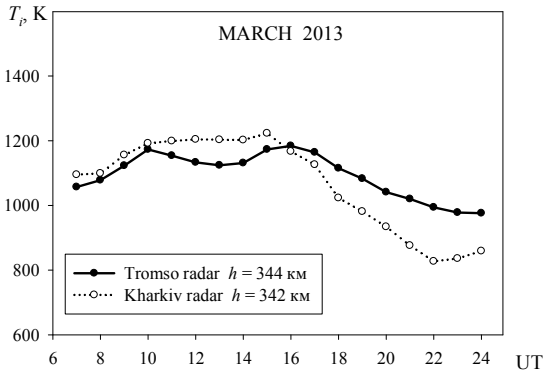

Fig. 3 – Comparison of time course T_i, according to Tromsø radar data for 14.03.2013 and Kharkov radar data for 20.03.2013

The figure shows that the temperature of ions in Kharkiv more than the temperature of ions in Tromsø on the time interval 07:00 – 15:00 UT, i.e. before sunset in Kharkiv on 15:49 UT. After sunset in Kharkiv temperature of ions in Tromsø in the time interval 16:00 – 24:00 UT was higher than the temperature of ions in Kharkiv.

The temperature of ions in Kharkiv, starting from 08:00 UT, gradually increases to its maximum value – 1223 K at 15:00 UT. After 15:00 UT with the sunset in Kharkiv temperature of ions monotonically decreases to its minimal value 827 K that it takes at 22:00 UT. The amplitude changes T_i, i.e. the difference between the maximum and minimum temperature of ions in Kharkiv is 396 K.

In Tromsø ion temperature has two local maximum at 10:00 and 16:00 UT and the local minimum at 13:00 UT. After 16:00 UT ion temperature slowly decreases until 17:00 UT, and after sunset in Tromsø at 16:40 UT ion temperature monotonically decreases to its minimal value 976 K that it takes at 24:00 UT. The amplitude changes T_i in Tromsø is 208 K, i.e. by 1.9 times less than in Kharkiv.

The temperature of ions in Kharkiv was higher than the temperature of ions in Tromsø in the interval 07:00 – 15:00 UT on 19 – 79 K, and the temperature of ions in Tromsø in the interval 16:00 – 24:00 UT higher than the temperature of ions in Kharkiv on 17 – 167 K.

Thus, in the period of the spring equinox, the temperature of ions in Kharkov higher than the temperature of ions in Tromsø on the time interval 07:00 – 15:00 UT, i.e. before sunset in Kharkov at 15:49 UT, and after sunset in Kharkiv temperature of ions in Tromsø was higher than the temperature of ions in Kharkiv.

After sunset in Kharkiv and Tromsø the temperature of ions in Kharkiv and Tromsø monotonically decreases to their minimum values, moreover, the decreasing of the temperature of ions in Kharkiv faster than descending T_i in Tromsø.

The amplitude changes T_i in Tromsø in 1.9 times less than in Kharkiv. This is because in Tromsø on the heights of 300 km and more 14.03.2013 the Sun never sets, and at these heights dominates the polar day.

The conclusions. 1. During the spring equinox n_{em}F2 in Kharkiv exceeds n_{em}F2 in Tromsø in the whole time interval joint observations from 08:00 to 24:00 UT.

2. Before-sunset highs n_{em}F2 in Tromsø and Kharkiv are not observed.

3. After sunset in Tromsø there is more rapid decrease n_{em}F2 compared with decrease n_{em}F2 after sunset in Kharkiv.

4. During the spring equinox the temperature of electrons in ionosphere over Tromsø exceeds the temperature of electrons in ionosphere over Kharkiv in the whole time interval joint observations from 07:00 to 24:00 UT.

5. During the spring equinox, the temperature of the ions in ionosphere over Kharkiv higher than the temperature of ions in ionosphere over Tromsø in the whole time interval 07:00 to 15:00 UT, i.e. before sunset in Kharkiv at 15:49 UT.

6. After sunset in Kharkiv and Tromsø the temperature of ions in ionosphere over Kharkiv and Tromsø monotonically decreases to their minimum values, moreover, the decrease of the temperature of ions in the ionosphere over Kharkiv faster than descending T_i in ionosphere over Tromsø.

7. The amplitude changes T_i in Tromsø in 1.9 times less than in Kharkiv. This is because in Tromsø on the heights of 300 km and more 14.03.2013 the Sun never sets, and at these heights dominates the polar day.

References: 1. *Zhivolup T.G.* Variations of parameters of the F2-layer in the spring equinox 2012, according to the Kharkiv and EISCAT incoherent scatter radars data // Bulletin of the National Technical University "Kharkiv Polytechnic Institute". Series: "Radiophysics and ionosphere". – 2013. – № 28 (1001). – P. 3-9. **2.** *Zhivolup T.G. , Dzyubanov D.A.* Variations of parameters of the F2-layer during the strong magnetic storm on 5 – 6 August 2011, according to the Kharkiv and EISCAT incoherent scatter radars data // Bulletin of the National Technical University "Kharkiv Polytechnic Institute". Series: "Radiophysics and ionosphere". – 2012. – № 57 (963). – P. 61-69. **3.** *Rishbeth H., Mendillo M.* Patterns of F2-layer variability // J. Atm. Sol.-Terr. Phys. – 2001. – V. 63. – P. 1661-1680. **4.** *Sharma D.K., Sharma P.K., Rai J., Garg S.C.* Effect of solar activity on ionospheric temperatures in F2 region. // Ind. J. Radio Space Phys. – 2008. – V. 37. – P.319-325.

Received 20.05.2014

UDC 550.388

The F2-layer parameter variations during spring equinox 2013, according to the Kharkiv and EISCAT incoherent scatter radars data / T.G. Zhivolup // Bulletin of the National Technical University "Kharkiv Polytechnic Institute". Series: "Radiophysics and ionosphere". - Kharkiv: NTU "KhPI", 2014. – No. 47 (1089). – P. 50-56. Ref.: 4 titles.

Проведено дослідження часових варіацій електронної концентрації в максимумі шару F2, іонної та електронної температур в середніх і високих широтах в період весняного рівнодення 2013 р. Виявлено особливості часових варіацій параметрів шару F2 в Харкові і Тромсьо в період весняного рівнодення. Встановлено, що в період весняного рівнодення амплітуди зміни температур електронів і іонів в іоносфері над Тромсьо менше, ніж амплітуди зміни температур електронів і іонів в іоносфері над Харковом на всьому часовому інтервалі спільних спостережень з 07:00 до 24:00 UT.

Ключові слова: весняне рівнодення, часові варіації параметрів шару F2 в середніх і високих широтах.

Проведены исследования временных вариаций электронной концентрации в максимуме слоя F2, ионной и электронной температур в средних и высоких широтах в период весеннего равноденствия 2013 г. Выявлены особенности временных вариаций параметров слоя F2 в Харькове и Тромсё в период весеннего равноденствия. Установлено, что в период весеннего равноденствия амплитуды изменения температур электронов и ионов в ионосфере над Тромсё меньше, чем амплитуды изменения температур электронов и ионов в ионосфере над Харьковом на всем временном интервале совместных наблюдений с 07:00 до 24:00 UT.

Ключевые слова: весеннее равноденствие, временные вариации параметров слоя F2 в средних и высоких широтах.

UDC 550.380:550.388.1:550.389.5: 537.67

T.A. SKVORTSOV, D.Sc., Prof., NTU "KhPI";
L.Ya. EMELYANOV, PhD, head of department, Institute of Ionosphere, Kharkiv;
A.V. FESUN, PhD student, NTU "KhPI";
D.P. BELOZEROV, PhD, junior research scientist, Institute of Ionosphere, Kharkiv

MEASUREMENT OF THE GEOMAGNETIC FIELD IN THE IONOSPHERE USING RADAR METHODS

A new method for measuring the geomagnetic field in the ionosphere by the integrated use of vertical sounding radar (ionosonde) and incoherent scatter radar, its capabilities and features of the technical implementation, as well as the first results of an experimental test are considered.

Key words: geomagnetic field, ionosphere, incoherent scatter radar, ionosonde.

Introduction. Currently, measurements of the geomagnetic field (GMF) in the ionosphere are realized at altitudes of flight of the Earth artificial satellites [1]. Currently, measurements of the geomagnetic field (GMF) in the ionosphere are realized at altitudes of flight of the Earth artificial satellites [1]. At first, the magnetic studies, which proved the presence of ionosphere sources, originative the changes of the GMF, have been carried out by the third Soviet satellite in 1958 [2].

However, measurements of the GMF in the ionosphere by satellites have the following weaknesses:

1. Area of the ionosphere near the ionospheric peak and below is practically beyond the observation zone due to short life of satellites in the specified area. At the same time, one can expect the greatest GMF variations associated with ionospheric currents just in this area.

2. Continuous monitoring of GMF in a fixed region of space is impossible due to the movement of satellites, making it difficult to study the temporal variations in GMF.

3. Simultaneous and continuous measurement of the characteristics of the ionosphere and magnetosphere in the area above IS radar is practically impossible. This reduces the possibility of studying magnetosphere-ionosphere coupling.

Thus, the topical problem is to develop methods for measuring the GMF in the region near the ionospheric peak and below.

To investigate the interaction of the magnetosphere and ionosphere, it is desirable to carry out combined in time and space measurement of the magnetosphere and ionosphere parameters.

Such measurements can be performed using the method developed at Institute of Ionosphere [3] and described below.

The method allows measuring the vertical component of intensity of the GMF in region near the ionospheric peak under ionospheric observatory by the integrated use of vertical sounding radar (ionosonde) and incoherent scatter (IS) radar.

Purpose is to consider the possibility of measuring the geomagnetic field at the dense ionosphere altitudes.

Method for measuring GMF in the ionosphere. The Faraday effect is used to measure GMF by IS radar. The effect appears that, when the radio wave passes through the magnetized ionospheric plasma from the radar up to a height h and backwards, its polarization ellipse is rotated by an angle

$$\Phi(h) = k\int_0^h H(l)N(l)dl\,, \tag{1}$$

where k =0,0594·f_0^{-2}, f_0 is operating frequency, $N(h)$ is the electron density, and H is the longitudinal component of the GMF intensity.

In accordance with (1) and the mean value theorem there is in a specified height interval [h_1, h_2] such height h_x, for which

$$\delta(h_x) = \Phi(h_2) - \Phi(h_1) = kH(h_x)\int_{h_1}^{h_2} N(h)dh\,. \tag{2}$$

Thus, we have from (2):

$$H(h_x) = \frac{\delta(h_x)}{kN_M I}\,, \tag{3}$$

where

$$I = \int_{h_1}^{h_2} F(h)dh \tag{4}$$

$F(h) = \dfrac{N(h)}{N_M}$ is normalized to the maximum height profile of the electron density.

As seen from (3), if we measure the Faraday effect, the normalized profile and maximum of the electron density, we can calculate the intensity of the GMF at a certain height within a specified interval of heights.

For measuring the Faraday effect, transmitter radiates a signal with linear polarization and we carry out reception of the left and right circular polarization components. At the same time, optimal algorithm of estimate formation is of the form [4]

$$\hat{\Phi}(h) = \frac{1}{2}arctg\left[\frac{r_{c1s2}(h) - r_{c2s1}(h)}{r_{c1c2}(h) + r_{s1s2}(h)}\right], \tag{5}$$

where r_{c1s2}, r_{c2s1}, r_{c1c2}, r_{s1s2} are estimates of the cross correlations of the signal quadrature components at the receiver outputs.

To determine the $F(h)$ function using the IS radar, the signal power $P(h)$, electron $T_e(h)$ and ion $T_i(h)$ temperatures are measured, and then we calculate and normalize a function

$$N(h) = CP(h)h^2\left(1+\frac{T_e(h)}{T_i(h)}\right), \tag{6}$$

where C is any constant. N_M is measured using ionosonde.

As it is necessary to radiate a long pulse with circular polarization for $T_e(h)$ and $T_i(h)$ measurement, we proposed to use the sound signal, consisting of the first pulse with circular polarization and the second pulse with linear polarization [1]. The first pulse has long duration to ensure the accuracy of temperature measurement, and the second pulse has short duration to ensure high correlation between ordinary and extraordinary waves, as well as high resolution of IS signal for power measurement.

Thus, we obtain the estimate

$$\hat{H}(h_x) = \frac{\hat{\delta}(h_x)}{k\hat{N}_M\hat{I}}, \tag{7}$$

where $\hat{H} = H + \varepsilon_H$, $\hat{\delta} = \delta + \varepsilon_\delta$, $\hat{N}_M = N_M + \varepsilon_N$, $\hat{I} = I + \varepsilon_H$, ε_δ, ε_I, ε_H, ε_N are errors of measurement.

Estimation of the method accuracy. Assuming smallness of ε_δ, ε_I, ε_H, ε_N measurement errors and under condition of absence of their cross-correlation, we obtain on basis of (7) a formula for the relative variance of measurement error of the longitudinal component of the GMF intensity at the height h_x

$$\frac{\sigma_H^2}{H^2} \approx \frac{\sigma_\delta^2}{\delta^2} + \frac{\sigma_N^2}{N^2} + \frac{\sigma_I^2}{I^2}, \tag{8}$$

where σ_δ^2, σ_N^2, σ_I^2 are variances of δ, N_m, and I measurement.

The error due to uncertainty of the height h_x can be significant in case of strong GMF change within the altitude range $\Delta = h_2 - h_1$ and high requirements to accuracy of binding measured GMF intensity to the height.

If we represent a law of change in the GMF intensity within this altitude range as Taylor series and confine oneself to linear approximation

$$H(h) \approx H_0 + \frac{1}{2}\gamma(h - h_0), \tag{9}$$

where H_0 – GMF intensity at the height $h_0 = \frac{h_1 + h_2}{2}$, we obtain

$$\frac{\sigma_H^2}{H^2} \approx \frac{\sigma_\delta^2}{\delta^2} + \frac{\sigma_N^2}{N_M^2} + \frac{\sigma_I^2}{I^2} + \frac{\beta^2}{H^2}, \tag{10}$$

where $\beta = \gamma \frac{I_1}{2I}$, $I_1 = \int_{h_1}^{h_2} F(h)(h - h_0)dh$.

The height profile of the electron density can be approximated by the function

$$F(h) \approx F(h_0) + a(h - h_0) + b(h - h_0)^2. \tag{11}$$

Then

$$\frac{\sigma_H^2}{H^2} \approx \frac{\sigma_\delta^2}{\delta^2} + \frac{\sigma_N^2}{N_M^2} + \frac{\sigma_I^2}{I^2} + \left(\frac{\gamma}{H} \frac{a(\Delta h)^2}{12F(h_0)} \right)^2. \tag{12}$$

We assume that the variance $\sigma_\delta^2 = 2\sigma_\Phi^2(1 - r)$ makes the main contribution to the variance (12). Here σ_Φ^2 is the variance of the error of the parameter Φ, and r is the cross-correlation of errors for the heights h_1 and h_2, which depends on the amplitude-frequency response of the receiver.

We can show that the Cramér–Rao bound for the variance σ_Φ^2 under optimal measurement algorithm (5) is defined by formula

$$\sigma_\Phi^2 = \frac{\left[1 - \rho^2 + \left(\frac{1}{q_2} + \frac{1}{q_1} \right) + \frac{1}{q_1 q_2} \right]^2}{4M\rho^2 \left\{ 1 - \rho^2 + \frac{1}{2q_2} + \frac{1}{2q_1} \right\}}, \tag{13}$$

where ρ is the coefficient of correlation between the ordinary and extraordinary waves, M is the number of processed sounding cycles, q_1 and q_2 are the signal-to-noise ratio at the receiver outputs. The values $\sigma_\Phi = \sqrt{\sigma_\Phi^2}$ for the case of M=5800 (accumulation during a 15-min session) are presented in Table 1.

Table 1 – Standard deviation of error in measurement of the angle of the polarization ellipse rotation

	$q_1 = q_2 = 2$	$q_1 = q_2 = 4$	$q_1 = q_2 = 10$	$q_1 = q_2 = 50$
ρ = 0.5	0.022	0.017	0.014	0.012
ρ = 0.7	0.0165	0.012	0.009	0.007
ρ = 0.9	0.0126	0.008	0.005	0.004

Such potential accuracy allows expecting the fact that measurement errors in intensity of GMF can be comparable with its disturbances during geomagnetic storms.

Results of experimental test of the method. Some results of the first test of the described method for measuring GMF are presented below. In this case, the one channel of the transmitter and one of two orthogonal antenna dipoles were used to emit linearly polarized waves. When sampling a signal, we used a step in height Δ=4550 m. Because of the small step, the integral (4) for the *i*-interval of heights was calculated by the formula

$$I(h_{xi}) = 0{,}5\Delta\left[F(h_{1i}) + F(h_{2i})\right]. \qquad (14)$$

Parameter Φ was determined according to the algorithm (5). The signal power was determined for the echo signal from the short pulse by equalizing the receiver gains, subtraction of the noise power from the signal plus noise power, accounting gain of antenna switches with gas-filled dischargers for each segment of the radar sweep, and summing the results.

Dependence of vertical component of intensity of GMF on a height, got at watching 15 minutes presented on Fig. 1.

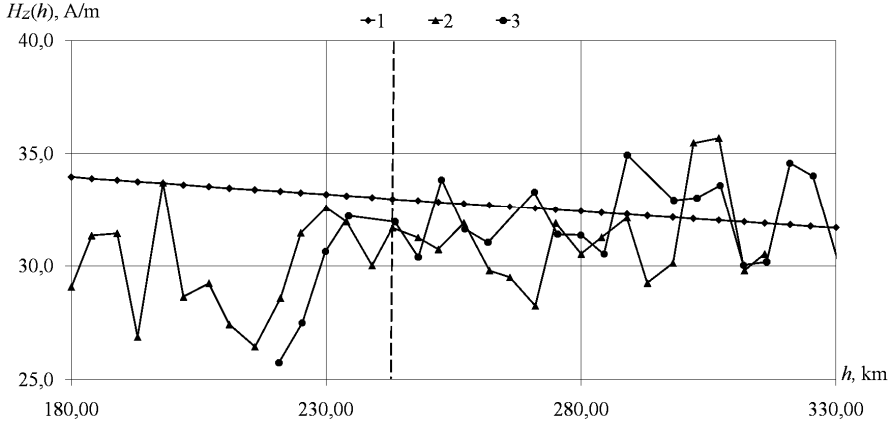

Fig. 1 – Intensity of H_z-component of geomagnetic field.
Local time in Kharkiv 13:20–13:36 (12.11.2012).

Curve 1 corresponds to the DGRF/IGRF Geomagnetic Field Model of [5], and curves 2 and 3 got experimentally. Curve 2 got with the use of temperatures in accordance with the model of IRI-2007 [6], and curve 3 – with the use of the temperatures measured by IS radar. A stroke vertical marks the height of a maximum of ionizing.

Apparently, in area of high concentration (230-300 kilometers) the measured values are near to the model.

It is of interest that the size of the measured intensity on the average a bit increases with a height, unlike the DGRF/IGRF model. In principle, such effect can be caused by the error of measuring of temperatures. A calculation was therefore produced with the use of model of temperatures of IRI-2007, that confirmed the effect of increase of vertical component of intensity with a height. This fact requires additional research. However it is known that GMF in an ionosphere can have noticeable local differences from the accepted models [1, 2].

Conclusion. Theoretical estimation and experimental test indicate that it is possible to measure the vertical component of the GMF intensity in the ionosphere by the proposed method with a relative root mean square error of a few percent. We can further improve the accuracy of these measurements, in particular due to the following:

– correction of errors due to errors in setting the polarization of the antenna;

– improving the signal-to-noise ratio by using two channels of the transmitter for formation of the sound signal with linear polarization;

– use of the polarization modulation of the sound signal, which allows to measure the electron and ion temperatures simultaneously with the signal polarization (Faraday rotation measurement).

Finally, we can evaluate quality of the GMF measurement using IS radar and ionosonde after optimization of equipment and measurement algorithms, and also the analysis of experimental data with the use of a sufficiently large statistical material.

References: 1. Ionosphere geomagnetic field: Comparison of IGRF model prediction and satellite measurements 1991 – 2010 [Электронный ресурс] // Radio Sci. – 2011. – № 46. – P. 1-10. – URL: http://onlinelibrary.wiley.com/doi/10.1029/2010RS004529/pdf (дата обращения: 25.05.2014). **2.** *Aleksandrov S.G.* Soviet satellites and spaceships / *S.G. Aleksandrov, R.E. Fedorov.* – Moscow: Academic Science, 1961. – 440 p. (in Russian). **3.** Patent 71162. Ukraine, G01S 13/95. A method of measuring the parameters of the ionosphere and magnetosphere / *L. Ya. Emelyanov*, *T. A. Skvortsov*, *I. B. Sklyarov*, *A. V. Fesun*.; patented 14.11.2011; published 10.07.2012, Bulletin № 13 (in Ukrainian). **4.** *Tkachev G.N.* The measurement of phase differential between ordinary and extraordinary waves which was scattered by thermal fluctuation electron density of ionosphere / *G.N. Tkachev, V.D. Karlov* // Harbinger KPU. – 1981. – № 183. – P. 18-27. (in Russian). **5.** http://ccmc.gsfc.nasa.gov/modelweb/models/igrf_vitmo.php. **6**. *Woodfield E. E.* Combining incoherent scatter radar data and IRI-2007 to monitor the open closed field line boundary during substorms / *E.E. Woodfield, J.A. Wild., A.J. Kavanagh, A. Senior, and S.E. Milan* // J. Geophys. Res. – 2010. – № 115. [Электронный ресурс] / URL: http://onlinelibrary.wiley.com/doi/10.1029/2010JA015751/pdf (дата обращения: 25.05.2014).

Received 16.05.2014

UDC 550.380:550.388.1:550.389.5: 537.67

Measurement of the geomagnetic field in the ionosphere using radar methods / **T. A. Skvortsov, L. Ya. Emelyanov, A. V. Fesun, D. P. Belozerov** // Bulletin of NTU "KhPI". Series: Radiophysics and ionosphere. – Kharkiv: NTU "KhPI", 2014. – No. 47 (1089). – P. 57-63. Ref.: 6 titles.

Рассмотрен новый способ измерения геомагнитного поля в ионосфере путем комплексного использования радара вертикального зондирования (ионозонда) и радара некогерентного рассеяния, его возможности и особенности технической реализации, а также первые результаты экспериментального испытания.

Ключевые слова: геомагнитное поле, ионосфера, радар некогерентного рассеяния, ионозонд.

Розглянуто новий спосіб вимірювання геомагнітного поля в іоносфері шляхом інтегрального використання радару вертикального зондування (іонозонду) і радару некогерентного розсіяння, його можливості й особливості технічної реалізації, а також перші результати експериментального випробування.

Ключові слова: геомагнітне поле, іоносфера, радар некогерентного розсіяння, іонозонд.

UDC 621.391

S.S. KOZLOV, PhD student, senior lecturer, NTU "KhPI"

AUTOMATIC DATA COLLECTION FOR INCOHERENT SCATTER COMPLEX

The creation of the automated data collection system for incoherent scatter complex is justified. The main part of the parameters influencing the control action was considered. The simplified implementation of automated data collection system is presented.

Keywords: automated data acquisition system, the control action, incoherent scatter radar, the program product.

Introduction. Changing settings on the radar systems of the Institute of the ionosphere will improve the information content of the data. Manage settings apparatus research observatory Institute ionosphere that affect the emission and reception mode, it is advisable to carry out, with the help of the control action. The control action is a requirement, which contains information about the required parameters of receiving and transmitting equipment and instruments, performing primary data processing.

Purpose of forming automation control action – more efficient use of the potential of the complex IS:

1. Providing operator relevant data for decision making.
2. Acceleration of certain operations to collect and process data.
3. Reducing the number of decisions on the measurement mode and the increased scrutiny.
4. Improving management efficiency.
5. Increasing the validity of decisions

On the formation of the content control action affects a large number of elements, differing in composition, characteristics, number of states, properties, significance, etc. In the process of analyzing the composition of the system, defining the control action, it was decided to divide the members into groups:

- Geophysical (current state of the ionosphere, the processes in the Sun);
- Technical (the technical condition of the complex Ionosonde);
- Geographic (geographical location of the radar);
- Information (set value and the study parameters, altitude range, temporal resolution);
- External (measured as part of an international network of radars HP);
- Energy (energy availability).

Automating the process of formation of the control action involves the need to describe the system model. A simplified model of the system is presented below (Fig. 1).

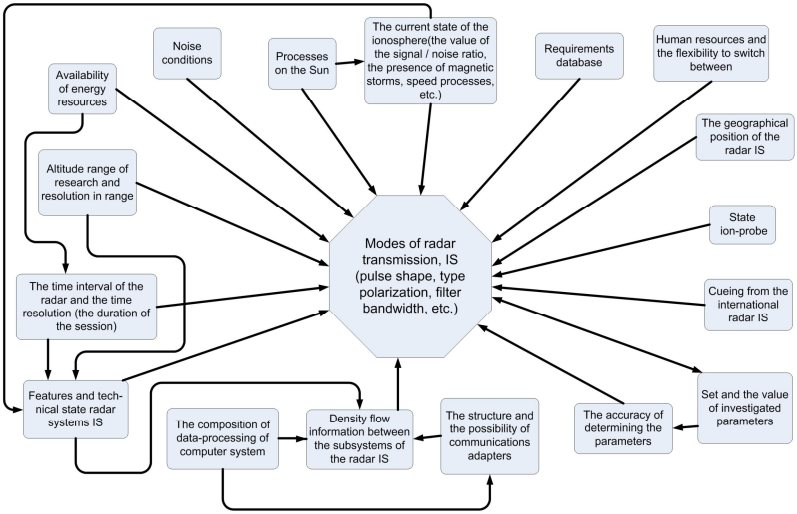

Fig. 1 – Simplified model of the automation system control action.

To resolve discrepancies between the degree of automation of complex IS to manage its energy resources, control and operation of the technical condition and degree of automation of process control information, a special operations support software of the automated data collection system.

Developed software written in HTML with the exception of under-and JavaScript library jQuery script itself. The client program is able to provide real-time information obtained from various sources, connect to the database of the Institute of Ionosphere and other research agencies. This software system is automatically gathering information. The software provides the operator with easy access to information, allows you to search values on the specified criteria, warns of excessive parameters thresholds, etc. Managing the measurements can be carried out at the request of the operator or to be automated in accordance with the output generated.

When designing a system was chosen programming language HTML, the body of which is connected script, which in turn is required for the program as script performs the basic function graph display an HTML page, the data output from the array with the definition of the maximum and minimum values of the subsequent construction schedules . Java script loosely connected to the body and the program runs without errors. Errors should be avoided, because this can cause erroneous results and conclusions of the program. When reading a web browser

page, the browser first tag finds <*script*>, executes its contents, and then continues reading the program code.

Data output from the array in graphical form is carried out through information from different websites and web-services.

To convert a given array and display it on a Web page, a table was used connect the special function: *function array2table ($ array, $ recursive = false, $ return = false, $ null = '')*, this function works with amounts of data, and outputs the result as a table on the html page. After the conclusion of the data is the possibility of their graphical representation of how the value of time.

Input parameters:
array $ array - array output
bool $ recursive - recursively nested arrays
bool $ return - displays the result on the screen (echo) or returns a string
string $ null - a string that is substituted for the empty cells.
Body of the function:

```
<?
function array2table ($ array, $ recursive = false, $ return = false, $ null ='')
{
/ / Check the input data
 if (empty ($ array) | |! is_array ($ array)) {
return false;
}
if (! isset ($ array [0]) | |! is_array ($ array [0])) {
$ array = array ($ array);
}
/ / Start the table
$ table = "<table> \ n";
/ / The table headings
$ table. = "\ t <tr>";
foreach (array_keys ($ array [0]) as $ heading) {
$ table. = '<th>'. $ heading. '</ th>';
}$ table. = "</ tr> \ n";
 foreach ($ array as $ row) {
$ table. = "\ t <tr>"; foreach ($ row as $ cell)
{
$ table. = '<td>';
if (is_object ($ cell)) {$ cell = (array) $ cell;}
if ($ recursive === true && is_array ($ cell) &&! empty ($ cell)) {
/ / Recursion
$ table. = "\ n". array2table ($ cell, true, true). "\ n";
} Else {
$ table. = (strlen ($ cell)> 0)?
htmlspecialchars ((string) $ cell): $ null;
}
$ table. = '</ td>';
```

```
}
$ table. = "</ tr> \ n";
}
/ / End
$ table. = '</ table>';
/ / Output
if ($ return === false) {
echo $ table;
}
Else {
return $ table;
}
?>
```

The function is written in php, which in turn can be connected to the html code using javascript. Javascript to connect php function is basically the program code.

Conclusions. The automation of the control action will facilitate the collection of information necessary to select the operating mode of the complex, more economical use of energy, improve information content of the data.

References: **1.** *Bogomaz O.V.* Unified Processing of the Results of Incoherent Scatter Experiments (UPRISE), a new generation program package for incoherent scatter radar data processing / *O.V. Bogomaz*, *D.V. Kotov* // Bulletin of National Technical University "Kharkiv Polytechnic Institute": Special Issue "Radiophysics and ionosphere". – Kharkiv: NTU "KhPI". – 2013. – N 28 (1001). – P. 29–37 (in Russian). **2.** *Miroshnikov A. E.* Kharkiv Institute ionosphere incoherent scatter radar (Ukraine) express data processing on a remote server and visualization of results / *A. E. Miroshnikov*, *O. V. Bogomaz* // 16th International EISCAT symposium, 12–16 August 2013, Lancaster, United Kingdom. – Lancaster, 2013. – http://eiscat2013.lancs.ac.uk/wp-content/uploads/2013/08/3 Miroshnikov_Miroshnikov_Abstract.pdf. **3.** *V.A. Semenov, S.V. Morozov*, Gunpowder SA Strategy object-relational mapping: systematization and analysis based on patterns / / Proceedings of the Institute for System Programming RAS. - 2004. - T. 8, part 2. - P. 53 - 92. **4.** *Puliaev V.A.* Software automated radar system incoherent scattering / / Vestn. NTU "KPI": team. scientific. tr. - Kharkov: NTU "KPI", 2003. – № 26. – P. 91-94. **5**. *Bogomaz A.V., Kozlov S.S., Pulyaev V.A.* The data base of the Institute for the ionosphere // Conference of Young Scientists "Remote radio soundings of the ionosphere (ION 2011)" (Kharkov, Ukraine, 12 – 15 April 2011). – Abstracts. – 2011. – P. 47.

Received 20.05.2014

UDC 621.391

Automatic data collection for incoherent scatter complex / S. S. Kozlov // Bulletin of NTU "KhPI". Series: Radiophysics and ionosphere. – Kharkiv: NTU "KhPI", 2014. – No. 47 (1089). – P. 64-68. Ref.: 5 titles.

Обосновано создание автоматизированной системы сбора информации для комплекса некогерентного рассеяния. Рассмотрен основной состав параметров, влияющий на управляющее воздействие. Представлена упрощённая реализация автоматизированной системы сбора информации.

Ключевые слова: автоматизированная система сбора информации, управляющее воздействие, радар некогерентного рассеяния, программный продукт.

Обґрунтовано створення автоматизованої системи збору інформації для комплексу некогерентного розсіяння. Розглянуто основний склад параметрів, що впливає на керуючий вплив. Представлена спрощена реалізація автоматизованої системи збору інформації.

Ключові слова: автоматизована система збору інформації, керуючий вплив, радар некогерентного розсіяння, програмний продукт.

UDC 621.3.095

S.I. RYMAR, PhD student, assistant, NTU "KhPI"

TECHNOLOGY AND EQUIPMENT FOR FAST OIL AND ADSORBENT REGENERATION WITH APPLICATION OF HIGH-POWER HF ELECTROMAGNETIC FIELD

The method of adsorbent drying by electromagnetic field is presented. Technology and equipment for fast oil and adsorbent regeneration with application of high-power HF electromagnetic field are shown.

Key words: adsorbent, regeneration, UF electromagnetic field.

Introduction. It is well-known, that one of the most critical problems in hi-power transformers usage is connected to quality of transformers oil. During the transformer operation oil absorbs atmospheric moisture and its dielectric strength decreases. To reduce the water content in the oil it is pumped through the tank containing the adsorbent such as zeolite or silica gel. Adsorbent, which had lost sorption capacity, can be restored by removing the moisture via heating. The treatment of the adsorbent can be produced by its calcinations on metal sheets or heating in sealed containers at reduced pressure by heating coils. Using the first method leads to destruction of the adsorbent during its transfer from the adsorber and back. Disadvantages of the second method are: adsorbent carbonization near heating coils due to overheating and lack of adsorbent drying in the area away from heaters. This is a due to low thermal conductivity of the adsorbent. To eliminate the shortcomings of the second method authors propose a technique of heating and regeneration of the adsorbent by using the HF powerful electromagnetic field.

The aim of the article is observe briefly the method of adsorbent drying by electromagnetic field.

Description of technology. To accelerate the regeneration of the adsorbent we use drying at reduced pressure. Another advantage of this method is application of a cartridge for oil regeneration "adsorber") as drying capacity. Application of the universal cartridge allows reducing the loss of adsorbent during operations of loading and unloading. Proposed cartridge (1), on figure 1, is a coaxial resonator. To enhance the distribution of the electromagnetic field, the center conductor (2) of the resonator is equipped with four bedded ribs (3). With such a construction the field distribution and, consequently heating of the substance becomes more uniform. Gates 7, 8 and 9 are used for the feeding and pumping of the oil in the cleaning oil mode of operation. In the adsorbent regeneration mode the vacuum pump has connected to those gates. Gates 10–12 are used for the emergency thermal control sensors connection. Mesh (4) prevents the adsorbent particles ingress into vacuum and oil pumps. Block (13) serves for matching of the output impedance of the generator to the input characteristic impedance of the cartridge.

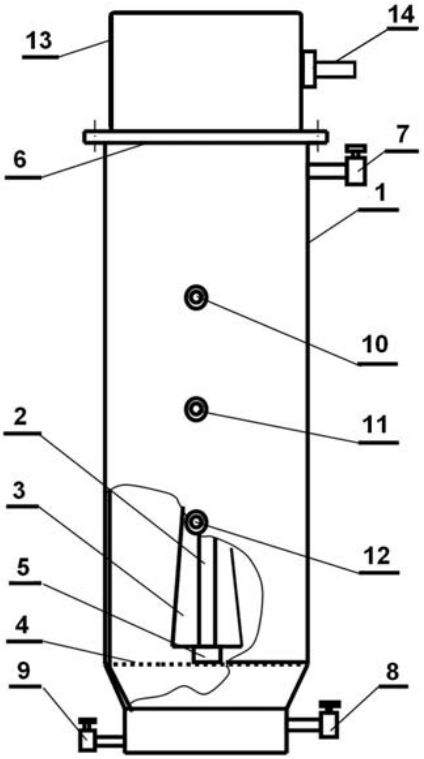

Fig. 1 – Universal regeneration cartridge
1 – external tube, 2 – center conductor, 3 – ribs for redistribution the electromagnetic field, 4 – filtering mesh, 5 – insulator, 6 – flange , 7-9 – oil and air gates, 10-12 – thermometer gates, 13 – device for electric matching, 14 – gate for UHF energy.

Modeling. To produce a uniform power distribution field modeling was carried out in specialized software.

Three were considered the embodiment: Non-ribbed (coaxial) resonator – the simplest variant; 4-ribbed resonator – *best RMS power distribution*; 8-ribbed resonator.

On fig. 3 can see the CAD model of this resonator. The shape of ribs allows matching an impedance of the resonator with the output resistance of the power generator.

Equipment for regeneration of transformer oil works on the two-cartridges scheme: one cartridge is used for transformer oil regeneration, second - for

adsorbent regeneration. After the regeneration of the adsorbent in the second cartridge, it replaces the first one in the scheme of recovery of the transformer oil.

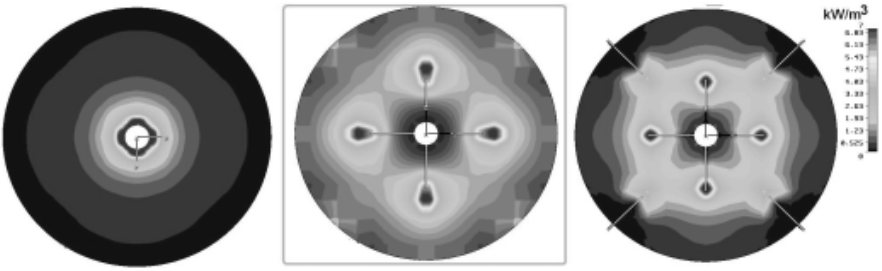

Fig. 2 – RMS power distribution in the different types of cartridges

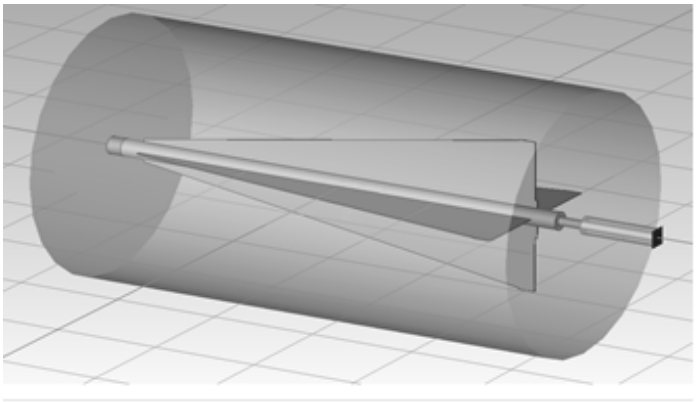

Fig. 3 – Cartridge for adsorbent regeneration

Industrial equipment. The construction of the universal cartridge presented on Fig. 1. Fig. 4 shows the outward of the device.

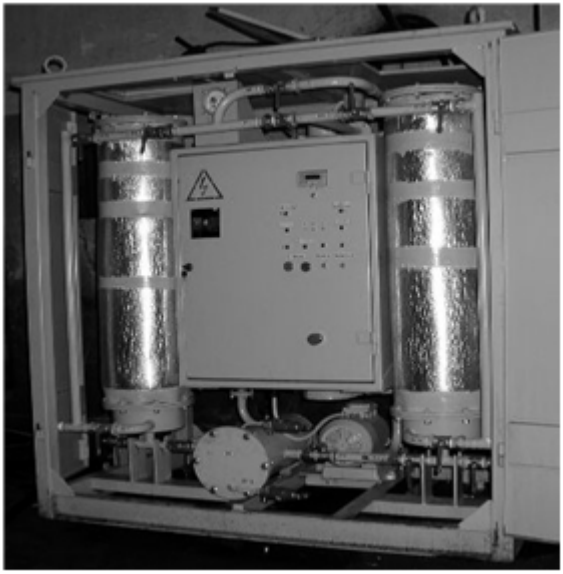

Fig. 4 – Industrial equipment for regeneration of transformer oil

Conclusion. The sorbent regeneration by proposed technique can increase the initial sorption capacity, prolong the life of sorbent, decrease a regeneration time and decrease the total energy consumption. Application of the presented technology and equipment allows to

- Increase the initial sorption capacity of the new zeolite in 15-20%
- Increase the number of cycles of zeolite usage from 3-4 to 8-10 (in comparison to the method of drying by heating coils).
- Decrease the time of regeneration from 15-16h to 7-8h (in comparison to the method of drying by heating coils).

References: 1. *Kivva F. V., Gorobets V. N., Zotov S. M. i dr.* New technologies of sorbents // Energy news. – 2003. – № 1-2. – P. 26–31 (in Russian). **2.** *Golovko M. I., Goncharenko Y. V., Gorobets V. N. i dr.* Installation for the regeneration of sorbents in the electromagnetic field // Technology and design of electronic equipment. – 2005. – № 5 (59). – P. 49–51 (in Russian). **3.** *Monastyrskiy A. E.* Regeneration, drying and degassing of transformer oil. Tutorial. – S-Peterburg, 1997. – P. 42 (in Russian). **4.** *Kel'tsev N. V.* Fundamentals of adsorption technology. – Moscow: Khimiya, 1984 (in Russian). **5.** *Lukin V. D., Antsipovich I. S.* Regeneration of the adsorbent. – Leningrad: Khimiya, 1983 (in Russian).

Received 26.05.2014

UDC 621.3.095

Technology and equipment for fast oil and adsorbent regeneration with application of high-power HF electromagnetic field / S. I. Rymar // Bulletin of NTU "KhPI". Series: Radiophysics and ionosphere. – Kharkiv: NTU "KhPI", 2014. – No. 47 (1089). – P. 69-73. Ref.: 5 titles.

Представлен способ сушки адсорбента электромагнитным полем. Показаны технология и оборудование для быстрой регенерации нефти и адсорбента с применением мощных ВЧ электромагнитных полей.

Ключевые слова: сорбент, регенерация, ВЧ электромагнитное поле.

Представлений спосіб сушіння адсорбенту електромагнітним полем. Показано технологію та обладнання для швидкої регенерації нафти і адсорбенту із застосуванням потужних ВЧ електромагнітних полів.

Ключові слова: сорбент, регенерація, ВЧ електромагнітне поле.

UDC 550.388.2

S.V. GRINCHENKO, scientific researcher, Institute of Ionosphere, Kharkiv

SEASONAL ANOMALY IN VARIATIONS OF GLOBAL DISTRIBUTIONS OF F2-LAYER ELECTRON DENSITY ACCORDING TO CCIR MODEL

There are presented the global distributions of electron density $n_{e\,max}$F2 and height h_{max}F2 of the main maximum of ionosphere. There are analyzed the basic regularities of longitude-latitudinal variations of these parameters in the northern and southern hemispheres. The main attention is given to the effect of seasonal anomaly. It is shown that, according to calculations by the CCIR model seasonal anomaly appears at latitudes between 15 and 60 degrees N. approximately from 9 to 12 hours of local time. In the southern hemisphere the seasonal anomaly is not observed.

Keywords: CCIR model, IRI, NeQuick model, global distribution of ionospheric parameters, geographical anomaly, seasonal anomaly, December anomaly, semiannual anomaly, Visual Fortran.

Statement of the problem. CCIR model of the distribution of electron density and height of F2-layer is constructed according to the data of the global network of vertical sounding stations. It is the basic empirical model of main maximum parameters of the quiet ionosphere. CCIR model allows to make daily calculations during various seasons at different levels of solar activity. The analysis of seasonal variations of F2-layer parameters according to CCIR model is important for confirmation of the results of theoretical simulation of quiet ionosphere parameters (electron density, transport plasma velocity, ion and electron temperatures) and comparisons with the incoherent scatter data. The main goal of this research is to construct global distribution of the main maximum parameters of the ionospheric plasma and to identify manifestations of seasonal anomalies and other features of the F2-layer morphology in longitude-latitudinal distributions of the northern and southern hemispheres.

The review of known anomalies of F2-layer morphology. F2-region (≈ 210-500 km) is the most difficult ionosphere area from the point of view of morphology of daily and seasonal variations of electron density altitude profile. The major ions in this region are the atomic nitrogen N^+ and atomic oxygen O^+ with a strong predominance of oxygen ions. Although the ion composition of F2-region is not complex, the electron density and height of layer F2 vary with complexity. It is a result of the dynamic processes peculiar to this area. Dynamic processes are determined by ambipolar diffusion and motion of ions and electrons in the magnetic and electric fields in the environment of horizontally moving neutral particles.

The behavior of F2-layer isn't described even in the first approximation by the theory of the Chapman layer. The regularities of F2-layer morphology which

don't keep within simple relations of Sun arrangement in the dome of the sky and values of maximum electron density and height of the F2-layer in the framework of Chapman theory are conventionally called "anomalies". The variations in the course of any year or day, changes with latitude are anomalous too.

The daily course of the electron density at F2-layer maximum is called anomalous, since diurnal variations can have one or two minima and one or two maxima, and the main maximum can be shifted relative to the noontime for a few hours (daily anomaly).

Geographical anomaly is manifested in the fact that the electron density maximum throughout the year shifts to the north of the geographic equator. Geographic anomaly is observed not only in the vernal and autumnal equinoxes, and even in the winter solstice.

It is accepted to understand the phenomenon of excess of winter day values of electron density $n_{e\ max}$F2 in maximum of layer over the summer ones as seasonal anomaly of F2-layer. The extent of this excess, as well as the behavior of other layer parameters – maximum height h_{max}F2, the upper and lower semithicknesses of the layer – are various for different geographic coordinates and levels of solar activity.

December anomaly is that in the range of the northern mid-latitudes to the southern mid-latitudes day values of electron density $n_{e\ max}$F2 are anomalously high in November, December and January. December anomaly strengthens seasonal one at northern mid-latitudes.

Also it is possible to note semiannual anomaly: during equinox periods day values of electron density are comparable with winter values (and hence exceed summer values).

General information about CCIR model. The full name of this model – CCIR f_0F2 and M(3000)F2 Model Maps 1982. Abbreviation CCIR is the reduced name of the International Radio Consultative Committee. The International Radio Consultative Committee was established in 1927. In 1992 the CCIR has been converted into Radiocommunication Sector of the International Telecommunication Union. The International Telecommunication Union (ITU) is a specialized agency of the United Nations Organization on information and communication technologies. The ITU Radiocommunication Sector (ITU-R) publishes regulations, recommendations, reports and handbooks compiled by research groups on a radio communication. In the ITU-R documents CCIR model is recommended for calculation of parameters of the F2-layer at modelling of radio pathes [10].

CCIR model contains a set of coefficients f_0F2 and M(3000)F2, allowing to calculate the ionospheric F2-layer parameters. Both parameters f_0F2 and M(3000)F2 are read from ionograms.

Propagation factor M(3000)F2=MUF(3000)/f_0F2. MUF(3000) is a maximum usable frequency, reflected from the F2 layer with a height of 3000 km.

The CCIR maps are received by the average values of a worldwide network of ionosondes. Mathematical bases of numerical methods used in the description of daily and geographic variations of these parameters are described in the papers by William B. Jones [1, 2]. At first, the data set of each station is represented by time Fourier series (in Universal Time). For according to the geographical latitude and longitude each Fourier coefficient is represented as a decomposition using Legendre functions. Series coefficients are calculated for the high and low solar activity. For intermediate levels of solar activity linear interpolation is used.

Database CCIR, currently known as a database ITU-R [10], consists of 12 files (on one for each month of the year). Files contains the coefficients needed to describe the time and geographical variations of the values M(3000)F2 and f_0F2. Each file contains: 1) 882 coefficients for M(3000)F2 (441 – for solar activity at Wolf number W=0 and 441 – for solar activity at W=100; 2) 1976 coefficients for f_0F2 (988 – for W=0 and 988 – for W=100). Thus, the whole CCIR model consists of (441+988)·2·12=34,296 coefficients.

Critical frequency of the electromagnetic wave reflected from the layer of electron density $f_0^2 = \dfrac{e^2 n_{e\,max}}{\pi m_e}$. From here the maximum of electron density in layer expresses as $n_{e\,max} = \dfrac{\pi m_e}{e^2} f_0^2$.

Considering, that $m_e = 9.1095 \cdot 10^{-28}\ g$, $e = 4.8034 \cdot 10^{-10}\ abstat\ unit$, we receive $\dfrac{\pi m_e}{e^2} = \dfrac{\pi \cdot 9.1095 \cdot 10^{-28}}{(4.8034)^2 \cdot 10^{-20}} = 1.2404 \cdot 10^{-8} \dfrac{g}{(abstat\ unit)^2}$.

If critical frequency f_0 is measured in MHz, and electron density concentration – in sm^{-3}, then $n_{e\,max} = 1.2404 \cdot 10^{-8} \cdot 10^{12} \cdot f_0^2 = 1.2404 \cdot 10^4 \cdot f_0^2$, $\lg n_{e\max} = \lg 1.2404 + 4 + 2 \cdot \lg f_0 = 4.0936 + 2 \cdot \lg f_0$. The square of critical frequency $f_0^2 = \dfrac{10^{-4}}{1.2404} \cdot n_{e\,max} = 8.0619 \cdot 10^{-5} \cdot n_{e\,max}$.

There are constantly improving techniques that allow on the critical frequency and f_0F2 propagation constant M(3000)F2 to calculate the height h_{max}F2 of the layer maximum F2 [3, 4, 5].

Comparisons of the planetary distributions of F2-layer parameters calculated from the empirical CCIR model and from theoretical calculations have shown a consistency of the general character of longitude-latitudinal variations [6, 7].

In spite of the continuously improvement of coefficient arrays with using of new ionospheric data [8, 9, 10], the same coefficient arrays of version 1982 are

applied in NeQuick model and in all versions of IRI model (from IRI-1990 to IRI-2011) presented on the Internet for free using.

Formulas of planetary distribution of f_0F2, M(3000)F2. To describe the global distribution of time dependences of ionospheric characteristics f_0F2, M(3000)F2 in CCIR model [10] it is used the time series Fourier which coefficients are expanded in spherical Legendre functions:

$$\Omega(\varphi,\lambda,T)=a_0(\varphi,\lambda)+\sum_{i=1}^{6}\left[a_i(\varphi,\lambda)\cos(iT)+b_i(\varphi,\lambda)\sin(iT)\right],$$

where Ω – ionospheric characteristics f_0F2, M(3000)F2; φ – geographic latitude ($-90°\le\varphi\le90°$); λ – geographic longitude ($0°\le\lambda\le360°$); T – Coordinated Universal Time (UTC), presented in the form of an angle ($0°\le T\le360°$).

Expansion coefficients in the Fourier series on variable T are represented as:

$$a_i(\varphi,\lambda)=\sum_{k=0}^{75}U_{2i,k}G_k(\varphi,\lambda)\qquad\left(i=\overline{0,6}\right),$$

$$b_i(\varphi,\lambda)=\sum_{k=0}^{75}U_{2i-1,k}G_k(\varphi,\lambda)\qquad\left(i=\overline{1,6}\right),$$

where $G_k(\varphi,\lambda)$ – spherical Legendre functions.

Thus, the numerical mapping function that describes the global distribution of ionospheric characteristics f_0F2, M(3000)F2, can be written as:

$$\Omega(\varphi,\lambda,T)=\sum_{k=0}^{75}U_{0,k}G_k(\varphi,\lambda)+$$

$$+\sum_{i=1}^{6}\left[\cos(iT)\sum_{k=0}^{75}U_{2i,k}G_k(\varphi,\lambda)+\sin(iT)\sum_{k=0}^{75}U_{2i-1,k}G_k(\varphi,\lambda)\right].$$

Since CCIR files contain values f_0F2, M(3000)F2 for two levels of solar activity, characterized by Wolf indices W=0 and W=100, the series expansion is carried out twice.

Remarks on the relationship of local time LT and Coordinated Universal Time UTC, used in the CCIR model. At the simulation of ionospheric processes it is convenient to use time directly connected with Sun hour angle t. For the zenith angle z, which determines the intensity of the ionizing radiation of the Sun, we have the formula: $\cos z=\sin\varphi\cdot\sin\delta+\cos\varphi\cdot\cos\delta\cdot\cos t$, where φ – latitude of the observation point, δ – declination of the Sun. The hour corner of the Sun $t=15^{\circ}(\mathrm{LT}-\mathrm{LT}_0)$, where LT – local time; at the moment of LT_0 the Sun is in upper culmination point, crossing the meridian of the observation point. Since the local time is determined by the Sun position, it is also called solar time.

Because of the Earth's orbit ellipticity the linear velocity of movement and the angular velocity of rotation of the Earth around the Sun varies throughout the

year. The Earth moves most slowly on its orbit, while it is at aphelion – the farthest point from the Sun, and most fast – while at perihelion. This is the significant cause of change in the duration of solar day during a year.

At apparent local time LT=12.00 the Sun is in the top culmination point. Since the duration of a day varies throughout a year, the researches use the mean solar day, tied to the so-called average Sun – a conditional point moving in regular intervals along the celestial equator (instead of on ecliptic, as the real Sun) and coinciding with the center of the Sun at the vernal equinox. There is a system of readout of average local time. Average local time of the upper culmination varies during a year approximately from 11 h 45 min to 12 h 15 min.

Further we will use the average local time, calling it for shot as local time. The local time (so we have agreed to call the average local time) of Greenwich meridian is Greenwich Mean Time (GTM).

There are various versions of universal time based on the rotation of the Earth relative to distant celestial objects (stars and quasars). The universal time UT1 is a basic version of a universal time. UT1 is calculated proportional to the angle of rotation of the Earth relative to the International Celestial Reference System (ICRS). The Coordinated Universal Time (UTC) is a time scale approximating UT1. UTC goes synchronously with the International Atomic Time (TAI).

Usually a UTC day consist 86,400 SI seconds. However for maintenance of divergence UTC and UT1 no more than 0.9 seconds with necessary of June, 30th or on December, 31st an additional second of coordination is added or subtracted. Besides the listed versions of universal time there are also others: UT0, UT1R, UT2, UT2R.

For ionospheric simulation differences between varioust versions of Universal Time and Greenwich Mean Time are insignificant. Therefore the local time on the zero meridian is assumed to be equal to a “certain” universal time. And as a universal time for ionospheric calculations it is possible to take any version of Universal Time.

The review of empirical models of altitude profiles of ionospheric parameters using CCIR model for calculation of F2-layer parameters. There are widely known the empirical model of ionosphere IRI (Fortran codes of various versions are on the NASA site), the European empirical model NeQuick (Fortran code can be found in the section of the free software of site ITU-R), the empirical model SPIM (Standard Ionosphere and Plasmasphere Model), codes various versions of which are available for public using on the IZMIRAN site. All of these programs to calculate electron density and height of the F2 maximum use CCIR model.

For using CCIR model in NeQuick it is necessary to input geographical longitude and latitude, number of month, Covington index $F_{10.7}$ and universal time.

For using CCIR model in IRI instead of a number of month it is necessary to input the concrete date (number and month) or corresponding number of day in a year. The IRI model has an interpolating dependence of monthly calculations, allowing to set not only a number of month, but also a number of day of the concrete month. The activity index $F_{10.7}$ is replaced by Wolf number W. These indexes are connected by the certain known dependence and easily recalculated into each other.

For values W ≤ 150 and $F_{10.7} \le 192.975$ the IRI model uses the following ratio: $F_{10.7} = 63.75 + W \cdot (0.728 + 0.00089 \cdot W)$.

And so, $0.00089 \cdot W^2 + 0.728 \cdot W - (F_{10.7} - 63.75) = 0$,

$$W = 33.5201 \cdot \sqrt{F_{10.7} + 85.122} - 408.989 =$$

$$= \sqrt{167271.8 + 1123.596 \cdot (F_{10.7} - 63.75)} - 408.989.$$

Value of $W = 11$ corresponds to $F_{10.7} = 71.87$. Value $F_{10.7} = 70$ corresponds to $W = 8.50$, and the value of $F_{10.7} = 100$ corresponds to $W = 47.08$.

The global longitude-latitudinal variations of electron density and height of the F2-layer maximum. To research the behavior of the maximum electron density $n_{e\,max}$F2 and height h_{max}F2 we'll build the longitude-latitudinal distribution of these values along the northern and southern hemispheres. Calculation of the electron density and height of the F2 layer are carried by CCIR model.

Figures 1-9 show the distributions of the decimal logarithm of electron density at the F2-layer maximum, measured in cm^{-3}. For the better perception of figures on schematic maps of hemispheres contours of continents and large islands are plotted. There are marked latitudes in 30 and 60 degrees and longitudes from 0 to 360 degrees with the step of 30 degrees.

To the each global distribution there corresponds some value of universal time UT. For example, at UT=0 local time LT for zero longitude equals 0 too. Through every 30 degrees for each of the 12 plotted longitudes there added 2 hours of local time.

On the northern hemispheres the point designates the location of the Kharkov Incoherent Scatter Radar. When universal time is 12 hours, at the Radar there is a little more than 14 hours of local time.

The presented figures are executed by programming in Visual Fortran language.

Before to analyze the manifestations of seasonal anomaly on the global distributions of electron density, there is of interest to dwell on an asymmetry of electron density distribution about rotation axis (i.e. the axis passing through the geographical poles).

Figures 1 and 2 show the $\lg n_{e\,max}$F2 December distributions in Covington index 71.87, and UT = 0, 12 respectively.

The axial asymmetry is the result of a mismatch of the Earth magnetic field poles with the geographic ones. Difference in geometry of the magnetic field lines relative to the geographical meridians, for example, in the North American and the European regions, leads to some quantitative differences of electron density variations. At a generality of physics of a middle-latitude ionosphere the ionosphere morphology in these regions has quantitative differences.

In both figures at middle latitudes there are well visible regions of the lowered $n_{e\,max}$F2 values in the morning and evening hours, corresponding to minima in the winter daily course. Around 12-14 hours of local time in both figures there is observed the maximum of F2-layer electron density.

The global distribution of F2-layer seasonal anomaly. The seasonal anomaly of electron density is illustrated in figure 2 and 3. The December distribution is characterized by high-amplitude variations of the electron density. If at night electron density in December is less, than in June, then at the mid-latitudes December daily values of electron density there are more than June ones. In winter at mid-latitudes daytime electron density at the F2-layer maximum is greater than the summer values. The effect of seasonal anomalies is observed, as seen from the figures, in the period 12-14 LT in the latitude range about from 15° to 60° N.

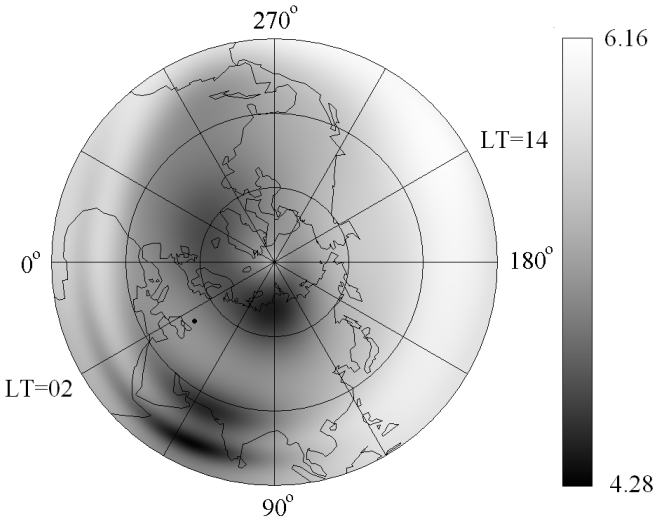

Fig. 1 – The December lg $n_{e\,max}$F2 distribution for northern hemisphere (UT = 00). The minimum value of lg $n_{e\,max}$F2 equals 4.31, maximum – 6.13.

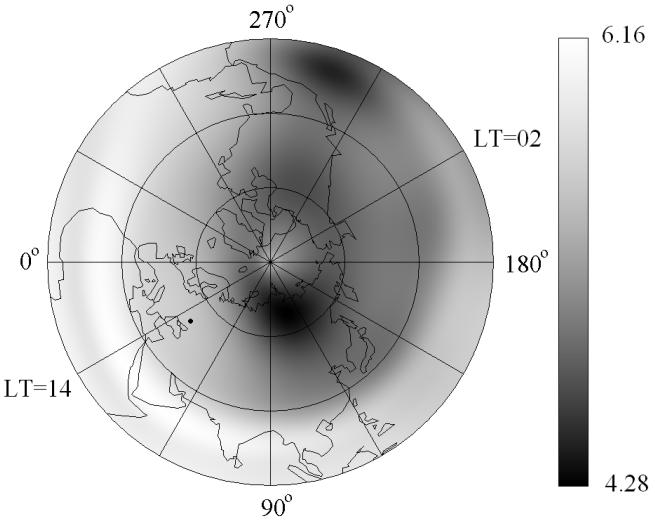

Fig. 2 – The December lg $n_{e\,max}$F2 distribution for northern hemisphere (UT=12). The minimum value of lg $n_{e\,max}$F2 equals 4.28, maximum – 6.16.

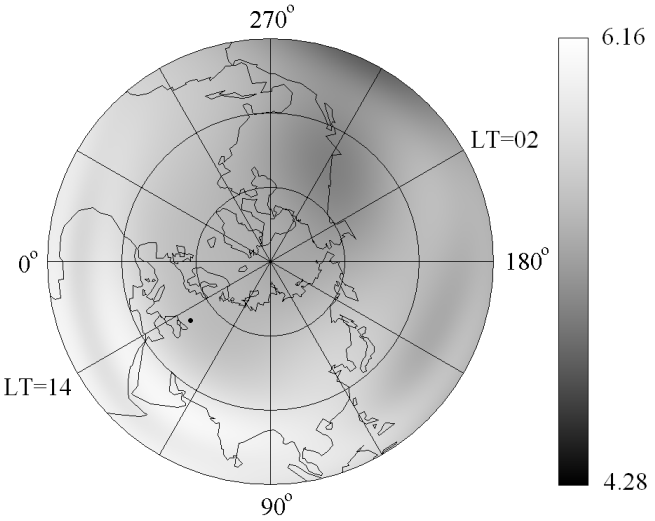

Fig. 3 – The June lg $n_{e\,max}$F2 distribution for northern hemisphere (UT=12). The minimum value of lg $n_{e\,max}$F2 equals 4.79, maximum – 6.07.

The sharper changes of electron density of the main maximum are observed during winter time in comparison with summer time. This is also true for the southern hemisphere in the conditions of local winter and local summer.

In southern hemisphere (fig. 4, 5) the phenomenon of seasonal anomaly is absent. In the southern hemisphere there is excess of electron density during the local summer over the winter ones in almost all latitudes and longitudes.

Naturally, in June the electron density values of the northern hemisphere is greater than values in the southern hemisphere. In December in the southern hemisphere it is so-called local summer, and the electron density values of the southern hemisphere is greater than values of the northern hemisphere.

Morphology of F2 maximum height. In northern hemisphere (fig. 6, 7) the summer values of F2-layer height are greater than the winter ones except for some equatorial regions. Calculations on CCIR model were made at $F_{10.7}$ = 71.87.

The sharper changes of height of F2 maximum are observed in winter time in comparison with summer time. For local winter and local summer of the southern hemisphere this is also true.

In southern hemisphere (fig. 8, 9) the height of layer F2 in the conditions of local summer is more than values of this height in the conditions of local winter practically at all values of co-ordinates.

In the southern hemisphere (fig. 8, 9), the height of the F2 layer in the conditions of local summer is greater than the height at the local winter conditions practically at all coordinates.

Quite naturally, in June the F2-layer height in the northern hemisphere is greater than the height in the southern hemisphere. In December in the southern hemisphere in the conditions of the local summer the F2-layer height is greater than the height in the northern hemisphere.

Thus, we can say that the phenomenon of seasonal anomaly (excess of the winter values of electron density of the F2 layer over the summer ones) is observed only in the northern hemisphere at mid-latitudes. Under other conditions there are exceeded the summer values of electron density and height of the F2-layer over the winter ones. Some equatorial regions can be an exception.

The daily variations of electron density and height of maximum F2 over a point of a location of Kharkov Incoherent Scatter Radar. Fig. 10 shows the daily variations of the electron density and height of F2-layer in June and December at $F_{10.7}$=72. If at night the summer values of electron density exceeds the winter values than approximately from 10 to 16 of local time there is observed an anomalous excess of winter values of electron density on the summer ones. At night seasonal anomaly is not observed.

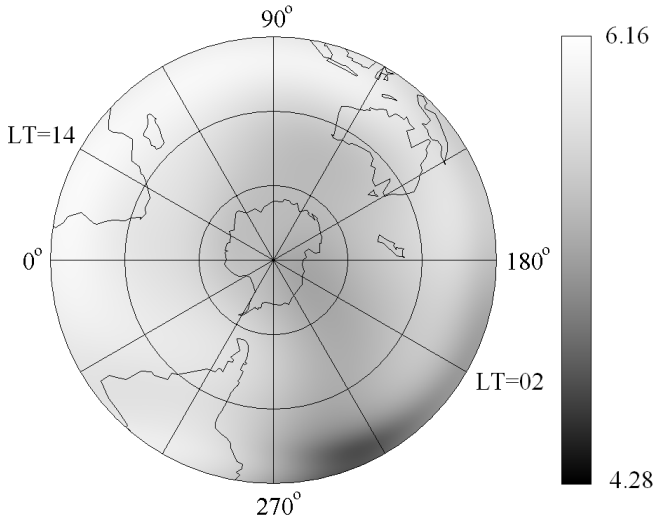

Fig. 4 – The December lg $n_{e\,max}$F2 distribution of southern hemisphere in the conditions of local summer (UT=12). The minimum value of lg $n_{e\,max}$F2 equals 4.69, maximum – 6.09.

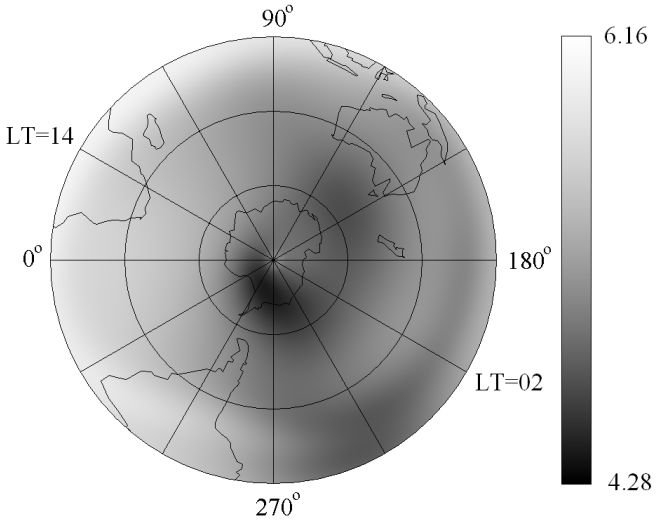

Fig. 5 – The June lg $n_{e\,max}$F2 distribution of southern hemisphere in the conditions of local winter (UT=12). The minimum value of lg $n_{e\,max}$F2 equals 4.41, maximum – 6.03.

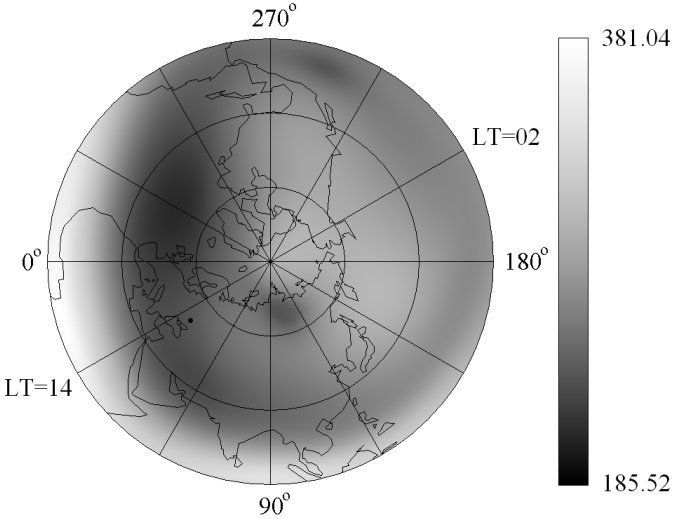

Fig. 6 – The December h_{max}F2 distribution of northern hemisphere (UT=12). The minimum value of h_{max}F2 equals 207.11 km, maximum – 381.04 km.

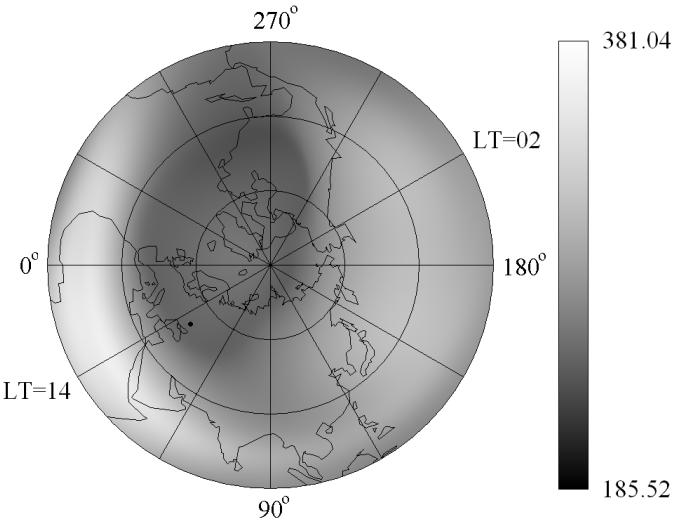

Fig. 7 – The June h_{max}F2 distribution of northern hemisphere (UT=12). The minimum value of h_{max}F2 equals 228.55 km, maximum – 360.84 km.

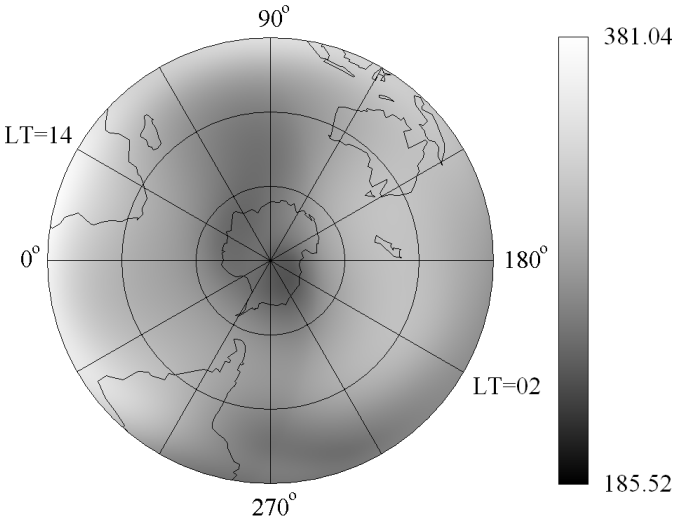

Fig. 8 – The December h_{max}F2 distribution of southern hemisphere in the conditions of local summer (UT=12). The minimum value of h_{max}F2 equals 231.96 km, maximum – 378.41 km.

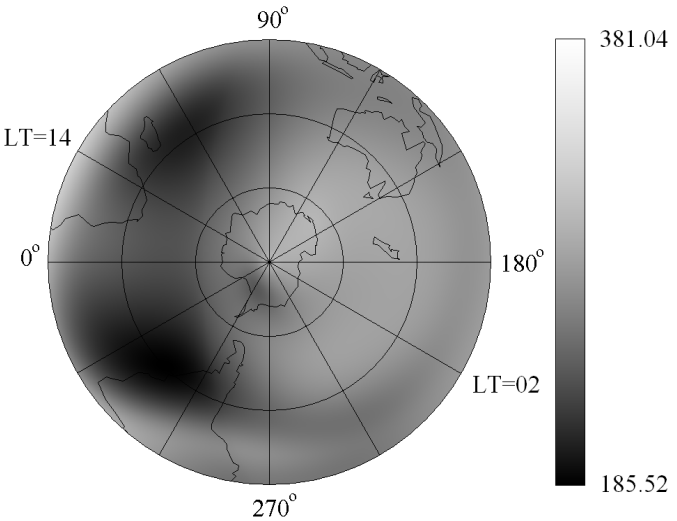

Fig. 9 – The June h_{max}F2 distribution of southern hemisphere in the conditions of local winter (UT=12). The minimum value of h_{max}F2 equals 185.52 km, maximum – 327.13 km.

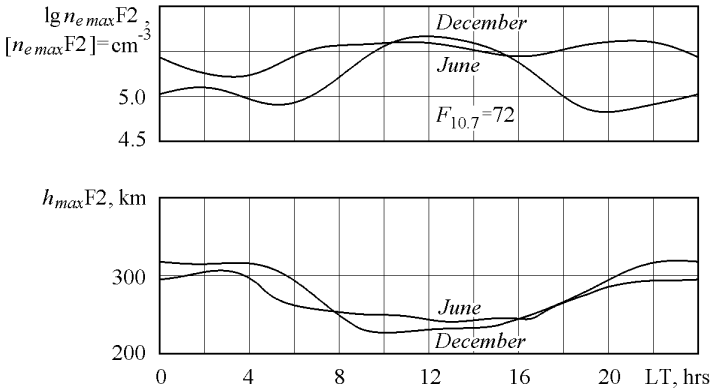

Fig. 10 – The daily variations of the electron density in the F2-layer maximum and maximum height above the point of a location of the Kharkov Incoherent Scatter Radar at $F_{10.7}$=72.

In the middle of June the sunrise time is about 4.6 LT, the sunset time – 20.8 LT. The sun doesn't disappear behind horizon approximately over 275 km. In the middle of December the Sun rises at LT≈7.9 and sets at LT≈16.0.

For winter the daily course is characterized by: 1) the considerable (to an order of values) variations of $n_{e\,max}$F2; 2) the pronounced pre-sunrise minimum, the fast growth in the morning; 3) a maximum in a daily course about 12 LT; 4) the decline in the afternoon.

The fast growth of the electron density in winter in the morning after a minimum is accompanied by the further lowering of height of the layer maximum. The time interval of the least heights coincides with the time interval of the maximum values of electron density. After this the layer F2 begins to rise. The greatest height of the layer is observed around midnight.

An interesting feature of the behavior of the winter ionosphere at middle latitudes is a night increase of electron density.

The summer type of daily variations is characterized by: 1) the inconsiderable daily variations (the diurnal values approximately twice more the night ones); 2) poorly expressed minimum at pre-sunrise time; 3) the presence of two maxima in a daily $n_{e\,max}$F2 course (day maximum – about 11 LT and evening one – about 21 LT; 4) the after-sunset decreasing of electron density until sunrise.

Fig. 11 shows the daily variations at higher solar activity (Covington index $F_{10.7}$=100). The seasonal anomaly is manifested already in a larger time interval – from 9 to 17 local time and not from 10 to 16, as in the previous case.

It should be noted a common pattern of change of electron density and height of the F2-layer maximum: an increase of electron density is almost always connected with a decrease of height of the layer and vice versa.

As it has been noted, the effect of seasonal anomaly of electron density is more expressed at higher solar activity (SA). This is due to the fact that although both in winter and summer at an increase of solar activity there are observed an increase of height of the layer and electron density during the whole day (figure 12, 13), the increase of electron density is more considerable during the winter daytime in comparison with summer increase.

The changes in solar activity does not affect the nature of the daily variations. A number of maxima and minima of the daily course remains invariable at SA changing. The moments of extrema of daily course of $n_{e\,max}$F2 and h_{max}F2 do not change with SA increasing.

Against the comparison of the daily courses in June and December it is represented interesting to compare the daily variations of electron density and height of F2-layer in March and September.

In the middle of March the sunrise time is about 6.3 LT, the sunset time – 18.0 LT. In the middle of September the Sun rises at LT≈5.6 and sets at LT≈18.2.

Although the March daytime values of electron density exceed September ones a little, the daily courses of electron density are generally similar. Also the daily courses of height of F2-layer are close. Thus, the spring and autumn variations of electron density and height of F2 maximum are approximately identical.

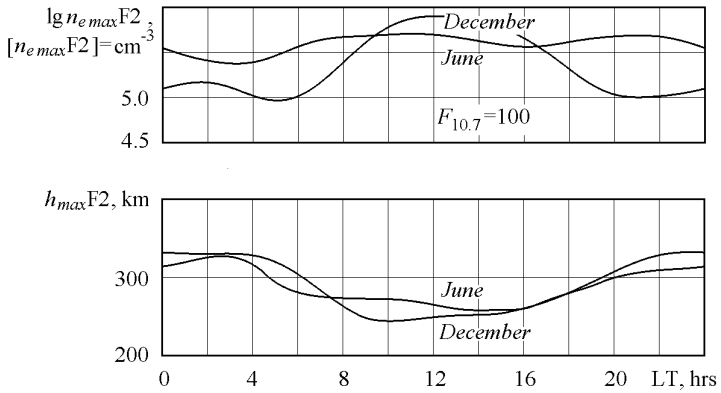

Fig. 11 – The daily variations of the electron density in the F2-layer maximum and maximum height above the point of a location of the Kharkov Incoherent Scatter Radar at $F_{10.7}$=100.

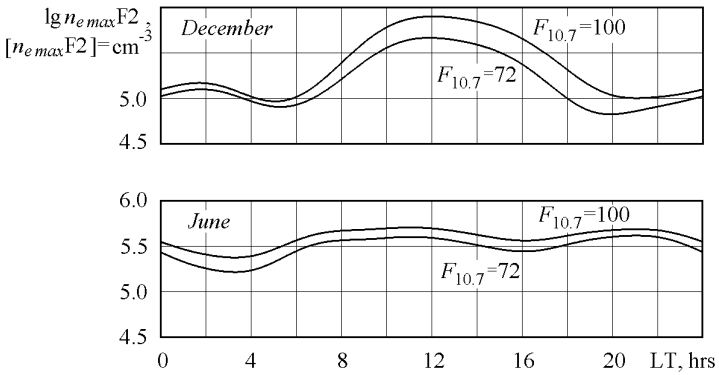

Fig. 12 – Increase of electron density of F2-layer at increasing of solar activity

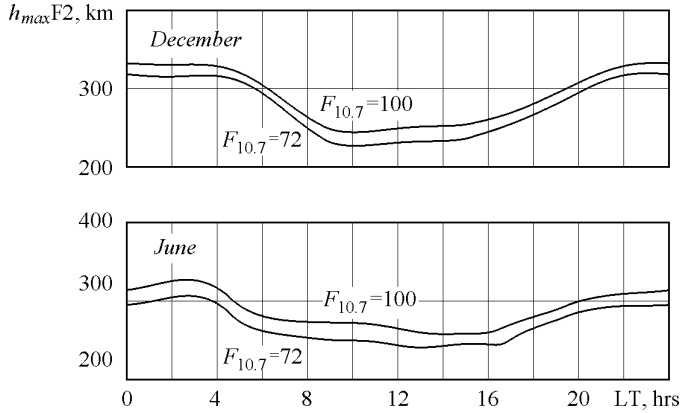

Fig. 13 – Increase of height of layer F2 at increase of solar activity

The daily variations of electron density and height of F2-layer maximum at mid-latitudes of the southern hemisphere. In the southern hemisphere the phenomenon of seasonal anomaly is absent: there is the excess of the local summer values of electron density over the electron density values in conditions of local winter practically at all latitudes and longitudes. This can be illustrated with fig.15 for 49.7° latitude south of the equator unlike northern latitude 49.7° of Kharkov Incoherent Scatter Radar used in the previous calculations. A comparison of the winter and summer variations do not carry in the southern hemisphere "anomalous" character. The values of electron density in the conditions of local

summer is greater than the values of local winter. And the heights of F2-layer in local summer are greater the heights in local winter.

In selected point of the southern hemisphere in the middle of June of local winter the sunrise time is about 8.6 LT, the sunset time – 16.7 LT. In the middle of December of local summer the Sun rises at LT≈3.8 and sets at LT≈20.0. In December the Sun doesn't disappear behind horizon approximately over 275 km.

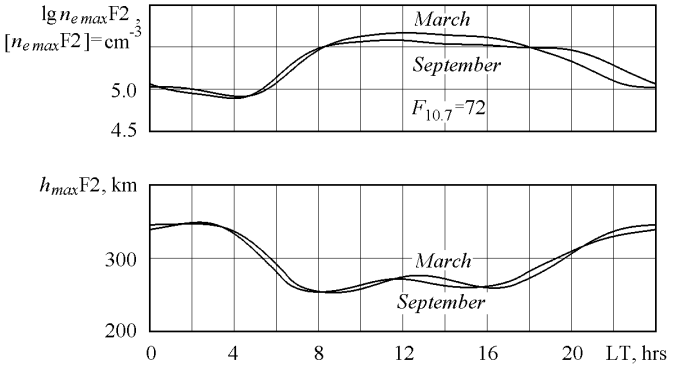

Fig. 14 – The spring and autumn variations of electron density and height of the F2-layer maximum

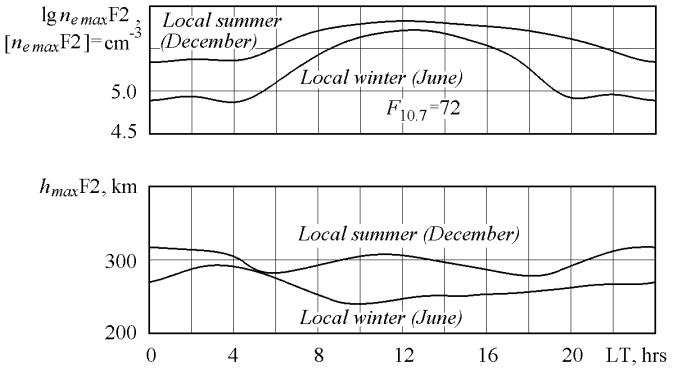

Fig. 15 – The daily variations $n_{e\,max}$F2 and h_{max}F2 in June and December in the southern hemisphere

The main feature of the variations of height h_{max}F2 at mid-latitudes of the southern hemisphere is relatively small change of values during the day.

Development of ionospheric models by dates receiving by the incoherent scatter method in Institute of Ionosphere of NAS and MES of Ukraine. The creation of empirical model CCIR became possible due to the statistically provided data of a world network of vertical sounding stations. Though the incoherent scatter data are the most informative ones in a wide altitude range, but they have the regional limitations. In Institute of ionosphere in the eightieth years there was developed an empirical model of the daily courses of the altitude profiles of electron density, ion and electron temperature by the incoherent scatter date, presented in tabular form for the different seasons and levels of solar and geomagnetic activity (E. I. Grigorenko, S. V. Grinchenko, et al). Now M. V. Lyashenko develops CERIM IION Model (Central Europe Regional Ionospheric Model) which allows to calculate seasonal and daily courses of electron density, ion and electron temperatures of ions, vertical velocity of the plasma transport, as well as some parameters of dynamic and thermal processes in ionospheric plasma.

Conclusions. The results of CCIR model calculations confirm axial asymmetry of ionosphere. The CCIR model calculations clearly demonstrate the phenomena of seasonal and geographical anomalies. The daily courses of the parameters of F2-layer maximum (h_{max}F2 and $n_{e\,max}$F2) have characteristic anomalies too. In winter the daily course $n_{e\,max}$F2 has well expressed the Chapman form with one midday maximum; in summer the daily course $n_{e\,max}$F2 has two maxima (day and evening), and the summer amplitude of a daily course is less than winter one. At northern mid-latitudes the winter excess of electron density $n_{e\,max}$F2 of quit ionosphere is observed approximately in the range of 9-17 LT. In the rest time of the day winter values $n_{e\,max}$F2 are less summer ones.

At increase of solar activity there is observed the increasing of h_{max}F2 and $n_{e\,max}$F2 during all time of days. The increase of $n_{e\ max}$F2 at increasing of solar activity is especially appreciable in winter daytime. Therefore, the effect of seasonal anomaly is more expressed at higher solar activity.

The spring and autumn values of electron density and height of F2 maximum are about the same.

References: **1**. *Jones W.B., Gallet R.M.* Representation of diurnal and geographic variations of ionospheric data by numerical methods // Journal of Research of the National Bureau of Standard – D. Radio Propagation. – 1962. – Vol. 66D, № 4. – P. 419-438. **2**. *Jones W.B., Stewart F.G.* A numerical method for global mapping of plasma frequency // Radio Sci. – 1970. – Vol. 5, № 50. – P. 773-784. **3**. *Brunini C., Conte J.F., Azpilicueta F., Bilitza D.* A different method to update monthly median h_mF2 values // Adv. Space Res. – 2013. – Vol. 51. – P. 2322-2332. **4**. *Hoque M.M., Jakowski N.* A new global model for the ionospheric F2 peak height for wave propagation // Ann. Geophysicae. – 2012. – Vol. 30. – P. 797-809. **5**. *Shubin V.N., Karpachev A.T., Tsybulya K.G.* Global model of F2 layer peak height for low activity based on GPS radio-occultation data // J. Atm. Sol.-Terr. Phys. – 2013. – Vol. 104. – P. 106-115. **6**. *Rush C.M., PoKempner M., Anderson D.N., Stewart F.G., Perry J.* Improving ionospheric maps using theoretically derived values of f_oF2 // Radio Sci. – 1984. – Vol. 18, № 1. – P. 95-107.

7. *Rush C.M., PoKempner M., Anderson D.N., Perry J., Stewart F.G., Reasoner R.K.* NTIA Report 84-140. Global Maps of f_0F2 derived from observation and theoretical values // Institute for Telecommunication Sciences. National Telecommunications and Information Administration. US Department of commerce, 1984. – 144 p. **8**. *Bradley P.A.* Mapping the critical frequency of the F2-Layer: Part 1 – requirements and developments to around 1980 // Adv. Space Res. – 1990 – Vol. 10, № 8. – P. 47-56. **9**. *Crane R.K.* Evaluation of global and CCIR models for estimation of rain rate statistics // Radio Sci. – 1985. – Vol. 20, № 4. – P. 865-879. **10**. ITU-R Reference ionospheric characteristics // Recommendation ITU-R P. 1239-3 (02/2012) – 29 p.

Received 08.08.2014

UDC 550.388.2

Seasonal anomaly in variations of global distributions of F2-layer electron density according to CCIR model / S. V. Grinchenko // Bulletin of NTU "KhPI". Series: Radiophysics and ionosphere. – Kharkiv: NTU "KhPI", 2014. – No. 47 (1089). – P. 74-91. Ref.: 10 titles.

Построены планетарные распределения электронной концентрации $n_{e\,max}$F2 и высоты h_{max}F2 главного максимума ионосферы. Проанализированы основные закономерности долготно-широтных вариаций этих параметров в северном и южном полушариях. Основное внимание уделено эффекту сезонной аномалии. Показано, что согласно расчётам по модели CCIR сезонная аномалия проявляется на широтах от 15° до 60° с. ш. примерно с 9 до 12 часов местного времени. В южном полушарии сезонная аномалия не наблюдается.

Ключевые слова: модель CCIR, IRI, модель NeQuick, планетарное распределение ионосферных параметров, географическая аномалия, сезонная аномалия, декабрьская аномалия, полугодовая аномалия, Visual Fortran.

Побудовано планетарні розподіли електронної концентрації $n_{e\,max}$F2 і висоти h_{max}F2 головного максимуму іоносфери. Проаналізовано основні закономірності довготно-широтних варіацій цих параметрів в північній і південній півкулях. Основна увага приділена ефекту сезонної аномалії. Показано, що згідно з розрахунками за моделлю CCIR сезонна аномалія проявляється на широтах від 15° до 60° пн. ш. приблизно з 9 до 12 години місцевого часу. У південній півкулі сезонна аномалія не спостерігається.

Ключові слова: модель CCIR, IRI, модель NeQuick, планетарний розподіл іоносферних параметрів, географічна аномалія, сезонна аномалія, груднева аномалія, піврічна аномалія, Visual Fortran.

UDC 550.388.2

S.V. PANASENKO, PhD, head of department, Institute of ionosphere, Kharkiv;
M.T. RIETVELD, Prof., senior scientist, EISCAT Scientific Association, Ramfjordmoen, Norway;
C. LA HOZ, Prof., UiT the Arctic University of Norway, Tromsø, Norway;
I.F. DOMNIN, D.Sc., Prof., director, Institute of Ionosphere, Kharkiv

TRAVELLING IONOSPHERIC DISTURBANCES OVER KHARKIV, UKRAINE, ACCOMPANYING THE OPERATION OF EISCAT HEATER FACILITY

We have detected the travelling ionospheric disturbances (TIDs) over Kharkiv with periods of 40 – 80 min occurring in the time range between 09:00 and 10:30 UT on November 22 and between 10:00 and 12:00 UT on November 23, 2012 during and after the operation of the EISCAT heater facility. The duration of these disturbances were less than 120 – 180 min. The relative amplitudes of the TIDs in electron density ranged from 0.05 to 0.15 and those in electron and ion temperatures were about 0.02 – 0.05. Assuming that these TIDs have been generated in the heated region, we described the possible mechanisms of their generation.

Key words: travelling ionospheric disturbances, powerful HF radio waves, incoherent scatter radar, heater facility.

Introduction. The ionospheric modification by high power HF radio waves is a kind of the active experiment conducted regularly after putting in use the ionospheric heating facilities in USA, Norway and Russia (former USSR). Powerful radio waves result in significant perturbations involving an increase in electron temperature, a change in electron density, low-frequency radiation of ionospheric current systems, generation of ionospheric irregularities with a wide range of scales, pump-induced artificial optical emissions, etc., in the irradiated ionospheric region [1, 3]. Some recent results of such experimental studies have been published in the papers [4, 5].

Large scale disturbances during heating experiments have been detected at the distances of the order of 1000 km, along with local ones. They appear in the F-region as traveling ionospheric disturbances (TIDs) related to generation and propagation of acoustic-gravity waves (AGWs) in the upper atmosphere. Such disturbances were determined to be strongly depending on space weather conditions, the time of day, season of the year, the mode of the heating facility operation, etc (see, e.g., [6]). Furthemore, since the parameters of these artificial disturbances appear to be close to the parameters of natural perturbations originating constantly in the ionosphere, it is often difficult to separate these two

types of events. Nevertheless, the efforts to detect the disturbances occurring far from the heated plasma volume have been continuing [7 – 9]. *Domnin et al.* [7] found wave disturbances in the ionosphere over Kharkiv, Ukraine during the operation of "Sura" facility. *Kunitsyn et al.* [8] reported about wavelike disturbances coming out from the ionospheric region over the "Sura" heater. *Mishin et al.* [9] observed AGWs induced by HAARP HF heating. *Pradipta and Lee* [10] presented the results indicating the origin of AGWs from the edge of the HAARP facility heated region.

The purpose of this paper is to present and analyze the TIDs in the ionospheric F region measured by the Kharkiv incoherent scatter radar during the operation of the EISCAT heating facility.

Instrumentation and data sets. In 2012 a coordinated experimental campaign was conducted. The facilities employed included the EISCAT Heater, Dynasonde and incoherent scatter (IS) radar, located near Tromsø, Norway as well as IS radar and ionosonde, located near Kharkiv, Ukraine. The experiments were done at the morning hours on November 22 – 24.

The ionospheric heater transmitted pump waves with O-mode polarization having a frequency from 4.04 to 7.10 MHz. On November 22, 2012, it was operated during 05:33 – 09:00 UT period in 15-min cycles (9 min on, 6 min off), after which the pump modulation of 15 min on, 15 min off was alternated with ± 2 min square wave modulation during 15-min period, 15 min off. On November 23, 2012, the heater operation with 15-min cycles was from 05:03 until 09:00 UT followed by such pump modulation as in previous day. On November 24, 2012, the HF pump cycles were different. A sporadic-E layer appeared during the observations, so this experiment was exluded from the study. The effective radiated power increased from 140 to 850 MW being dependent on pump frequency and antenna array. The antenna beam was directed to the magnetic zenith which is 12° south of zenith.

The diagnostics of ionospheric plasma was performed by the Kharkiv IS radar being at the distance of about 2400 km. The time variations in incoherent scatter power, electron density and electron and ion temperatures being observed at different altitudes have been analyzed.

Results. Figure 1 presents temporal variations of pump frequency as well as F2-region critical frequency f_oF2 over EISCAT heater site. As seen in this figure, the heating was in underdense conditions from the experiment start to about 08:00 UT both on November 22 and November 23, followed by overdense conditions. After about 08:00 UT, the pump frequency increased stepwise to be slightly less than f_oF2 (see Figure 1). The F2-region critical frequency over Kharkiv during these experiments was greater and fell within the range of 5.0 to 10.6 MHz and 5.4 to 10.0 MHz on November 22 and 23, respectively.

The temporal variations of the main ionospheric parameters over Kharkiv obtained from the IS radar data are indicated in Figures 2 and 3. These data covering the height range of 200 – 325 km have been filtered to detect the oscillations initiated by AGWs. The analysis shows that the fluctuations with the largest relative amplitudes were in the range of 40 – 80 min.

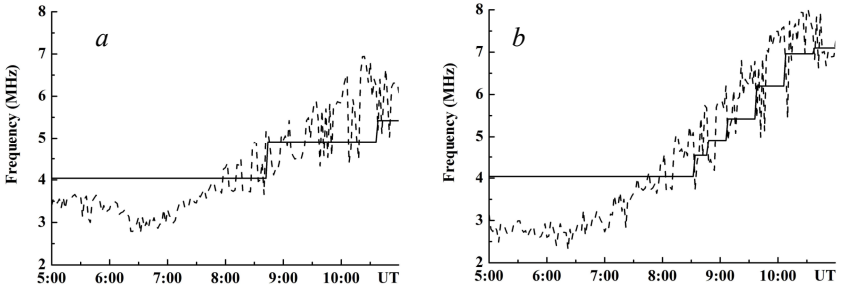

Fig. 1 – Pump frequency (solid line) and F2-region critical frequency measured by the Dynasonde (dashed line) during the EISCAT heating experiments conducted on: *a* – November 22; *b* – November 23, 2012

The main criterion for TIDs selection was the occurrence of fluctuations with close dominant periods in the electron density, the electron temperature and the ion temperature simultaneously during almost the same time interval. Moreover, these fluctuations must cover a height range more than 50 km.

The strong variations in all ionospheric parameters being analysed occured between 04:00 – 07:00 UT and again 12:00 – 17:00 UT on November 22, 2012. Their relative amplitude values reached 0.05 – 0.2 for different parameters depending on the height (see Figure 2). On November 23, 2012, such fluctuations with similar relative amplitudes were observed during 04:30 – 07:30 UT and 14:00 – 17:00 time intervals (see Figure 3). These TIDs arose before the start or after the end of heating experiments. They are likely to be caused by the passage of solar terminators over Kharkiv IS radar site.

A pronounced TID was observed during the time interval from about 09:00 to 10:30 UT on November 22, 2012. As illustrated in Figure 2, the fluctuations with the dominant period of about 60 min were primarily observed at heights of 200 – 290 km. The values of the relative amplitude ranged from 0.05 to 0.15 for the electron density and 0.02 – 0.05 for the electron and ion temperatures. The duration of oscillations was usually about 2 periods. The TID was also detected during the heating experiment conducted on November 23, 2012. Its parameters

were similar to that described above, but the time interval with oscillations was from about 10:00 to 12:00 UT (see Figure 3).

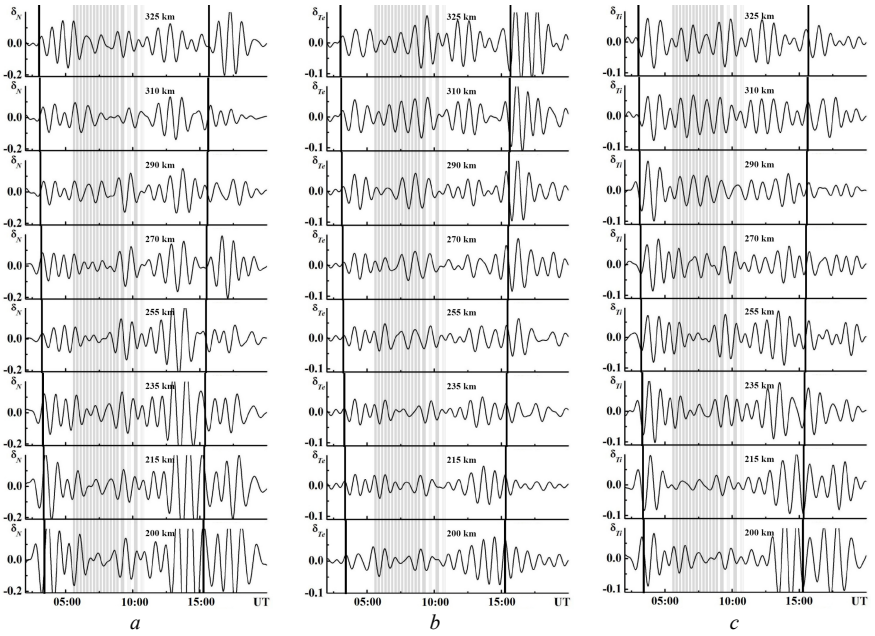

Fig. 2 – Relative fluctuations of *a* – electron density, *b* – electron temperature and *c* – ion temperature filtered in 40 – 80 min band, at different altitudes on November 22, 2012. The shadow strips indicate heater-on times. The solid lines mark the times of sunrise and sunset terminator moving in the atmosphere above the Kharkiv incoherent scatter radar location.

Discussion. As is well known (see, e. g., [9]), the strong effects of high power HF radio wave on the F2 region are produced when the pump frequency is equal to the upper hybrid resonance (UHR) frequency near the F2-peak. This became possible only after a change in the heating conditions from underdense to overdense, i.e after about 08:00 UT. Thus, if the TID observed after 09:00 UT on November 22 and after 10:00 UT on November 23, 2012 originated in the heated ionospheric region, their apparent horizontal velocity are not less than 330 – 660 m/s taking into account a transit time of 1 – 2 hours and the distance of about 2400 km. Such apparent horizontal velocities are associated with AGWs. However, since the exact time of wave disturbance onset is unknown, we

can not exclude the propagation of waves of another type, e. g. magnetohydrodynamic in nature.

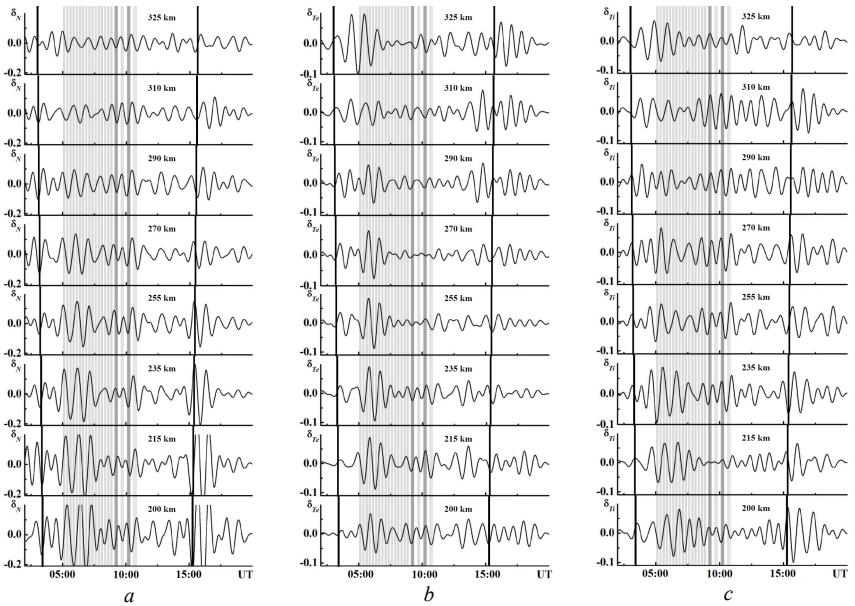

Fig. 3 – Same as Fig. 2 but for relative fluctuations on November 23, 2012

Possible mechanisms for AGW generation in the heated region have been proposed in [7, 8, 10]. The authors of [8] indicated the heater-induced wave disturbances to be generated at the edge of the heated region by sharp thermal gradients. *Mishin et al.* [7] and *Chernogor* [10] concluded that such disturbances can be produced by periodic heating of neutral gases. Moreover, other mechanisms may involve the modulation of ionospheric currents in the dynamo region, UHR region and in the ionospheric F-region by the propagating radio wave [10]. The detailed estimations made by *Chernogor* [10] showed the most effective mechanism of TIDs generation during the ionospheric heating is modulation of the effective electron collision frequency in the UHR region.

The main problem we met is that we have no possibility to obtain the arrival direction of TIDs. Therefore, based only on the results of these measurements we can not assert that the observed TIDs arrived from the heated region. However, even in the case of finding the arrival detection, the origin of the observed TIDs is not obvious. The AGWs producing the TIDs are known to be omnipresent in the atmosphere due to a large number of their natural and man-made sources. In

particular, the detected TIDs could be generated in the polar region, although the experiments have been conducted during magnetically very quiet conditions when the planetary *Ap* and *Kp* indexes not exceed 7 and 1, respectively. Thus, long-term, regular measurements are needed to detect and identify high-power radio wave-induced TIDs as well as estimate their parameters during different space weather conditions.

Conclusions. TIDs in electron density, electron and ion temperatures have been detected in the ionospheric F2-region with Kharkiv IS radar during the operation of the EISCAT heating facility. An increase in relative amplitudes of wave disturbances with periods of 40 – 80 min in the height range from 200 to 290 km has been observed. Such disturbances are likely caused by AGW propagation generated by periodic HF modification of the ionosphere, although they can be generated by many other natural or man-made origins of AGWs and TIDs. The possible mechanisms for AGW generation in the modified region are the modulation of ionospheric currents in the UHR region or in the dynamo region by high power radio waves, the periodic heating of neutral gas and sharp thermal gradients at the edge of the heated region.

References: 1. *Stubbe P.* Ionospheric modification experiments the Tromsø Heating Facility / *P. Stubbe, H. Kopka, M.T. Rietveld, A. Frey, P. Høeg, H. Kohl, E. Nielsen, G. Rose, C. LaHoz, R. Barr, H. Derblom, Å. Hedberg, B. Thidé, T. B. Jones, T. Robinson, F. Brekke, T. Hansen, O. Holt* // J. Atm. Terr. Phys. – 1985. – Vol. 47, No 12. – P. 1151-1163. **2.** *Fejer J.A.* Ionospheric modification experiments with the Arecibo Heating Facility / *J.A. Fejer*, *C.A. Gonzales*, *H.M. Ierkic*, *M.P. Sulzer, C.A. Tepley, L.M. Duncan, F.T. Djuh, S. Ganguly, W.E. Gordon* // J. Atm. Terr. Phys. – 1985. – doi: 10.1016/0021-9169(85)90086-8. **3.** *Migulin V.V.* Investigation in the U.S.S.R. of non-linear phenomena in the ionosphere // *V.V. Migulin, A.V. Gurevich* // J. Atm. Terr. Phys. – 1985. – Vol. 47, No 12. – P. 1181-1187. **4.** *Vierinen J.* High latitude artificial periodic irregularity observations with the upgraded EISCAT heating facility / *J. Vierinen, A. Kero*, *M.T. Rietveld* // J. Atm. Sol.-Terr. Phys. – 2013. – V. 105 – 106. – P. 253-261. **5**. *Frolov V.L.* Sounding of the ionosphere disturbed by the "Sura" heating facility radiation using signals of the GPS satellites / *G.P. Komrakov*, *V.E. Kunitsyn*, *A.M. Padokhin*, *A.E. Vasiliev*, *G.A. Kurbatov* // Radiophys. Quantum Electron. – 2010. – Vol. 53, No 7. – P. 379-400. **6.** *Garmash K.P.* Elegtromagnetic and geophysical effects in the near-Earth plasma, stimulated by high power high frequency radio waves / *K.P. Garmash, L.F. Chernogor* // Electromagnetic phenomena. – 1998. – V. 1. No 1. – P. 90-110. (in Russian) **7.** *Mishin E.* F2-region atmospheric gravity waves due to high-power HF heating and subauroral polarization streams / *E. Mishin, E. Sutton, G. Milikh, C. Roth, M. Förster* // Geophys. Res. Lett. – 2012. – Vol. 31, L11101, doi: 10.1029/2012GL052004. **8.** *Domnin I.F.* Results of Radiophysical Study of Wave Disturbances in the Ionospheric Plasma During Its Heating by High-Power HF Radio Transmission of "Sura" facility / *I.F. Domnin*, *S.V. Panasenko, V.P. Uryadov, L.F. Chernogor* // Radiophysics and Quantum Electronics. – 2012. – Vol. 55, No 4. – P. 253-265. **7.** *Kunitsyn V.E.* Sounding of HF heating-induced artificial ionospheric disturbances by navigational satellite radio transmissions / *V.E. Kunitsyn, E.S. Andreeva, V.L. Frolov, G.P. Komrakov, M.O. Nazarenko, A.M. Padokhin* // Radio Sci. – 2012. – Vol. 47, RS0L15, doi:10.1029/2011RS004957. **8.** *Pradipta R.* Investigation of acoustic gravity waves created by anomalous heat sources: experiments and theoretical analysis / *R. Pradipta, M.C. Lee* // Physica Scripta. – 2013. – Vol. 155, 014028, doi:10.1088/0031-8949/2013/T155/014028. **9.** *Gurevich A.V.* Nonlinear Phenomena in the Ionosphere / *A.V. Gurevich* – New York, Heildelberg,

Berlin: Springer – Verlag, 1978. – 465 pp. **10.** *Chernogor L.F.* The mechanisms for generation of infrasound oscillations in the upper atmosphere by high power radio transmission / *L.F. Chernogor* // Radio Physics and Radio Astronomy. – 2012. – Vol. 17, No 3. – P. 240-252. (in Russian)

Received 08.09.2014

UDC 550.388.2

Travelling ionospheric disturbances over Kharkiv, Ukraine, accompanying the operation of EISCAT heater facility / S. V. Panasenko, M. T. Rietveld, C. La Hoz, I. F. Domnin // Bulletin of NTU "KhPI". Series: Radiophysics and ionosphere. – Kharkiv: NTU "KhPI", 2014. – No. 47 (1089). – P. 92-98. Ref.: 10 titles.

Обнаружены перемещающиеся ионосферные возмущения (ПИВ) над Харьковом с периодами 40 – 80 мин, имевшие место в течение 09:00 – 10:30 UT 22 ноября и с 10:00 до 12:00 UT 23 ноября 2012 г. в период и после работы нагревного стенда EISCAT. Продолжительность этих возмущений не превышала 120 – 180 мин. Относительные амплитуды ПИВ концентрации электронов составляли 0.05 – 0.15, а ПИВ температур электронов и ионов равнялись 0.02 – 0.05. В предположении, что эти ПИВ были сгенерированы в нагретой области, описаны возможные механизмы их генерации.

Ключевые слова: перемещающиеся ионосферные возмущения, мощные радиоволны, радар некогерентного рассеяния, нагревный стенд.

Виявлено рухомі іоносферні збурення (РІЗ) над Харковом з періодами 40 – 80 хв, що мали місце впродовж 09:00 – 10:30 UT 22 листопада та з 10:00 до 12:00 UT 23 листопада 2012 р. в період і після роботи нагрівного стенда EISCAT. Тривалість цих збурень не перевищувала 120 – 180 хв. Відносні амплітуди РІЗ концентрації електронів складали 0.05 – 0.15, а РІЗ температур електронів та іонів дорівнювали 0.02 – 0.05. За припущення, що ці РІЗ були згенерровані в нагрітій області, описано можливі механізми їх генерації.

Ключові слова: рухомі іоносферні збурення, потужні радіохвилі, радар некогерентного розсіяння, нагрівний стенд.

UDC 550.388.2

S.V. GRINCHENKO, scientific researcher, Institute of Ionosphere, Kharkiv;
D.A. DZIUBANOV, PhD, senior scientific researcher, associate professor, NTU "KhPI";
Iu.E. ZIUZGINA, student, NTU "KhPI"

SIMULATION OF IONOSPHERIC PLASMA VELOCITY ALONG THE GEOMAGNETIC FIELD LINES DUE TO THE HORIZONTAL NEUTRAL WINDS

With use of horizontal neutral winds model HWM93 there are calculated the elements of a global picture of thermosphere circulation, the changes of value and direction of thermosphere wind over Kharkiv. The calculations of constituent part of vertical component of ionospheric plasma velocity caused by horizontal neutral winds were made.

Keywords: horizontal wind model HWM93, dynamics of an ionosphere, ionospheric plasma velocity.

Statement of the problem. Motion of the ionospheric plasma is determined by the processes of diffusion, dragging by neutral wind and electromagnetic drift. The dragging by neutral wind characterizes the global processes in the ionosphere and, in some cases, may be the determining factor. Now the empirical model of horizontal neutral winds HWM93 [1] is successfully used. In general, it presents satisfactorily a global picture of the atmospheric circulation. However HWM93 as any empirical model, requires constant addition of observational data obtained in different regions. One of such informative tools of observation is incoherent scatter radar of the Institute of ionosphere. It gives possibility to determine the overall velocity of the plasma in the vertical direction. From these data, at the further processing, the component determined by neutral winds can be calculated [2]. Therefore it is necessary to know kind of data, given with the model, as these data are determined by time and solar activity. Subsequently, these data will be compared with the results of observations and used for model development.

The work purpose. Using the model HWM93 to calculate and interpret the dynamic processes in the upper atmosphere, caused by neutral winds at thermospheric altitudes.

Dynamic processes modeling. Dynamics of the upper atmosphere is one of the most important problems of geospace. This applies both to dynamics of neutral components and dynamics of an ionosphere. The dynamics of the neutral components is determined mainly by the tidal forces caused by heating of the upper atmosphere by solar radiation and, in a minor part, lunar tides. These movements are often decisive in the dynamic processes of the ionosphere and play the important role in formation of global distribution of electron density.

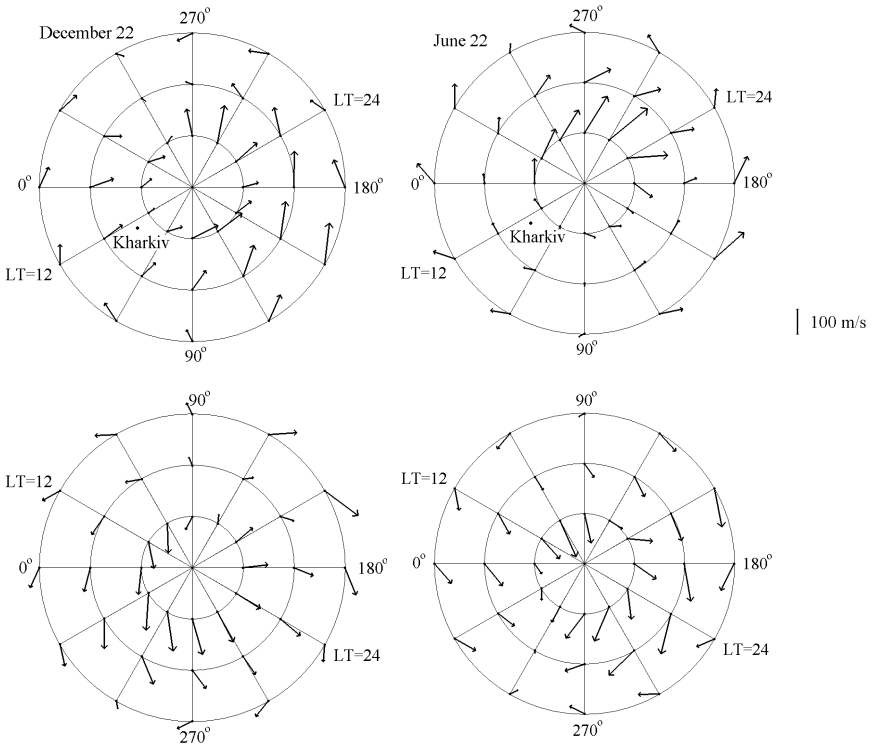

Fig. 1 – Distributions of the horizontal neutral winds in northern and southern hemispheres at altitude of 300 km in the winter and summer solstices when $F_{10.7}$=100 and A_p=2

Fig. 1–2 shows the global distribution of neutral velocity vectors for winter and summer solstices, vernal and autumnal equinoxes at low solar activity. The calculations are executed on model HWM93 [3 – 5] of horizontal winds of neutral components. For the calculations there were taken magnetically quiet conditions (A_p=2); the level of solar activity (SA) was characterized by index $F_{10.7}$=100. The calculations of neutral winds were carried out for altitude of 300 km.

The graphs show that there is a significant difference between the summer and winter periods. It is noteworthy that in the local summer almost round the clock thermospheric wind is directed toward equator, changing in value and direction. In local winter one can see a clear change of direction during the day: in

the afternoon – in a direction of a corresponding pole, at night – through the pole in the opposite direction.

As to the equinox periods, the same tendency of change of a wind vector direction is shown, as well as in local winter time. It can be seen that both in direction and value of velocity, the equinox periods are very similar.

Now we will show the variations of thermospheric wind direction over Kharkiv (see Fig. 3–4).

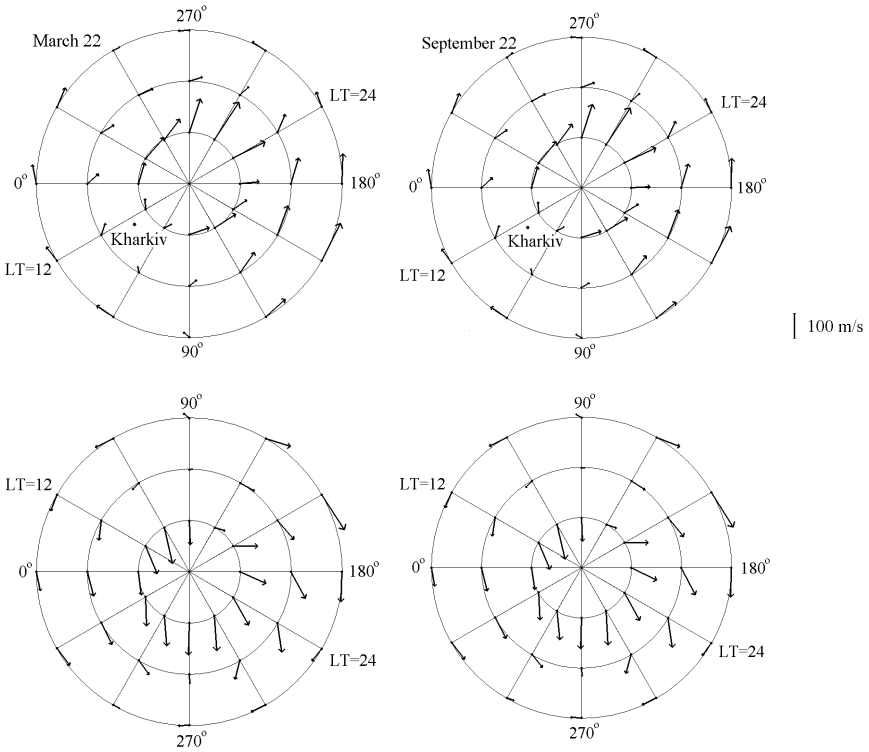

Fig. 2 – Distributions of the horizontal neutral winds in northern and southern hemispheres at altitude of 300 km in days of vernal and autumnal equinoxes. Character of the distributions of velocity vectors is almost the same

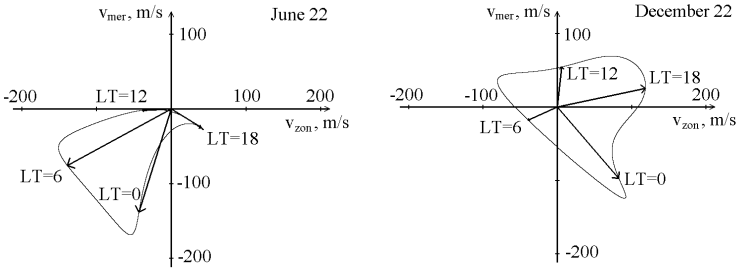

Fig. 3 – Variation of value and direction of horizontal wind over Kharkiv in winter and in summer during the day. In summer at low solar activity in magnetically quiet conditions during all time a northern wind component is absent

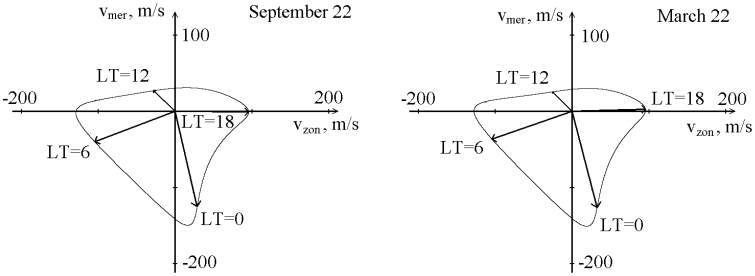

Fig. 4 – Variation of value and direction of horizontal wind over Kharkiv at vernal and autumnal equinoxes during the day

Finally, to connect the given model calculations with studies of the ionosphere by incoherent scatter method, we calculated the vertical component of the velocity of the ionospheric plasma dragged by thermospheric wind. The fact is that due to the magnetization of ionospheric plasma horizontal wind forces the plasma to move along the geomagnetic field lines. In turn, this movement has a vertical projection, which can later be compared with the ionospheric observations data. The results of calculations are shown in Fig. 5–6.

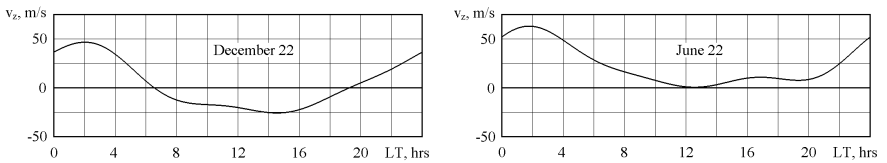

Fig. 5 – The vertical component of the drag plasma velocity in the summer and winter time

It is seen that in summer at low SA thermospheric wind during the whole day gives a contribution to upward component of overall plasma velocity. In winter during the daytime there is a significant downward movement.

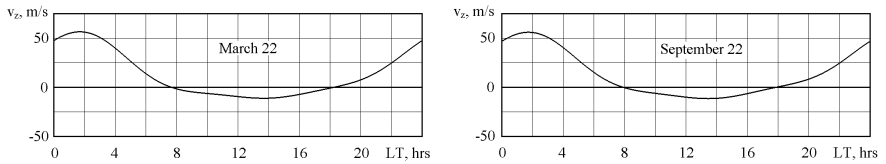

Fig. 6 – The vertical component of the plasma drag velocity in the vernal and autumnal equinoxes

Equinox periods occupy an intermediate position and are almost identical in nature.

Conclusions. There are analyzed the details of a global picture of thermosphere circulation for Kharkiv region during various seasons. There is executed the simulation of constituent part of vertical component of ionospheric plasma velocity caused by horizontal neutral winds. To confirm or to correct the presented model calculations will be possible by processing of ionospheric plasma velocity observations obtained by incoherent scatter method.

References: 1. *Hedin A.E.*, *et al*. Empirical Wind Model for the Upper, Middle and Lower Atmosphere // J. Atmos. Terr. Phys. – 1996. – Vol. 58. – P. 1421-1447. **2**. *Dziubanov D.A., Emelyanov L.Ya. , Loiko A.A*. Estimation of velocity of neutral atmosphere motion at the altitudes of F-layer maximum according to incoherent scatter data // Bulletin of National Technical University "Kharkov Polytechnic Institute": Series "Radiophysics and ionosphere". – 2013. – № 28 (1001). – P. 75-81 (in Russian). **3**. *Grinchenko S.V.* Construction of vector field of the horizontal neutral winds // Bulletin of National Technical University "Kharkov Polytechnic Institute": Special Issue "Radiophysics and ionosphere". – 2011. – № 44. – P. 130-137 (in Russian). **4**. *Grinchenko S.V.* Global distributions of temperature, mass density and horizontal winds according to empirical models // 13th Ukrainian Conference on Space Research. Abstracts Yevpatoria, Crimea, Ukraine, September 2-6, 2013. – Kyiv. – 2013. – P. 49 (in Russian). **5**. *Grinchenko S.V.* Global distributions of temperature, mass density and horizontal winds of neutral atmosphere // Bulletin of National Technical University "Kharkov Polytechnic Institute": Series "Radiophysics and ionosphere". – 2013. – № 28 (1001). – P. 82-96 (in Russian). **6**. *Grinchenko S.V.* The effect of horizontal neutral winds upon formation of middle-latitude ionospheric F2-region // 11th Ukrainian Conference on Space Research. Abstracts. Yevpatoria, Crimea, Ukraine, August 29 – September 2, 2011. – Kyiv. – 2011. P. 25.

Received 09.09.2014

UDC 550.388.2

Simulation of ionospheric plasma velocity along the geomagnetic field lines due to the horizontal neutral winds / S. V. Grinchenko, D. A. Dziubanov, Iu. E. Ziuzgina // Bulletin of NTU "KhPI". Series: Radiophysics and ionosphere. – Kharkiv: NTU "KhPI", 2014. – No. 47 (1089). – P. 99-104. Ref.: 6 titles.

С использованием модели горизонтальных нейтральных ветров HWM93 рассчитаны элементы глобальной картины термосферной циркуляции, изменения величины и направления термосферного ветра над Харьковом. Проведены расчёты компоненты вертикальной составляющей скорости движения ионосферной плазмы, обусловленной горизонтальными нейтральными ветрами.

Ключевые слова: модель горизонтальных нейтральных ветров HWM93, динамика ионосферы, скорость движения ионосферной плазмы.

З використанням моделі горизонтальних нейтральних вітрів HWM93 розраховані елементи глобальної картини термосферной циркуляції, зміни величини і напряму термосферного вітру над Харковом. Проведено розрахунки компоненти вертикальної складової швидкості руху іоносферної плазми, зумовленої горизонтальними нейтральними вітрами.

Ключові слова: модель горизонтальних нейтральних вітрів HWM93, динаміка іоносфери, швидкість руху іоносферної плазми.

CONTENT

NOTE

NOTE

НАУКОВЕ ВИДАННЯ

ВІСНИК
Національного технічного університету
“Харківський політехнічний інститут”

Збірник наукових праць

Серія
Радіофізика та іоносфера

№ 47 (1089)

Науковий редактор: д.т.н., проф. Пуляєв В.О.
Технічний редактор: к.ф.-м.н. Ляшенко М.В.
Відповідальний за випуск: к.т.н. Обухова І.Б.

Адреса редколегії: 61002, м. Харків, МСП, вул. Червонопрапорна, 16
тел. +38 (057) 707-65-27; *e-mail: iion@kpi.kharkov.ua*

Об. вид. № 86-14

Підписано до друку 21.10.2014 р. Формат 60×90 1/16.
Папір офсетний. Друк – ризографія. Гарнітура Times New Roman.
Умовн. друк. арк. 6,00. Наклад 300 прим. Зам. № _____.

Видавничий центр НТУ “ХПІ”. Свідоцтво про державну реєстрацію суб’єкта видавничої справи ДК № 3657 від 24.12.2009 р.

61002, Харків, вул. Фрунзе, 21

Надруковано у СПДФО Ізрайлєв Є.М.
Свідоцтво № 24800170000040432 від 21.03.2001 р.
61002, м. Харків, вул. Фрунзе, 16